# UC Irvine
## UC Irvine Electronic Theses and Dissertations

### Title
Image Based Interrogation of Brain and Body Composition in Human Newborns

### Permalink
https://escholarship.org/uc/item/266667qm

### Author
Rasmussen, Jerod Michael

### Publication Date
2016

### Copyright Information
This work is made available under the terms of a Creative Commons Attribution-NonCommercial-ShareAlike License, availalbe at https://creativecommons.org/licenses/by-nc-sa/4.0/

Peer reviewed|Thesis/dissertation

eScholarship.org Powered by the California Digital Library
University of California

UNIVERSITY OF CALIFORNIA,
IRVINE

# Image Based Interrogation of Brain and Body Composition in Human Newborns

DISSERTATION

submitted in partial satisfaction of the requirements
for the degree of

DOCTOR OF PHILOSOPHY

in Biomedical Engineering

by

Jerod Michael Rasmussen

Dissertation Committee:
Professor Frithjof Kruggel, Chair
Professor Pathik Wadhwa
Professor Gultekin Gulsen

2016

© 2016 Jerod Michael Rasmussen

# Table Of Contents


Page

**List of Figures** vii

**List of Tables** ix

**Acknowledgments** x

**Curriculum Vitae** xi

**1 Abstract** xiv

**2 Introduction** 1

**3 Background** 4

**3.1 Body Composition**

*3.1.1 Energy Homeostasis, White/Brown Fat, Adiposity/BMI, and Outcomes Related to Early Life Obesity* 4

*3.1.2 Autonomic Control of Energy Homeostasis* 7

*3.1.3 Brain Control of Feeding Behavior: Reward, Salience, Satiety, and Interoception* 8

*3.1.4 Early Life Fat Gain as an Outcome Variable* 10

**3.2 Infant Brain Development**

*3.2.1 Quantifying Infant Brain Development: Structure, Connectivity and Function* 11

*3.2.2 Age in Linear Models of Infant Brain Development* 15

**3.3 The Obese Brain: The Current State of Research in Adults and Children**

*3.3.1 Brain Size/Shape and Obesity* 17

*3.3.2 Structural Brain Connectivity and Obesity* 18

*3.3.3 Brain Function and Obesity* 19

**4 Research Design and Methods**

**4.1 Fat Quantification**

*4.1.1 DXA: Theory, Implementation, and Considering Covariates of Non-Interest* 22

*4.1.2 Central Adiposity: MRI Acquisition and Segmentation* 25

*4.1.3 Brown Adipose Tissue: MRI Acquisition, Segmentation, Validation and Estimates of Repeatability/Reliability* 28

**4.2 Quantifying Infant Brain Development**
*4.2.1 Brain MRI Acquisition: Structure/Anatomy, Structural Connectivity, Functional Connectivity* 33
*4.2.2 Maturation Index (MI) Defined* 37

**4.3 Prospective Associations Between Brain Phenotypes and Infant Adiposity: Modeling**
*4.3.1 Newborn Insula Volume and Early Life Adiposity Gain* 41
*4.3.2 Newborn White Matter Properties and Early Life Adiposity Gain* 42
*4.3.3 Newborn Functional Connectivity to the Amygdala and Early Life Adiposity Gain* 43

**5 Results**

**5.1 Fat Quantification**
*5.1.1 Age, Sex and Breastfeeding Status: Associations with Newborn BF%, Six-month BF% and Six-month Change in BF%* 45
*5.1.2 Challenges in Visceral Adipose Tissue Segmentation and Quantification* 49
*5.1.3 Validation, Segmentation and Repeatability/Reliability of Imaging Brown Adipose Tissue (BAT)* 51

**5.2 Infant Brain Development**
*5.2.1 Maturation Index Reflects Typical Perinatal White Matter Development* 57

**5.3 Prospective Associations Between Newborn Brain MRI-Phenotypes and Early Life Adiposity Gain**
*5.3.1 Newborn Insula Volume and Early Life Adiposity Gain* 64
*5.3.2 Newborn White Matter Properties and Early Life Adiposity Gain* 68
*5.3.3 Newborn Functional Connectivity to the Amygdala and Early Life Adiposity Gain* 70

**6 Discussion**

**6.1 Fat Quantification**
*6.1.1 Gestational and Postnatal Age at Birth are Important Covariates of Non-Interest in Quantification of Six-month Change in BF%* 75
*6.1.2 MRI-Based Visceral Adipose Tissue Quantification Is Questionable* 76
*6.1.3 Brown Adipose Tissue (BAT) Composition Quantification Using MRI is Reliable and Repeatable* 77

**6.2 Infant Brain Development**
*6.2.1 Maturation Index Reflects Typical Perinatal White Matter Development* 81

**6.3 Prospective Associations Between Newborn Brain MRI-Phenotypes and Early Life Adiposity Gain**
*6.3.1 Newborn Insula Volume is Prospectively Associated with Early Life Adiposity Gain* 87
*6.3.2 Newborn White Matter Microstructure Proximal to the Amygdala and Thalamus are Prospectively Associated with Early Life Adiposity Gain* 91
*6.3.3 Newborn Amygdala Functional Connectivity to the Insula, Thalamus and Putamen are Prospectively Associated with Early Life Adiposity Gain* 92

**7 Conclusion/Summary** 95

**References** 97

# List of Figures


| | | Page |
|---|---|---|
| Figure 3.1.3 | Cartoon Representation of Hormonal Signaling. | 10 |
| Figure 3.2.1 | Example Tissue Contrast in a Single Participant Near Birth and at One Year of Age. | 12 |
| Figure 4.1.1a | Schematic of DXA acquisition and calculations. | 23 |
| Figure 4.1.1b | Early Life Growth Variable Definition. | 24 |
| Figure 4.1.2a | Relaxation Curves for Kidney, Fat and Muscle. | 26 |
| Figure 4.1.2b | Pipeline for Visceral Fat Segmentation. | 27 |
| Figure 5.1.1a | K-means Clustering of Feeding Status. | 46 |
| Figure 5.1.1b | Newborn Age-correction of Global Body Fat Percentage (BF%). | 47 |
| Figure 5.1.1c | Six-month Age-correction of Global Body Fat Percentage (BF%). | 48 |
| Figure 5.1.1d | Inter-individual Variability in Body Fat Percentage Change in Early Life. | 48 |
| Figure 5.1.2a | Example Regions Manually Sub-classified. | 49 |
| Figure 5.1.2.b | MRI-Based Subcutaneous Fat Mass and DXA-Based Body Fat Percentage. | 50 |
| Figure 5.1.3a | Fat Fraction in Rodent. | 52 |
| Figure 5.1.3b | Fat Fraction In Three Planes. | 53 |
| Figure 5.1.3c | Neonatal Segmentations. | 53 |
| Figure 5.1.3d | Acquisition Repeatability. | 55 |
| Figure 5.1.3e | Voxelwise Repeatability. | 55 |
| Figure 5.1.3f | Segmentation Reliability. | 56 |
| Figure 5.2.1a | Splitting Postmenstrual Age (PM) into Gestational Age (GA) and Age at Scan (SA). | 58 |
| Figure 5.2.1b | Explanatory Power Increase as a Function of Maturation Index. | 59 |

| | | |
|---|---|---|
| Figure 5.2.1c | Cumulative Distribution Function of $MI_{FA}$, $MI_{RD}$, and $MI_{AD}$. | 60 |
| Figure 5.1.2d | Whole Brain Maturation Index Map. | 60 |
| Figure 5.2.1e | Detailed Features Along the Left Premotor Tract. | 63 |
| Figure 5.3.1a | Insula Gray Matter Volume Predicts Adiposity Change in the First Six Months of Life. | 65 |
| Figure 5.3.1b | Receiver Operating Characteristic Curve. | 66 |
| Figure 5.3.1c | Sub-parcellation of the Insula Suggests a Central-Posterior Pattern of Association between Insula GM Volume and Infant Adiposity. | 67 |
| Figure 5.3.2a | Tract-Based Statistics of Association Between DTI Diffusion Properties and Gestational Age at Birth, Postnatal Age at Scan, and Early Life Fat Gain in the Left Fornix. | 68 |
| Figure 5.3.2b | Tract-Based Statistics of Association Between DTI Diffusion Properties and Gestational Age at Birth, Postnatal Age at Scan, and Early Life Fat Gain in the Gustatory Pathway. | 69 |
| Figure 5.3.3a | Whole Brain Amygdala Connectivity Map. | 70 |
| Figure 5.3.3b | Whole Brain Left Amygdala Connectivity Associations with Gestational Age at Birth. | 71 |
| Figure 5.3.3c | Whole Brain Amygdala Connectivity Associations with Early Life Fat Gain. | 72 |
| Figure 5.3.3d | Graph Representation of Feeding-Relevant Functional Connections Modified by Gestational Age at Birth. | 73 |
| Figure 5.3.3e | Graph Representation of Feeding-Relevant Functional Connections Prospectively Associated with Early Life Fat Gain. | 73 |
| Figure 6.2.1 | The sign of $MI_{RD}$ Predicts $MI_{AD}$ and $MI_{FA}$. | 84 |

# List of Tables


| | | Page |
|---|---|---|
| Table 5.1.2 | Absolute and Relative Fat Compartment Size in the Newborn. | 50 |
| Table 5.1.3a | Summary of Brown Adipose Tissue Depot Volume and Fat Fraction. | 54 |
| Table 5.1.3b | Inter- and Intra-rater Reliability Results. | 56 |
| Table 5.2.1a | Interquartile Values of $MI_{FA}$, $MI_{RD}$ and $MI_{AD}$ by Fiber Group. | 61 |
| Table 5.1.2b | Estimated Rates of Change for, and Coordinates of, Significant Clusters of *Positive* $MI_{RD}$. | 62 |
| Table 5.1.2c | Estimated Rates of Change for, and Coordinates of, Significant Clusters of *Negative* $MI_{RD}$. | 62 |

# Acknowledgments

I would like to express profound appreciation for my committee chair, Professor Frithjof Kruggel, who has provided unwavering support throughout my endeavors. His knowledge and guidance has made this work possible.

The following individuals have also made significant academic and/or inspirational contributions towards the completion of this dissertation: Claudia Buss, Sonja Entringer, Steven Potkin, and Liv McMillan.

To my parents, who have provided, unendingly, on every level throughout the years, thank you.

Finally, for my wife who has taken every arduous step along this journey always at my side, thank you. We did it. Jude, Anders and Oliver: follow your own path but let your mother be your template for love, devotion, intelligence and humor.

Financial support was provided by NIH grants R01 MH091351 to Claudia Buss and Pathik D. Wadhwa, R01 HD-065825 to Sonja Entringer and Pathik D. Wadhwa, R01 HD-060628 to Pathik D. Wadhwa, and UCI Institute for Clinical and Translational Science (CTSA grant) UL1 TR000153.

# Curriculum Vitae

## Jerod Michael Rasmussen

2002-04 Undergraduate Researcher in Machine Learning at Sextant Engineering

2004 B.S. in Physics, University of California, Irvine

2007 M.S. in Physics, University of Cincinnati

2007-09 Research Assistant, Pediatric Brain Imaging, Cincinnati Children's Hospital

2009-14 Research Assistant, Biomedical Informatics Research Network, University of California, Irvine

2014-16 Research Assistant, Development, Health and Disease Research Program, University of California, Irvine

2015 M.S. in Biomedical Engineering, University of California, Irvine

2016 Ph.D. in Biomedical Engineering, University of California, Irvine

### FIELD OF STUDY

Neurobiological underpinnings of infant, childhood and adult obesity.

### SELECTED PUBLICATIONS


1. Hibar, DP., …, **Rasmussen J.,** …., ENIGMA Consortium. (2016). Subcortical Volumetric Abnormalities in Bipolar Disorder. *Molecular Psychiatry*, doi: 10.1038/mp.2015.227.
2. Graham, A. M., Buss, C., **Rasmussen, J**. M., Rudolph, M. D., Demeter, D. V., Gilmore, J. H., ... & Fair, D. A. (2015). Implications of newborn amygdala connectivity for fear and cognitive development at 6-months-of-age. *Developmental Cognitive Neuroscience*.
3. **Rasmussen J.,** Casey BJ, van Erp T., Tamm L., Epstein J., Buss C., Bjork J., Molina B., Velanova K., Mathalon D., Somerville L., Swanson J., Wigal T., Arnold L., Potkin S., MTA Neuroimaging Group (2015). ADHD and Cannabis Use in Young Adults Examined Using fMRI of a Go/NoGo Task. Brain Imaging and Behavior. 1-11.
4. Lee, K., …, ; **Rasmussen, J**., …, Styner, M.. (2015). Early postnatal myelin content estimate of white matter via T1/T2w ratio. *SPIE Medical Imaging.* doi: 10.1117/12.2082198.
5. **Rasmussen, J**., Entringer, S., Nguyen, A., Van Erp, T., Guijarro, A., Oveisi, F., Swanson, J., Piomelli, D., Wadhwa, P., Buss, C., Potkin, S.. (2013). Brown adipose tissue quantification in

human neonates using water-fat separated MRI. *PLOS ONE*. Provisionally Accepted July 2013.

6. Guffanti, G., Torri, F., **Rasmussen, J**., Clark, A., Lakatos, A., Turner, J., Fallon, J., Saykin, A., Weiner, M., Vawter, M., Knowles, J., Potkin, S., Macciardi, F.. (2013). Increased CNV-Region deletions in mild cognitive impairment (MCI) and Alzheimer's disease (AD) subjects in the ADNI sample. *Genomics*, 102(20, 112-122.
7. Stein, J., …, **Rasmussen J.,** …., ENIGMA Consortium. (2012). Identification of common variants associated with human hippocampal volumes and intracranial volumes. *Nature Genetics*, 44, 552-561.
8. Glover G., …, **Rasmussen J**., …, Potkin, S., FBIRN Consortium. (2012). Functional Biomedical Informatics Research Network recommendations for multi-center functional Magnetic Resonance Imaging Studies. *JMRI*, 38(1), 39-54.
9. **Rasmussen, J**., Lakatos, A., van Erp, T., Kruggel, F., Keator, D., Fallon, J., Macciardi, F., Potkin, S., ADNI Consortium. (2012). Empirical derivation of the reference region for computing diagnostic sensitive 18-FDG ratios in Alzheimer's disease based on the ADNI sample. Biochim Biophys Acta, 1822(2), 457-466.
10. Vannest J., **Rasmussen, J**., Eaton, K., Patel, K., Schmithorst, V., Karunanayaka, P., Plante, E., Byars, A., Holland, S. (2010). FMRI activation in language areas correlates with verb generation performance in children. *Neuropediatrics*, 41(5), 235-239.
11. Vannest., J., …, **Rasmussen, J**., …, Holland, S. (2008) Comparison of fMRI data from passive listening and active-response story processing tasks in children. JMRI, 29(4), 971-976.
12. DiFrancesco, M., **Rasmussen, J**., Yuan, W., Pratt, R., Dunn, S., Dardzinski, B., Holland, S. (2008) Comparison of SNR and CNR for in vivo mouse brain imaging at 3T and 7T using well matched scanner configurations. Medical Physics, 35(9), 3972-3978.

## FIRST AUTHOR POSTERS AND TALKS

1. Newborn Insula Volume is Prospectively Associated with Early Life Fat Gain, Poster, Flux Congress St. Louis, 2016.
2. Inhibition Network Differences Between ADHD and Healthy Adults Are Unbiased by Cannabis Use, Talk, American Academy of Adolescent and Childhood Psychology, San Antonio, 2016.
3. Longitudinal Changes In Brown Fat Composition Over the First Year of Life, Poster, NIH BAT, Workshop Bethesda 2014.
4. A Novel Maturational Index for Cross-Sectional Characterization of White Matter Ontology in Early Life. Selected talk, Flux Congress Los Angeles 2014.
5. Inhibition Network Differences Between ADHD and Healthy Adults Are Unbiased by Cannabis Use, Poster, ISMRM Salt Lake City 2013.
6. CBF Differences Between Healthy and Schizophrenic Brains, Presented, ISMRM Salt Lake City 2013.
7. Imaging Brown Adipose Tissue in Neonates Using Fat-Water Separated MRI, Poster, ISMRM Workshop Long Beach, 2012.
8. Measurement Stability in Arterial Spin Labeling Using Multiple Sites, e-Poster, ISMRM Stockholm 2010.

9. The Nintendo Wii Remote as an MR-Compatible Interface to Cognitive Studies Using fMRI, Poster, ISMRM Hawaii 2009.
10. Breath Hold Task Significantly Correlates With Cognition Across Run and Visit, Poster, ISMRM 2009.
11. High Dynamic Range Processing Improves Global Contrast, Poster, ISMRM 2009.
12. MR microscopy in studying the development of the chick inner ear, Poster, ISMRM 2009.
13. Comparison of Methods Used in Calibrated fMRI, Poster, ISMRM 2009.
14. The Relationship Between Verbal IQ and Language Lateralization in Children and Adolescents with Epilepsy. Poster 2009 International Neuropsychological Society Meeting.
15. Neural Activity in Language Areas Reflects Verb Generation Performance in Children. Poster 2008 Cognitive Neuroscience Society Annual Meeting.
16. MR Microscopy in Studying the Development of the Embryonic Chick Inner Ear. Poster 2008 Association for Research in Otolaryngology MWM.
17. Comparison of SNR and CNR for *in vivo* Mouse Brain Imaging at 3T and 7T Using Well Matched Scanner Configurations. Poster 2006 ISMRM.
18. The Use of an Ellipsoidal Basis Function in the Detection and Classification of Underwater Sea Mines. Poster/Talk 2004 UCI UROP.

## AWARDS AND HONORS

New Mexico Legislative Lottery Scholarship, Undergraduate

2014 NIH Travel Award: "Exploring the Roles of Brown Fat In Humans," Bethesda, MD. February 2014.

2016 Flux Congress Travel Award: "Newborn Insula Gray Matter Volume is Prospectively Associated with Early Life Fat Gain," St. Louis, MO. September 2016.

2016 Sugar, Stress, Environment and Weight Symposium Fellowship, San Francisco, CA. October 2016.

# Abstract

Image Based Interrogation of Brain and Body Composition Development in Newborn Humans

By

Jerod Michael Rasmussen

Doctor of Philosophy in Biomedical Engineering

University of California, Irvine, 2016

Professor Frithjof Kruggel, Chair

Storage of adipose tissue is a trait belonging to all humans, historically borne from the necessity to survive extended periods of famine. Yet, there is clear inter-individual variability in our propensity to accumulate excess fat. In addition, this variability is present as early as infancy and persists into adulthood. In adults, the regulation of energy homeostasis (balance) by the brain is evident not only through signaling provided by peripheral systems to the hypothalamus, such as fat (leptin) and the stomach (ghrelin), but also by the downstream cognition required to decide what, when and how much to eat. Magnetic Resonance Imaging has been instrumental in identifying the brain regions and circuitry involved in food-related behaviors as well as the identification of brain differences between obese and normal weight adults. It is, however, unclear whether the observed differences in brain regions and circuitry in obese relative to normal weight individuals are a cause, consequence, or both, of the obese state. Moreover, relatively little is known about the developmental ontogeny of these food-related brain regions and circuitry, particularly during the period of intrauterine development (when the postnatal obesogenic environment could not yet have affected this circuitry), and its prospective role in shaping propensity for childhood obesity. Knowledge of early life brain structure and function in the context of energy imbalance would contribute to an improved understanding of propensity for obesity, early identification of at-risk individuals, and intervention targets for primary prevention. This thesis has addressed this fundamental knowledge gap by using an imaging based approach to: 1) quantify and describe early life patterns of fat deposition, 2) shed new insights on perinatal brain development, and 3) identify prospective associations between interoceptive, reward, and gustatory properties of the newborn brain and subsequent early life fat gain.

## 2 Introduction

Obesity represents one of the most urgent national and global health challenges because of its established health risks and high prevalence(A. S. Kelly et al., 2013; McPherson, 2014; Lim et al., 2012). Childhood obesity is a particularly grave concern because obese children are substantially more likely to be obese as adults(Serdula et al., 1993; Whitaker, Wright, Pepe, Seidel, & Dietz, 1997), and to develop obesity-related diseases at earlier ages(Dabelea & Harrod, 2013; Freedman, Khan, Dietz, Srinivasan, & Berenson, 2001) and of greater severity(Doak, Visscher, & Renders, 2006; Forgat-Campagna & Narayan, 2001; Ghoorah, Campbell, & Kent, 2014). Established genetic and lifestyle risk factors currently explain only a modest proportion of the observed intra-individual variation in obesity risk(Locke, Kahali, Berndt, Justice, & Pers, 2015), thus highlighting the need for new, innovative approaches. Moreover, once established, obesity is extremely difficult to reverse(Doak et al., 2006), underscoring the critical importance of primary prevention.

**Commonly Used Abbreviations**

MRI (Magnetic Resonance Imaging)
fMRI (functional MRI)
RS-fMRI (Resting State fMRI)
DXA (Dual X-Ray Absorptiometry)
PET (Positron Emission Tomography)
PM (Postmenstrual Age)
GA (Gestational Age)
SA (Postnatal Scan Age)
ICV (Intracranial Volume)
GM (Gray Matter)
WM (White Matter)
DMN (Default Mode Network)
MI (Maturation Index)
FD (Framewise Displacement)
FA (Fractional Anisotropy)
RD (Radial Diffusivity)
AD (Axial Diffusivity)
BAT (Brown Adipose Tissue)
WAT (White Adipose Tissue)
BMI (Body Mass Index)
BF% (Body Fat Percentage)
ΔBF% (Change in Body Fat Percentage)

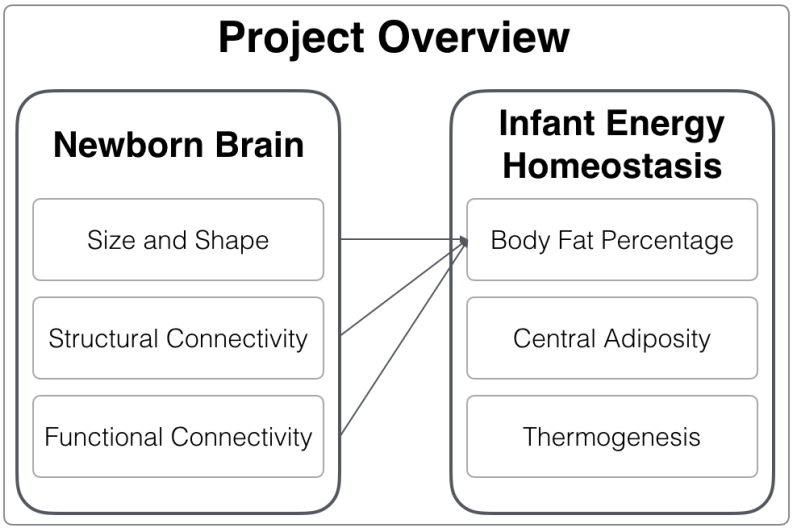
Obesity is a complex, multi-factorial phenotype(Finegood, Merth, & Rutter, 2010). Among these multiple factors, energy homeostasis and the importance of the hypothalamic-limbic-cortical brain circuits that regulate energy homeostasis is well established(Morton, Meek, & Schwartz, 2014). The anatomy and function of these brain circuits are described in adult humans and other animals, and reviewed in detail below (see Section 3.1.3). MRI-based studies have been instrumental in demonstrating altered connectivity of, and impaired GM(Pannacciulli et al., 2006; Raji et al., 2009) and WM fiber integrity(Kullmann, Schweizer, Veit, & Fritsche, 2015; Stanek, Grieve, Brickman, & Korgaonkar, 2011) in, energy homeostasis-related brain circuits in obese relative to normal-weight adults. However, very little is known about the integrity and function of such circuits in the human neonate.

The doctoral work contained here addresses this knowledge gap by observing and documenting the consequences of MRI-based measures of newborn energy homeostasis brain circuitry on infant adiposity outcomes. The following precepts guide the conceptual framework and research design contained here:

- Substantial and meaningful markers of inter-individual variation in infant adiposity exist.
- Energy homeostasis brain circuitry is established and functional by the time of birth (*i.e.*, in the newborn) and can be characterized using MRI.
- This variation is prospectively associated with markers of childhood obesity risk (*e.g.*, change in adiposity over the early postnatal period).

Therefore, the general narrative of the experimental design was to:

- Operationalize a measure of infant body composition reflective of childhood obesity risk. Sections 3.1, 4.1, 5.1 and 6.1.
- Characterize inter-individual variation in newborn homeostasis-related brain circuitry. Sections 3.2, 4.2, 5.2 and 6.2.
- Test for the prospective association between plausible biomarkers of homeostasis brain circuitry and infant body composition (and by extension, childhood obesity risk). Sections 3.3, 4.3, 5.3 and 6.3.



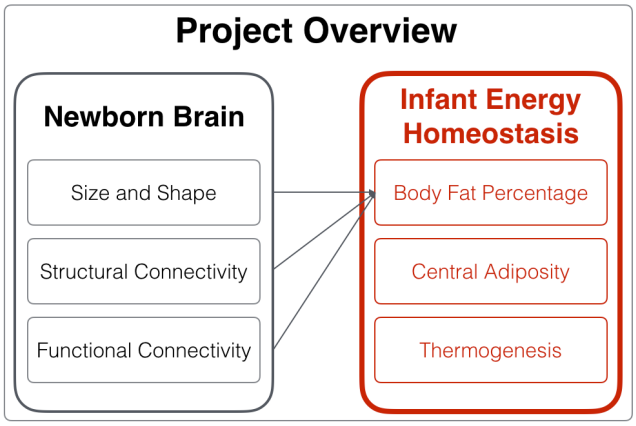

**Project Overview.** The general structure of this thesis is shown using a simple overview. Here the newborn brain (left panel, chapter sections N.1) and metabolism relevant (right panel, chapter sections N.2) measures are connected by a prospective association (black arrows, chapter sections N.3). Throughout this text, this image will be used as a guide for the reader as to the relevant sections at hand (to be highlighted in red).

In otherwise healthy adults, structural and functional measures of energy homeostasis-related brain circuits are associated with obesity. *It is, however, unclear whether these observed differences are a cause or consequence of the obese state.* Furthermore, relatively little is known about the developmental ontogeny of these brain regions and circuitry. With respect to the developmental ontogeny of this circuitry, I posit that it is particularly insightful to start at birth as this represents a developmental time point when key postnatal influences including infant feeding and dietary intake have not yet had an impact on this system. Additionally, investigating the relationship between brain structure/ function and early life weight-gain allows for a more optimally controlled experimental design relative to child or adult research, as infants are: 1) free of the cumulative postnatal exposures to neuroinflammation associated with excess weight(Miller & Spencer, 2014), 2) not exposed to day to day stresses of modern life that may play into food choices(Dallman, Pecoraro, & la Fleur, 2005; Dallman, Pecoraro, & Akana, 2003; Oliver, Wardle, & Gibson, 2000), 3) less confounded by behavioral inhibition differences related to food choice(Guerrieri, Nederkoorn, & Jansen, 2008; Guerrieri, Nederkoorn, Stankiewicz, & Alberts, 2007; Nederkoorn, Braet, Van Eijs, & Tanghe, 2006), 4) not susceptible to the effects of food advertising(A. S. Bruce, Bruce, & Black, 2014; Lobstein & Dibb, 2005), 5) naïve to anti-psychotic prescriptions associated with weight gain(Allison, Mentore, & Heo, 1999), 6) in a relatively standardized physical activity environment(Gordon-Larsen, Nelson, Page, & Popkin, 2006), and 7) devoid of the social stigmas and pressures associated with feeding and body image(Puhl & Heuer, 2010; Puhl & Latner, 2007). Certainly, as any new parent can attest to, the main priority of a newborn is to procure the food resources necessary for rapid and expansive growth in both fat stores and brain structures. Therefore, linking neurophenotypes of the newborn brain to indicators of childhood obesity risk (such as early postnatal adiposity gain) provides the opportunity to identify alterations of this circuitry at birth that *precede* the outcome and contribute towards an understanding of the temporality of effects independent of the confounding obesogenic factors present in later life.

## 3 Background

The primary objective of this thesis is to demonstrate prospective associations between newborn homeostasis brain circuitry and early life fat deposition. In this chapter, I first provide the relevant material pertaining to body composition including aspects of thermogenesis, a life preserving mechanism in infants with profound metabolic significance. Second, I describe aspects of normative brain development as well as provide an introduction to the nuances of regressing out age effects in the rapidly developing newborn brain. Third, a discussion covering the majority of existing MR-based characterizations of the obese adult brain including aspects of brain morphology, structural connectivity and functional connectivity is given.

### 3.1 Body Composition




The three measures of infant adiposity discussed in this thesis were motivated by their relevance to early life adiposity, metabolism, and later life obesity outcomes. First, infant BF% is a direct gold-standard measure for body composition and a proven risk factor for childhood obesity. Second, central adiposity (i.e. visceral fat) is metabolically distinct from subcutaneous fat deposits and increasingly recognized as being of metabolic importance. Third, BAT is known to be metabolically active and ubiquitous in the newborn infant.

The rationale for newborn brain systems as a predictor of infant adiposity is established in the following sections.

#### *3.1.1 Energy Homeostasis, White/Brown Fat, Adiposity/BMI, and Obesity Outcomes Related to Early Life Adiposity*

Energy homeostasis is the biological manifestation of the law of the conservation of energy. Simply put, intake energy will either be consumed by biological processes or stored in the form of fat. The Basal Metabolic Rate (BMR) is a summary measure of energy expenditure that, void of activity, makes up roughly 70% of Total Energy Expenditure (TEE) and is dominated by processes in the lean mass tissue of an individual. Roughly two-thirds of human BMR variability is due to fat-free mass contribution with another 8% contributed by fat mass and age differences combined, leaving over 25% of variation between individuals unexplained(Johnstone, Murison, Duncan, Rance, & Speakman, 2005). Because BMR is so dependent on lean tissue mass it can be estimated on height, mass, sex and age alone(Mifflin et al., 1990). The other two components of TEE, thermogenesis and activity, contribute roughly 10% and 20% respectively to adult TEE(McArdle, Katch, & Katch, 2010). Dietary induced thermogenesis is largely nutrition dependent as the energy required to digest, absorb and distribute proteins is greater than that required to process carbohydrates, for example. Activity dependent energy expenditure is generally expressed as a ratio of TEE over 24 hours to BMR. Those that are highly active may have a more than 50% increase in this ratio relative to those that are considered sedentary(Alfonzo-González, Doucet, Alméras, Bouchard, & Tremblay, 2004).

Energetic imbalance occurs when caloric intake either exceeds or falls short of TEE and results in a weight increase or decrease respectively. In the case of excess, the body will store energy in adipose tissue for retrieval in times of need. The tissue composed of large uni-locular adipocytes that store this energy is termed WAT. Under energetic stress, WAT will supply energy in the form of fatty acids and glycerol. In contrast to WAT, BAT (popularly called the “good fat”), is perhaps best known as a life-preserving source of non-shivering thermogenesis in neonates. At birth, humans do not possess the ability to shiver and due to a large volume to surface ratio rapidly exchange heat with their environment. BAT, via the uncoupling protein 1 (UCP1), is able to rapidly convert lipid stores into heat. Until recently, it was thought that BAT was not present after early childhood. However, PET studies have demonstrated glucose uptake in supraclavicular regions in adults under cold exposure(Cypess et al., 2009; van Marken Lichtenbelt et al., 2009). More recent studies have demonstrated the presence of active BAT in other regions including interscapular(Lidell et al., 2013), axillary and parathoracic(Rasmussen et al., 2013) using

MRI. *Because BAT is so active and ubiquitous in the neonate it becomes imperative to consider its contribution when discussing energetic imbalance in early life.*

Characterizing the weight gain resulting from excess intake relative to expenditure can be done in multiple ways. Two global approaches to fatness are BMI and BF%. While the two are inherently related to each other, as much as 50% of variance in measures of body fat percentage by DXA is unexplained by BMI(Flegal et al., 2009). Furthermore, disparities in ethnic differences between BMI-BF relationships exist as Asian populations have been shown to have disproportionately high body fat relative to BMI when compared to western populations(Deurenberg-Yap & Schmidt, 2000). *It is necessary to also address not just how much fat is present but where such fat is present.*

WAT can be loosely subdivided into subcutaneous and visceral tissue, each having it's own unique metabolic profile. Excess visceral fat is considered to be a risk factor for metabolic syndrome(Matsuzawa, Funahashi, & Nakamura, 2011) and cardiovascular disease independent of BMI(Donahue, Bloom, Abbott, Reed, & Yano, 1987). While central adiposity can be loosely characterized by waist circumference, it fails to account for differences in subcutaneous fat layers. Alternatively, DXA is able to quantify visceral fat(Kaul, Rothney, Peters, & Wacker, 2012), yet it can not subdivide the compartment into organ specific depots like perirenal and omental, whose activity is differential to that in subcutaneous compartments(Hube et al., 1996). Whole body MRI is the current gold standard for tissue specific quantification of fat deposition in the research environment(Brennan, Whelan, & Robinson, 2005; Engelson, Kotler, Tan, & Agin, 1999; Kullberg, Brandberg, Angelhed, & Frimmel, 2014) due to it's high spatial resolution.

The links between obesity in later life and adverse metabolic outcomes as well as risk for cardiovascular disease are well established. Developmentally, one of the greatest periods of susceptibility to future adult obesity is adolescence. It is therefore imperative to consider the predictive value of obesity in infancy to both that of adolescence and adult BMI. One systematic review suggested that an excessive rate of fat accrual in infancy leads to increased levels of central adiposity and insulin resistance(Ong & Loos, 2006). Of 16 papers reviewed, all had significantly positive associations between infant obesity and later obesity status (range 4-32 years old) with a total odds-ratio of 1.84 when accounting for parental size and 2.76 when not adjusting for parental size. A second review looked at 18

studies, 16 of which identified an increased likelihood of later obesity when the infants were at the high end of the weight distribution(Baird, Fisher, Lucas, Kleijnen, & Roberts, 2005). The studies reviewed showed an odds-ratio ranging from 1.35(P. O. A. Monteiro, Victora, Barros, & Monteiro, 2003) to 9.38(Poskitt & Cole, 1977) for later life obesity when comparing obese infants to those who were considered non-obese.

### *3.1.2 Autonomic Control of Energy Homeostasis*

The majority of genes associated with obesity are thought to affect food intake as opposed to energy expenditure(Farooqi & O'Rahilly, 2006). It is believed that "thrifty" genes were preferentially selected during a time in which food was scarce, giving a natural advantage to those who had a regulatory system efficient in finding, utilizing and storing energy. Such regulatory systems are still in place in modern environments; yet now represent a disadvantage in food abundant societies. The lower-level homeostatic regulatory system is largely autonomic and functions through the hypothalamus. The arcuate nucleus of the hypothalamus receives signaling from the two main hunger-related hormones: leptin and ghrelin. Leptin originates from adipose cells throughout the body increasing energy expenditure, acting as a satiety signal and reducing hunger(Frederich et al., 1995). Leptin is highly correlated with BMI in overweight and obese humans(Daghestani, Ozand, Al-Himadi, & Al-Odaib, 2007) and sensitivity to leptin signaling is reduced in obese populations(Pan, Guo, & Su, 2014). Ghrelin acts in opposition to leptin and originates in ghrelin cells in the gastrointestinal tract. As the stomach contracts/expands, ghrelin signaling is increased/decreased. Increased ghrelin signaling to the arcuate nucleus of the hypothalamus increases hunger(Malenka, Nestler, Hyman, Sydor, & Brown, 2009). Both leptin and ghrelin also mediate the ventral tagmentum area, a region with strong implications in the reward network as part of the mesolimbic dopaminergic pathway(Simerly, 2006). Finally, Neuropeptide (NPY) is also a key mediator in food intake and is produced, among other locations, in the hypothalamus. Food intake has been shown to increase in rodents with injections of dexamethasone, an NPY agonist, into the third ventricle(Hanson & Dallman, 1995). In addition, NPY acts directly on adipose tissue, mediating stress-induced obesity as stress up-regulates NPY in a glucocorticoid dependent

manner in visceral fat. This in turn leads to the proliferation and differentiation of new adipocytes(Kuo et al., 2007). Together, leptin, ghrelin and NPY form a basis for autonomic control of feeding behaviors driven by internal cues of energy homeostatic status. While these mechanisms are central to feeding behaviors, the majority of structures involved in autonomic control of energy homeostasis are too small for characterization using traditional MRI as described in section (4.2.1).

### *3.1.3 Brain Control of Feeding Behavior: Reward, Salience, Satiety, and Interoception*

While leptin, ghrelin and NPY provide the internal cues for intake, there is a complex higher-order cortical network responsible for internalizing the external cues, motivating and prioritizing the procurement of food and, once satiated, re-prioritizing other advantageous behaviors. As opposed to the autonomic aspects of feeding cues present (yet plastic(Steculorum, Collden, & Coupe, 2015)) at birth, the extent to which higher order systems are relevant to the neonate is largely unknown and a focus of this work. As a basis for this discussion, the four canonical energy homeostasis related networks in adults (reward, salience, satiety and interoceptive) are briefly reviewed here.

The reward system provides motivation for behaviors indispensible to a species (i.e. eating, drinking, reproducing) by releasing dopamine in response to gustatory, visual and olfactory cues. The link between feeding and the mesolimbic dopaminergic pathway has been established through lesion studies showing decreased desire for food after experimental damage, much in the same way as narcotics(Wise & Rompré, 1989). The traditional reward network centers on projection between the ventral tagmentum area and the nucleus accumbens but includes projections between the amygdala, hippocampus, striatum, prefrontal/orbitofrontal cortex, insula, thalamus and pituitary gland(Bassareo & Di Chiara, 1999). However, reinforcement is crucial to the reward dopamine hypothesis and also includes aspect of learning, reinforcement (strengthening reward stimulus-response relationships) and priming (learned response to one stimulus from a separate, but related, stimulus), suggesting it is almost certain that other brain regions are involved(Wise, 2004). Because dopamine and the reward network play such a prominent

role in motivating food intake behaviors, it has been suggested that obesity is an affliction similar to other addictive behaviors including narcotics abuse(Volkow & Wise, 2005).

As humans have difficulty maintaining attention on more than one task at a time, the need for focusing attention on obtaining food, in proportion to the demand for food, is one that is necessary for survival. The salience network produces this increased focus on procuring food sources when the body is especially deprived of energy. The salience network is centered on bilateral orbital frontoinsular and dorsal anterior cingulate cortices(Ham, Leff, de Boissezon, Joffe, & Sharp, 2013) with connectivity to ventral tagmentum area, thalamus, hypothalamus and amygdala(Menon & Uddin, 2010; Seeley et al., 2007). Insular dysfunction in the salience network has been implicated in an array of neurocognitive disorders including frontotemporal dementia(Schroeter, Raczka, Neumann, & Cramon, 2008), autism(Di Martino et al., 2009) and schizophrenia(H. Li, Chan, McAlonan, & Gong, 2010). The salience network is also likely important for switching between internal (default mode network) and external modes (central executive network) of thought(Uddin, 2015), a property necessary in the context of feeding behaviors. Finally, it has been shown that salience network alterations predicts food intake under stressful conditions(Z. Fang et al., 2015), and aberrations in the salience network are present in obese populations(García-García et al., 2013; Kullmann et al., 2013).

Satiety is responsible for deprioritizing food procurement and allows for behaviors deprioritized in times of hunger to return to the forefront. While not a well-defined network, brain regions associated with satiety have been identified using differential functional activation(Stoeckel et al., 2008) and cerebral blood flow(Gautier et al., 2000; 2001) between lean and obese people in response to food cues. Regions implicated in these studies are also central to reward and salience networks and include: ventromedial prefrontal cortex, insula, putamen, caudate, and hippocampal formation. The default mode network in particular has been useful in understanding internal versus external task switching in response to state of caloric demand. Obese individuals in the eucaloric state have been shown to have greater default mode network connectivity than lean individuals. The suggested interpretation of this is that obese relative to lean individuals are more internally focused when hungry(Tregellas et al., 2011). However, it may be difficult in any experimental design to disentangle satiety and salience networks, as they ought to be

inversely associated with one another. That is, as satiety increases, the need for internal focus, or salience, will decrease. A schematic of these three networks and their respective functions are shown below (Figure 3.1.3).

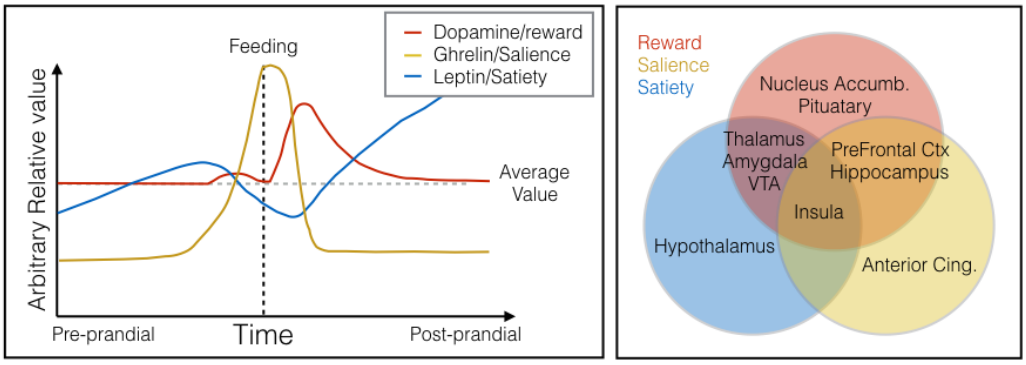



**Figure 3.1.3. Cartoon Representation of Hormonal Signaling.** Cartoon representation of hormonal signaling as it relates to feeding (left) and intersection of brain regions involved in feeding behaviors (right). Schematics re-interpreted based on Volkow et. al.(Volkow & Wise, 2005) and Cummings et. al. (Cummings et al., 2001).

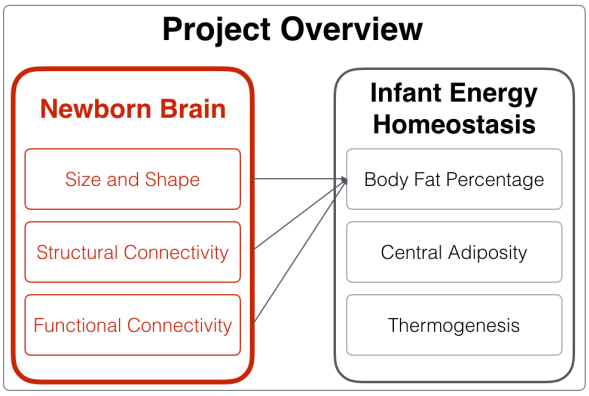
Interoception refers to the internal sensation of internal stimuli (i.e. stomach extension) related to food intake control(Kanoski & Grill, 2015). In this context, the importance of the insula is well established(Morton, Meek, & Schwartz, 2014; Simon, de Araujo, Gutierrez, & Nicolelis, 2006; Volkow, Wang, Tomasi, & Baler, 2013). The insula receives visceral afferent projections along the gustatory pathway. It has been suggested that the mid-insula serves as a modulator of feeding behaviors by integrating metabolic and visceral sensory information(de Araujo, Geha, & Small, 2012), ultimately as a means of homeostasis. In support of this, Avery et al. have identified anatomical overlay between gustatory and interoceptive networks in the mid-insula(Avery et al., 2015). Pre-surgical electrocortical stimulation in humans(Stephani, Fernandez-Baca Vaca, Maciunas, Koubeissi, & Lüders, 2010) and optogenetic manipulation of the insular cortex in rodents(Y. Peng et al., 2015) has provided direct evidence that the central insula provides gustatory sensation and that neuronal activation alone can modulate complex-feeding behaviors.

### *3.1.4 Early Life Fat Gain as an Outcome Variable*

Converging evidence suggests child size and growth velocity (particularly during the period of early infancy) represent among the most reliable, valid, and strongest predictors

of childhood obesity risk. Increased size or rapid weight or fat gain during this phase is associated with increased infant cardiovascular risk factors(McCloskey et al., 2016), increased childhood (and adult) obesity risk(Baird, Fisher, Lucas, Kleijnen, & Roberts, 2005; Druet et al., 2012; Koontz, Gunzler, Presley, & Catalano, 2014; Kruithof, Gishti, Hofman, Gaillard, & Jaddoe, 2016; Monteiro & Victora, 2005; Ong & Loos, 2006; Stettler, Kumanyika, Katz, Zemel, & Stallings, 2003) and related outcomes including type 1 diabetes(Magnus et al., 2015), metabolic disorders(Ekelund et al., 2007), hypertension(Huxley, Shiell, & Law, 2000), and asthma(Sonnenschein-van der Voort et al., 2014) in later life. A recent study reported that change in infant fat mass during early infancy was a much stronger predictor of childhood obesity risk than weight gain alone(Koontz et al., 2014). These findings support the critical importance of longitudinal assessments of body composition particularly during the period of early infancy and the validity of their use as outcomes in the context of the current work. It is for this reason that serial changes in infant adiposity, specifically from birth to six-months of age have been chosen as the operationalized outcome variable for quantifying infant adiposity.

### 3.2 Infant Brain Development




MRI-based measures of newborn brain networks are the primary predictors of obesity risk in this thesis. Below, I first provide a normative description of the rapidly developing newborn brain from the perspective of MRI phenotypes. Second, a brief discussion addressing the use of linear modeling to regress out the effects of age on the rapidly developing newborn brain is given.

#### *3.2.1 Quantifying Infant Brain Development: Structure, Connectivity and Function*

Early life development of the human brain is both rapid and complex. Most processes follow a sigmoidal trajectory described by a rapid acceleration at initiation, a period of

linear growth and finally an exponentially decreasing rate towards an asymptotic value. The first two years is especially rapid as white matter increases roughly 50% in volume and the cortex nearly triples in size(Knickmeyer, Gouttard, & Kang, 2008). Subcortical structures see similar changes in volume, increasing roughly 100% over the first year of life(Gilmore, Shi, Woolson, & Knickmeyer, 2012). Other morphometric features such as cortical thickness and gyration also see consistent patterns of rapid maturation in early life(Nie, Li, Wang, Shi, & Lin, 2014). These rapid structural changes accompany swift increases in overall cognition through early life.

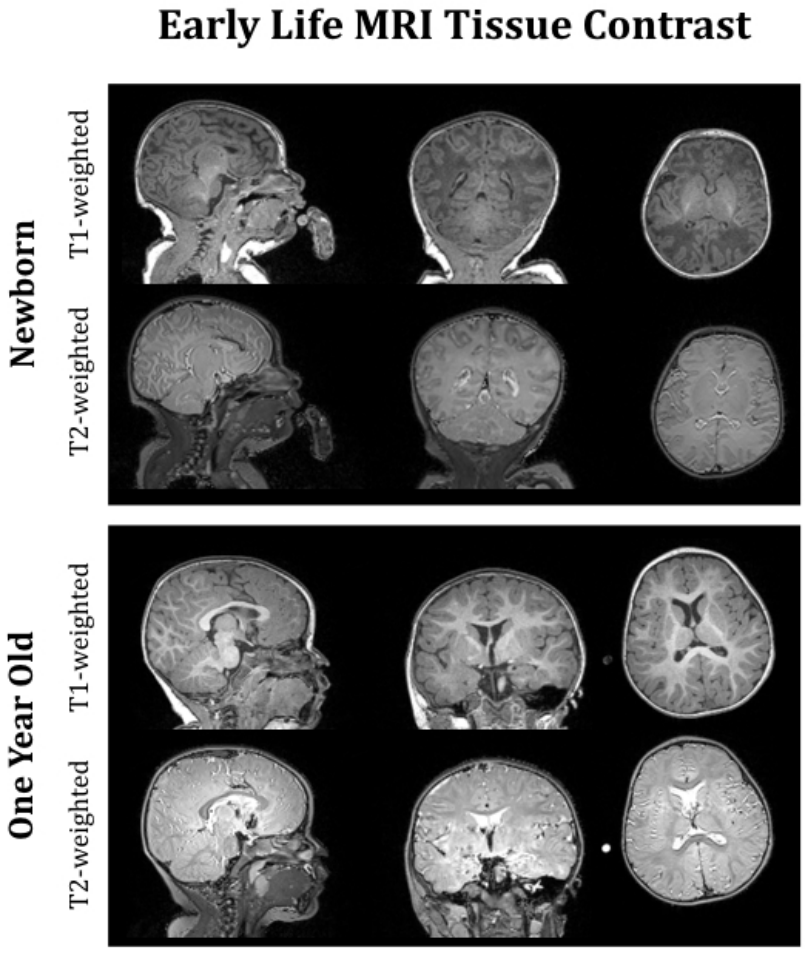



**Figure 3.2.1. Example Tissue Contrast in a Single Participant Near Birth and at One Year of Age.** Note the inversion of tissue contrast between white and gray matter tissues.

The gray-white matter contrast in the neonatal brain (Figure 3.2.1) is opposite that found in the mature adult brain. Adult T1-weighted images are typified by high signal

intensity in the white matter and low signal intensity in gray matter. In neonates, the T1-weighted gray matter appears brighter than the white matter signal. Furthermore, increased signal intensity in the periolandic cortex is present in neonates. The source of the contrast inversion is debated but it is thought that early life water retention and myelination processes(K. Lee, Cherel, & Budin, 2015) are at play. At birth, water makes up 92-95% of the brain composition and is decreased to 80-85% at two years as lipid rich myelin forms throughout(Counsell, 2002). Contrast inversion occurs at roughly 6 months of age, limiting the ability to differentiate between white and gray matter using T1 and T2-weighted acquisitions(Hazlett, Gu, & McKinstry, 2012). However, as white matter demonstrates anisotropic diffusion of water even as a fetus, alternative methods for white matter segmentation (and therefore gray matter) are available at 6 months(Oishi, Faria, & Mori, 2012). By one year of age the infant brain approaches a mature pattern of signal intensity in T1 and T2 weighted images.

The ontogeny of white matter is well described from the fetus(Huang et al. 2009; Kostović & Jovanov-Milošević, 2006), into early life(Fan et al., 2011), and beyond(Bhadelia, Price, Tedesco, Scott, & Qiu, 2009). Briefly and generally, the first trimester is dominated by neuronal proliferation, in the second trimester neural migration occurs, followed by oligodendrocyte proliferation and very limited myelination in the third trimester(Tau & Peterson, 2009). Despite the abundance of descriptive work, white matter maturation is asynchronous and complex (Dubois et al., 2008) enough that more work remains in fully understanding normative growth. The logistic model is considered to be the best theoretical descriptor of white matter growth trajectory(Deoni, Dean, O'Muircheartaigh, Dirks, & Jerskey, 2012), particularly during the years of life where changes in diffusion parameters are rapid(Gao et al., 2008). The time around birth also represents a period of non-linear growth(Ball et al., 2013) and is often characterized using studies of premature neonates scanned at birth and at term age(Partridge et al., 2004). However, it is unclear what role the factors that caused prematurity may play in both the state of maturation at birth and at term. I address this further down by considering the relative rates of change before and after birth estimated using a general linear model. This is only possible because of the strong dependence of diffusion parameters on age variables, despite the narrow range observed. At birth, most of the white matter fascicles are in place and organized.

Myelination is mostly limited to the inner capsule where the cortico-spinal fibers run through. Over the first year of life, most of the brain has begun to myelinate, albeit at different rates(Kinney, 2014) and will continue to do so until at least early adulthood. Because the pace of development is so rapid in early life, it is thought that the brain is susceptible to environmental perturbations that may be the root of future psychiatric illness(Arndt, Stodgell, & Rodier, 2005).

Multiple functional networks have been robustly detected in adults including the DMN, salience, frontoparietal, limbic, ventral attention, dorsal attention, somatomotor and visual networks(Thomas Yeo et al., 2011). Additional networks of interest to this discussion are the hypothalamic network(Kaufmann, 2006) and temporal lobe network both of which need not be exclusive to the DMN(Grecius et al., 2003). The DMN is the most oft-characterized resting state network in the brain and is thought to signify introspective thought during wakeful rest. DMN is de-activated during active thought, earning itself the label task-negative network and in competition with the task-positive network. A number of disorders have been shown to alter the DMN including schizophrenia(Garrity, Pearlson, McKiernan, & Lloyd, 2007; Pomarol-Clotet et al., 2008), bipolar disorder(Ongür et al., 2010), depression(Coutinho et al., 2015), Alzheimer's, ADHD, and as will be discussed in detail further down, obesity. Because aberrations in the DMN appear relevant to psychiatric disorders in later life, it becomes imperative to understand early life causes of DMN development and dysregulation.

Converging evidence suggests an early pattern of developmental change that can be described as a decrease in short range connectivity coupled with an increase in long range activity(Fair et al., 2008; 2009; 2007; A. M. C. Kelly et al., 2009). The period from birth to two-years of age has been found to be consistent with this pattern(Gao, Alcauter, Smith, Gilmore, & Lin, 2015; Gao et al., 2011; 2013; 2009; Homae et al., 2010), and likely logistical in nature as demonstrated by a rapid increase in network complexity and path length from birth to one-year followed by a slowing rate of increase from one to two years of age(Gao et al., 2009; 2011; 2013). Such changes in functional connectivity in early life are thought to reflect increasing network integration and segregation(Fair et al., 2007; 2009; Gao et al., 2013) concomitant with increasing richness in environmental interaction and structural changes within the brain. Because RS-fMRI (see section 3.3.3) is a measure of intrinsic

connectivity independent of external stimuli, it is thought that it allows for an assessment of higher order cognitive processing ability that may not be reliably assessed in behavioral testing of infants(Graham et al., 2015). These processes include goal driven selective and sustained attention(Corbetta, Patel, & Shulman, 2008) as found in dorsal attention networks(Gao et al., 2013) and other higher order networks probed in infancy include the salience and frontoparietal networks(Gao et al., 2015). While the use of resting state connectivity in infants is now well established, there remain a number of networks with known properties in adulthood not yet probed in neonates.

### *3.2.2 Age in Linear Models of Infant Brain Development*

Human birth presents an abrupt transition from intrauterine to extrauterine life. Profound physiological changes occur with the cessation of maternal provision, including the re-organization of the neonate's cardiovascular system and the onset of pulmonary function. Within 8 minutes of delivery, oxygen saturation levels increase from roughly 60% to over 85%(Rabi, Yee, Chen, & Singhal, 2006). From the perspective of a single cell in the neonatal brain, these are dramatic changes that, based on in vitro work, may represent a shift from a local environment that promotes oligodendrocyte proliferation to one that drives oligodendrocyte maturation(Pistollato, Chen, Schwartz, & Basso, 2007). Toda et al.(Toda et al., 2013) have demonstrated the initiation of barrel formation in the somatosensory cortex of mice through a reduction in serotonin signaling at birth. Birth also presents an abrupt increase in external sensory stimuli that may promote maturation through axonal signaling(Coman, Barbin, Charles, & Zalc, 2005). In addition, recent work has highlighted perinatal changes in physiological dehydration, skull contraction and cerebrospinal fluid reductions as possible mediators of increased gyrification in pre-term versus fetal brains matched for postmenstrual age(Lefèvre, Germanaud, Dubois, & Rousseau, 2015). Based on these dramatic changes at the time of birth, the transition from intrauterine to extrauterine life is likely to present a significant inflection point in brain maturation, including the maturation of white matter fiber tracts. In this work, we aim to identify white matter regions with significant inflection points in maturation near the time of birth and establish a metric for characterizing the relative average rates of maturation

before and after birth.

Cross-sectional Diffusion Tensor Imaging (DTI) studies aimed at describing perinatal brain maturation trajectories typically apply univariate analyses using postmenstrual age as a predictor of microstructural maturity(Hüppi et al., 1998; Oishi et al., 2011; Ou, Andres, Pivik, Cleves, & Badger, 2015; Provenzale, Isaacson, & Chen, 2012; A. Qiu et al., 2013) or using postmenstrual age while correcting for age at scan (or gestational age)(Van Kooij, De Vries, & Ball, 2012) in a linear model. In the former case, the assumption is made that growth is linear with time from conception, despite the environmental shift that occurs when the developing brain is first exposed to the postnatal environment. Using postmenstrual age as the predictor but correcting for age at scan (or gestational age) adequately adjusts for inter-individual variation in time spent *in utero*. Although this may often be an appropriate choice, this approach neglects potentially interesting information about prenatal versus postnatal developmental changes when the rate of maturation may not follow a linear trajectory from conception. It is for this reason that early stages of the thesis project focused on the appropriate modeling of age in newborn MRI regression analyses.

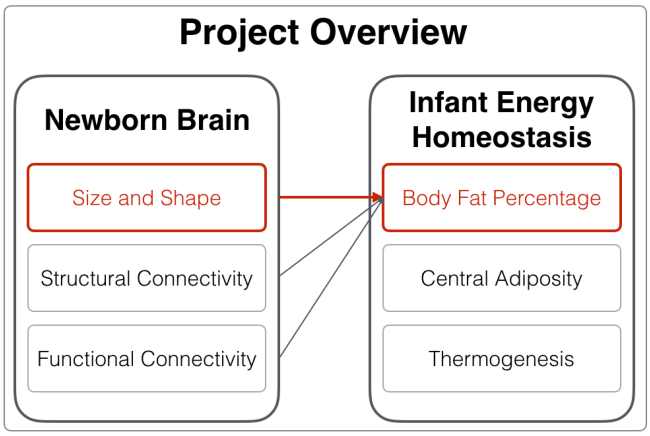
Previous work describing white matter maturation has been instrumental in describing the formation, organization and maturation of white matter in early life, yet lacks a quantitative description of maturational trajectories surrounding birth. By first separating PM into GA and SA (chronological age) for regression analysis, we examine and demonstrate the ability to describe inflection points in developmental trajectories near the time of birth. Second, using tract-based statistics we propose that the newly described MI is potentially indicative of spatially asynchronous perinatal maturation in white matter microstructure.

### 3.3 The Obese Brain: The Current State of Research in Adults and Children

In adults, structural and functional measures of energy homeostasis-related brain circuits are associated with obesity. It is, however, unclear whether these observed differences are a cause or consequence of the obese state. Furthermore, relatively little is known about the developmental ontogeny of these brain regions and circuitry. The

following sections provide the current state of research concerning associations between the obese state and brain anatomy, structural connectivity and functional connectivity.

### *3.3.1 Brain Size/Shape and Obesity*

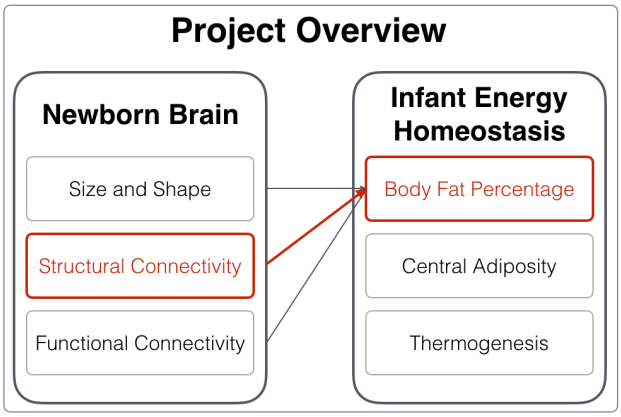



Excess weight has been associated with decreased global and regional gray matter volumes in adolescents(Alosco et al., 2014; Maayan, Hoogendoorn, Sweat, & Convit, 2011) and adults(Kurth et al., 2013; Raji et al., 2009). However, the mechanisms for, and causal direction of these findings is not clear. Gray matter volume is an indirect measure of a number of properties including: amount and size of neurons, glial cells, and dendritic processes. It is plausible that gray matter reductions in areas relevant to feeding networks (inhibition, satiety, salience and reward) are responsible for changed feeding behaviors. On the other hand, adiposity is known to be associated with neurotrophic factors such as leptin, insulin and pro-inflammatory cytokines whose influence may lead to excessive burden on the brain and subsequent neurodegeneration. Recent evidence has shown that gray matter volume differences may not even be present in young children(R. J. Sharkey, Karama, & Dagher, 2015) suggesting that alterations to gray matter are due to long term exposures to the burdens of excess adiposity. Despite this evidence, the authors concede that while the age range used captured a diverse demographic (4-18 years old) it is entirely possible that age specific effects were not captured. It has been recently established, in rodent models, that maternal obesity programs the reward system in the fetal brain in a sex dependent manner(Grissom et al., 2014). Such evidence makes it clear that the newborn is born with inter-individual variability in motivation and may explain such variation in early life feeding habits and weight gain as opposed to higher order level deficits in the frontal cortex.

As executive functioning is very limited in early life, it is likely that higher order inhibitory networks play a very minor role in the feeding habits of newborns. This suggests

that feeding behaviors will be largely driven by reward, satiety and salience networks. In contrast, interoception is a lower-level sensory function, more likely to play a central role in infant appetite and feeding. Structurally, obesity-related reductions in insula GM volume have been reported in multiple, large population-based studies(Carnell, Gibson, Benson, Ochner, & Geliebter, 2011; Janowitz et al., 2015; Kurth et al., 2012; Pannacciulli et al., 2006). More nuanced structural obesity-insula findings include negative associations between frontal operculum GM volume and blood leptin concentration(Pannacciulli, Le, Chen, Reiman, & Krakoff, 2007), positive associations between insula GM volume and aerobic capacity(Peters et al., 2009), and reduced brain metabolism coupled with insula GM atrophy in obese participants.(Jauch-Chara et al., 2016) Finally, reduced insula GM in individuals identified as obese-prone relative to those categorized as obese-resistant supports the notion that reduced insula volume is itself a risk factor for future weight gain(Smucny et al., 2012).

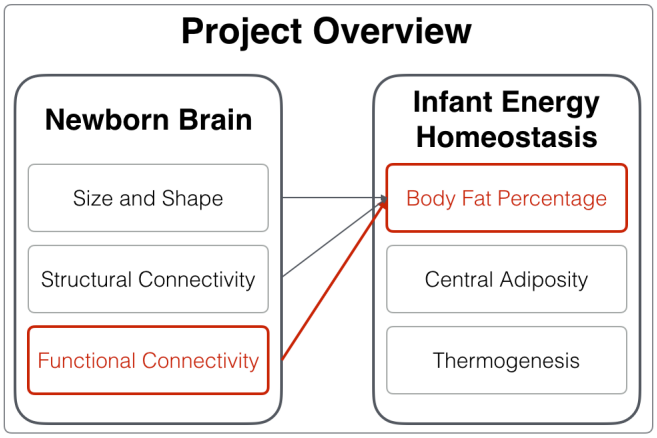
*3.3.2 Structural Brain Connectivity and Obesity*




Structural connectivity is a measure derived from the diffusion properties throughout long-range white matter fibers connecting processing nodes in the cortex. While they are often presented as measures of the efficiency in which signals travel from one processing region to another, it is likely that the measure is more nuanced due to methodological limitations(Jones, Knösche, & Turner, 2013) and the presence of short range fibers allowing for alternative pathways of information propagation. Nevertheless, DTI has been shown to be associated with a wide range of mental disorders(Ellison-Wright & Bullmore, 2009; Groen, Buitelaar, & Van Der Gaag, 2011) and reflective of developmental efficiency for visual processing in the newborn(Dubois et al., 2008). In adults, obesity is associated with reduced white matter anisotropy(Kullmann et al., 2015; Stanek et al., 2011) and volume(Karlsson et al., 2013). However, this does not

appear to be the case in children. Ou et al(Ou et al., 2015) have demonstrated increased anisotropy in a number of tracts related to food intake and suggest fatty acid presence in the extracellular space surrounding the axons as a cause. Analogous with gray matter, the leading theory of white matter degeneration in obese subjects posits that neuroinflammation from circulating inflammatory markers makes for a neurotoxic environment. However, it is likely, based on the current evidence, that this prolonged exposure is not present in children and inflammation may even be neuroprotective during the periods of development associated with rapid synaptic pruning that creates a need for cleaning up the dead cells. However, this pertains to a consequence of obesity and not to a cause of obesity, as is the focus here.

*3.3.3 Brain Function and Obesity*




Multiple overlapping networks control feeding-behaviors. The reward system drives an individual to procure sustenance through motivation. Salience causes the drive for sustenance to become a priority by de-prioritizing other functional tasks of less importance. Satiety does the opposite when food has been consumed, re-prioritizing those tasks that were attenuated during periods of hunger. Interoception provides internal cues of fullness provided by stomach sensation. All four of these networks are inter-related as they respond to internal hunger and external environmental cues. The DMN is a prominent brain network primarily recruited during wakeful rest and becomes inactive during task positive cognition. Because the DMN is considered a task negative system, it is also thought that interference from the DMN may cause task positive deficits. Overweight and obese subjects have demonstrated an array of functional connectivity deficits over a wide age range. DMN connectivity in young adults has been associated with BMI (positive association with precuneus, negative association with anterior cingulate) and insulin levels were negatively correlated with temporal lobe

connectivity (insular cortex)(Kullmann et al., 2011). The salience network has been implicated in obesity through increased connectivity to the putamen in adults aged 16 to 40 years old(García-García et al., 2013). Exercise intervention has also been shown to reduce DMN connectivity in the precuneus and was associated with greater fat mass loss, and reduced perceived hunger(McFadden, Cornier, Melanson, Bechtell, & Tregellas, 2013). Using a method to infer short-range functional connectivity, Zhang et al. demonstrated decreased connectivity in the orbitofrontal and medial prefrontal cortex and increased connectivity in the putamen of obese subjects(Zhang et al., 2015), suggesting a failure to inhibit reward circuitry. In one of only two known studies to consider hypothalamic functional connectivity, Wijngaarden et. al. observed greater connectivity in lean subjects relative to obese subjects after prolonged fasting in salience related regions(Wijngaarden et al., 2015) including the anterior cingulate cortex and greater connectivity between hypothalamus and left insula in obese subjects. The second study of hypothalamic connectivity identified greater connectivity between the orbitofrontal cortex and the medial hypothalamus(Kullmann et al., 2014). Differential insula activation in obese relative to non-obese participants when presented with food-related visual(Martin et al., 2010; Rothemund et al., 2007; Stoeckel et al., 2008) and gustatory stimuli(DelParigi, Chen, Salbe, Reiman, & Tataranni, 2005) has been widely reported and highlights the insula's functional importance in homeostasis. Functional activation of the insula has also been associated with ghrelin administration(Malik, McGlone, Bedrossian, & Dagher, 2008), stomach extension(Vandenbergh et al., 2005), and leptin replacement(Baicy et al., 2007). Finally, one recent study of obese participants who have sustained a 5-10% weight loss were scanned for DMN connectivity relative to lean participants. A decrease in DMN (posterior cingulate and parietal lobe) in the obese participants was observed as well as a strong association between the parietal cortex connectivity and appetite. Together, these results suggest altered salience, satiety, reward and interoception network connectivity between the obese and lean states.

To some degree, the amygdala is participant in each of the major energy homeostasis-relevant networks (salience(Anderson & Phelps, 2001), satiety(Yan & Scott, 1996), reward(Baxter & Murray, 2002; Murray, 2007), interoception(Knuepfer, Eismann, & Schutze, 1995)). Therefore, given its history in researching functional activation and

connectivity of the obese brain(Lips & Wijngaarden, 2014; Stoeckel, Kim, Weller, Cox, & Cook, 2009; Wijngaarden et al., 2015), the amygdala was chosen as an effective seed region to probe functional connectivity across domains in the human newborn.

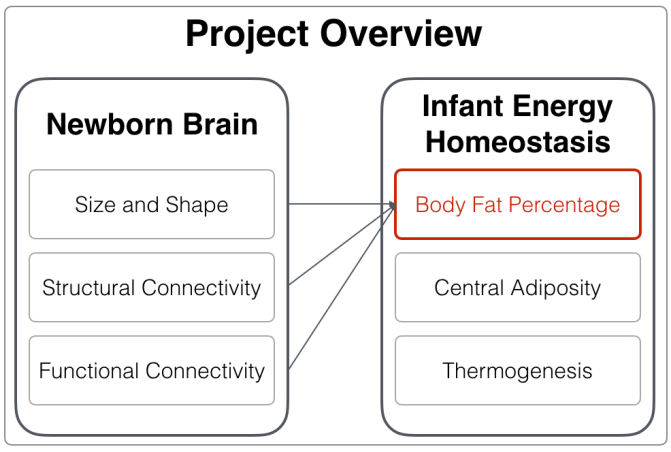
## 4 Research Design and Methods

The method and study design for elucidating the prospective association between newborn energy homeostasis relevant brain circuitry and early life fat gain is provided below. In this chapter, the material focuses on: 1) methodological issues relevant to fat quantification in the human newborn, 2) characterization of the human brain at birth, and 3) the approach used for testing the prospective associations between the newborn brain and subsequent accumulation of fat in the first six months of life.

### 4.1 Fat Quantification

The primary outcome (early life fat gain) operationalized in this project is provided below. First, I outline DXA methods for quantification of white adipose tissue (WAT) compartments and body fat percentage (BF%). Second, MRI acquisition methods and analytical approaches to segmenting visceral fat are provided. Lastly, the metabolically active Brown Adipose Tissue (BAT) and *novel* methods related to its quantification are discussed. Collectively, subcutaneous WAT, visceral WAT, and BAT comprise the major constituents of adiposity in the human infant.

#### *4.1.1 DXA: Theory, Implementation, and Considering Covariates of Non-Interest*




DXA is the gold standard for the rapid measurement of lean, bone and soft tissue mass(Laskey, 1996). In addition, DXA is considered safe due to its low dose of radiation, comparable to the amount absorbed during a commercial transatlantic flight. Compartment masses are estimated using two X-ray sources of differing energies, or frequencies, coupled with corresponding detectors. The relative amount of attenuation of the source X-rays due to Compton

scattering and optical absorption are made (R-values). Attenuation is related to the mass of scattering medium, M, and the absorption coefficient, $\mu_M$. Specifically, the R-value is the ratio of the low-energy mass attenuation to the high-energy mass attenuation. Because the R-value is linearly proportional to the fat percentage in a given sample, fat percentage can be estimated from the dual-energy attenuation in soft tissue. Furthermore, by simultaneously considering the body to be composed of two, two compartment systems (fat/fat-free mass and bone/soft-tissue mass), a three-compartment estimation is possible using only two energy sources.

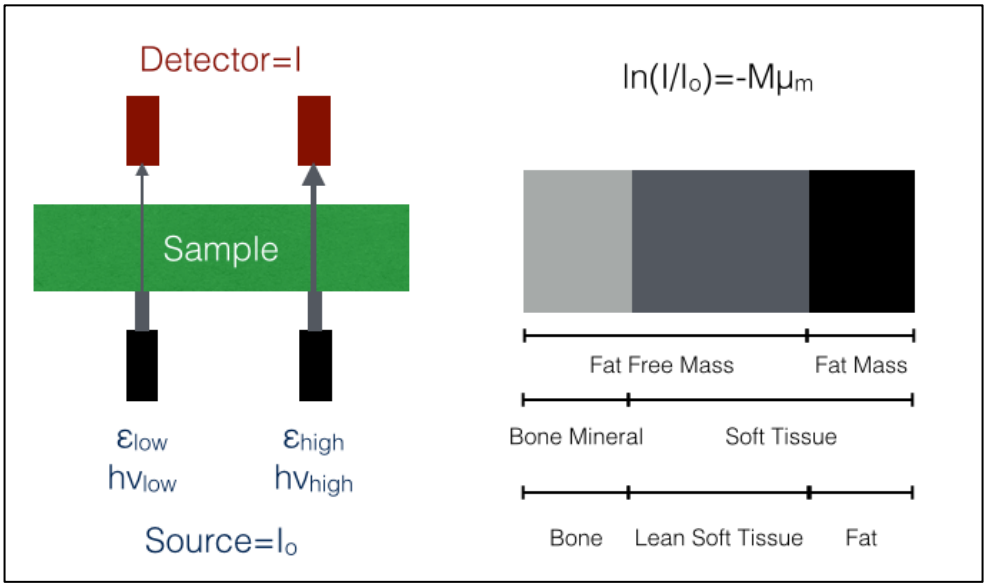



**Figure 4.1.1a. Schematic of DXA acquisition and calculations.** Detector setup for interrogating sample with dual detectors and sources (left). Simple calculation of fat mass, bone and fat free mass is possible with two sources/detectors.

Body fat percentage over the first year of life can described as a rapid accrual of fat over roughly the first six months of life followed by a normalizing period and slight decrease in adiposity after this point(Andres, Casey, Cleves, & Badger, 2013; Kulkarni, Mamidi, Balakrishna, & Radhakrishna, 2014). BMI peak can be characterized as either the age at peak, the BMI at peak or jointly. Age and maximum BMI have been associated with sex(Johnson, Choh, Lee, & Towne, 2013) and adolescent BMI(Silverwood, De Stavola, Cole, & Leon, 2009). The average peak BMI occurs at roughly 9 months and is associated with BMI in early adolescence(Hof, Vrijkotte, de Hoog, van Eijsden, & Zwinderman, 2013)

though not blood pressure. By 12 months of age BMI and adiposity is relatively stable through early adolescence(Adair, 2007).

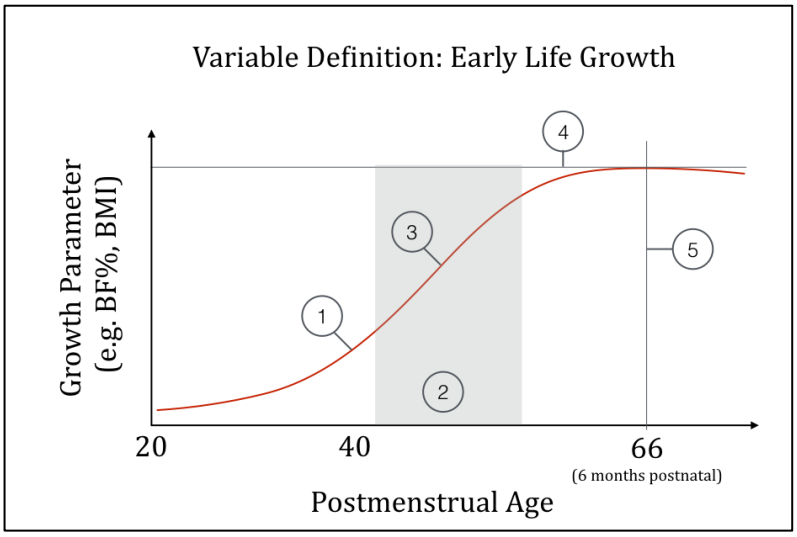



**Figure 4.1.1b. Early Life Growth Variable Definition.** 1) birth magnitude (e.g. birthweight, ponderal index), 2) period of peak gain velocity, 3) age at peak velocity, 4) peak magnitude (e.g. BMI, BF%, weight), 5) age at peak magnitude.

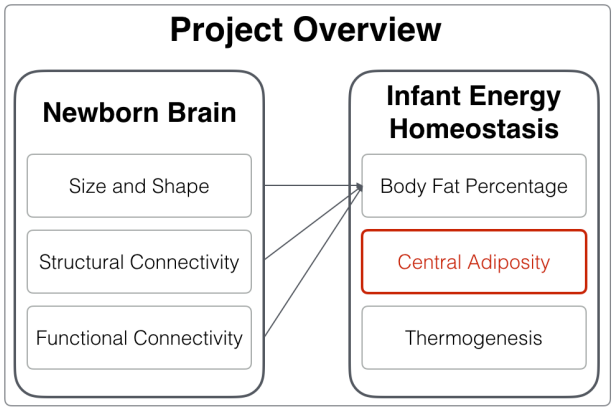
In practice, whole body DXA scans were obtained using a Hologic Discovery Scanner (A, QDR 4500 series, Hologic Inc., Bedford, MA, USA) in pediatric scan mode to define global BF%. Calibration using Hologic's anthropomorphic Spine QC Phantom was performed before each scan. During the scan, sleeping infants lay supine while swaddled in a light cotton blanket wearing only a disposable diaper. If the baby moved during the scan, a single repeat was performed once the baby had been pacified. BF% was defined as 100 times the ratio of global fat mass to the sum of global fat mass and global fat-free mass. Initial analyses exploring the relationships between BF% and gestational age at birth, postnatal age at scan, sex, and feeding practices determined demographic dependencies and identified an optimal model for residualization of the BF% outcome variable (see results 5.1.1). BF% was residualized for gestational age at birth and postnatal age at scan. The longitudinal ΔBF% was then defined as the change between newborn and six-month time points.

Breastfeeding status was defined using a monthly maternal report of categorical feeding (exclusively breastfed, exclusively formula fed, mixed feeding). Breastfeeding

status categorization used a k-means clustering algorithm to define 3 groups based on monthly reports. Gestational age was determined by best obstetric estimate with a combination of last menstrual period and early uterine size, and was confirmed by obstetric ultrasonographic biometry before 15 weeks using standard clinical criteria(O'Brien, Queenan, & Campbell, 1981). Postnatal age at scan was defined as the number of days elapsed since birth on the day of scan. Sex was treated as a categorical variable.

Linear regression was used to assess the contribution of these categorical variables and consider the validity of a priori correction. The newborn BF% model did not consider breastfeeding status due to its limited and variable exposure times given the distribution of postnatal scan ages. Therefore, the newborn model considered the following predictors of newborn BF%: gestational age at birth, postnatal age at scan, and infant sex. The six-month model considered: gestational age at birth, postnatal age at scan, breastfeeding status and infant sex. A third model considered the age-corrected change in BF% from birth to six-months as the outcome and breastfeeding status and sex as categorical predictors.

### *4.1.2 Central Adiposity: MRI Acquisition and Segmentation*




WAT is distributed throughout the body acting as an energy reserve when excess caloric intake coupled with low energy expenditure results in the accumulation of fat. Childhood obesity is relevant for assessing risk of obesity in later life and may lead to lower quality of life(Reilly, Methven, & McDowell, 2003) and reduced lifespan(Zeller & Modi, 2006). Because intra-abdominal fat is highly predictive of such adverse consequences(Y.-C. Hwang et al., 2015; Seidell, Björntorp, Sjöström, & Kvist, 1990), central body composition was considered in detail.

T1-weighted spin-echo sequence imaging has been used to image whole body adiposity in the neonate in previous studies(N. Modi et al., 2009). The signal originating from fat

comes from the aliphatic chains (-$CH_2$-) in fatty acids. These freely rotating chains create magnetic field fluctuations that result in short T1 times, or quick longitudinal magnetization recovery. The short T1 times mean that adequate signal contrast can be achieved simply by choosing a short TR, making fat hyper-intense relative to other signal contributions (Figure 4.1.2a).

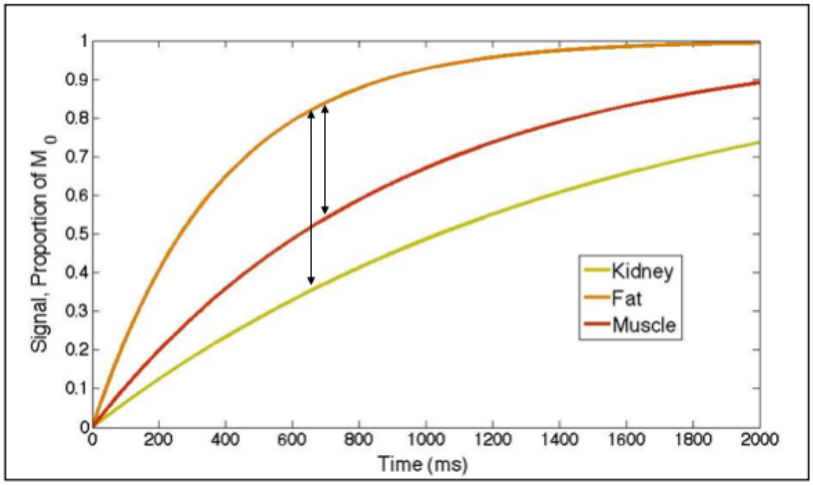



**Figure 4.1.2a. Relaxation Curves for Kidney, Fat and Muscle.** Longitudinal relaxation curves can help determine ideal repetition time for hyper-intense fat signal and tissue contrast.

The signal contrast generated from T1-weighted imaging with short TR results in hyper-intense signal from fat and moderate signal from other tissues partially based on their respective water densities. The quantification of fat then becomes a problem of identifying fat based signal intensities in a multivariate distribution. While conceptually straightforward, the lack of homogeneity from the RF excitation results in local variations in signal intensity. A novel semi-automatic processing pipeline was designed and implemented with the aim of addressing the following challenges: 1) standardized definition of "torso", 2) minimizing motion artifact, 3) correcting RF inhomogoneity artifact, 4) identification of voxels belonging to a "fat" class, and 5) sub-classification of specific fat compartments. Because fat segmentations are typically given in absolute terms (i.e. grams), a standardized definition of the torso is required for inter-subject comparison. For this project, the volume of interest was manually identified as the most inferior slice containing the diaphragm and the most superior slice containing the sigmoid process. Signal

intensities exterior to the torso were masked out using a slice-based automatic k-means (3 class) segmentation to roughly identify the torso for B1 correction. RF inhomogeneity and tissue classification/segmentation were addressed in parallel using a Hidden Markov Random Field – Expectation Maximization framework(Y. Zhang, Brady, & Smith, 2001) implemented in FSL FAST. Three tissue classes were identified containing: 1) fat hyper-intense in signal, 2) moderate and low signal intensities corresponding to non-fat tissues, and 3) background noise. Finally, a manual based sub-classification was applied to the fat tissue classes to identify the key compartments with appreciable fat signal. The manual sub-classification was performed using ITK-SNAP(Yushkevich et al., 2006). In sum, the pipeline yields fat compartment volumes for subcutaneous fat, deep subcutaneous fat, paraspinal fat, retroperineal fat, signal hyper-intense stomach and visceral fat.

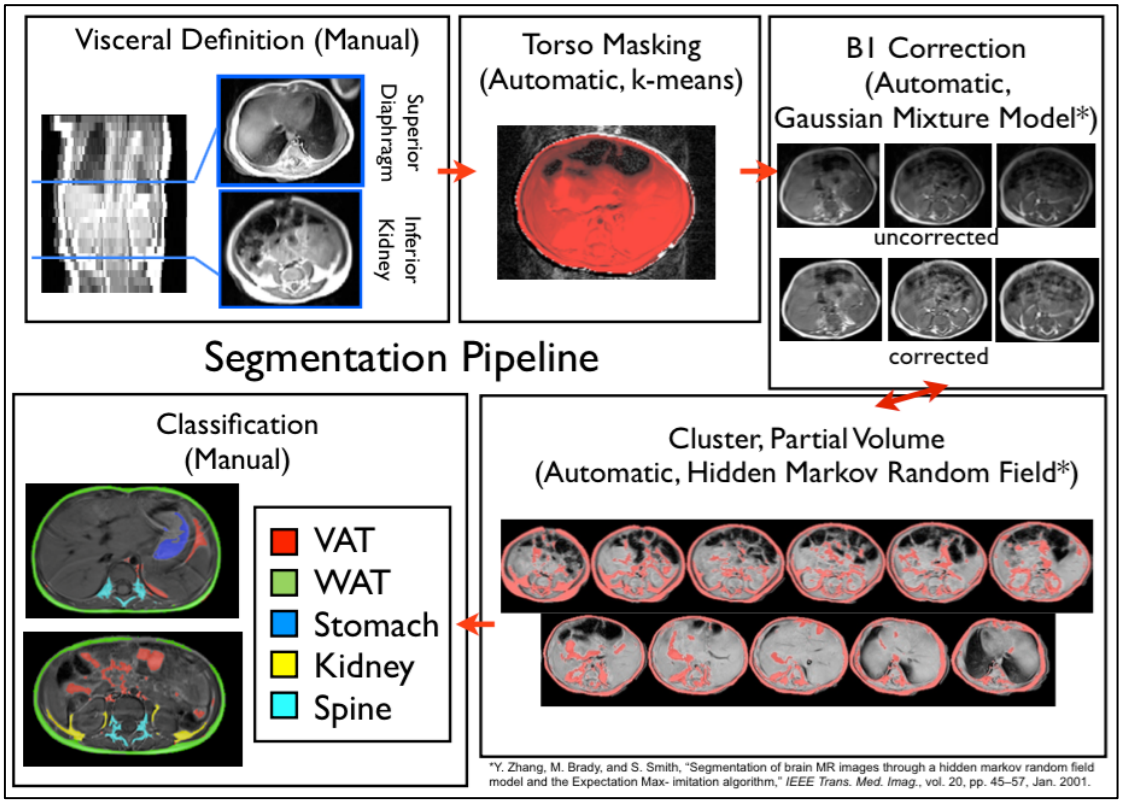
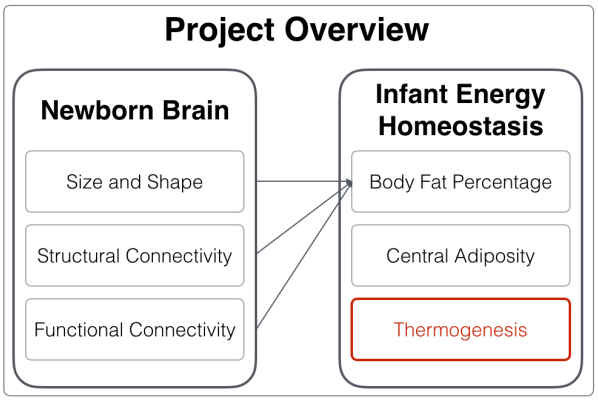



**Figure 4.1.2b. Pipeline for Visceral Fat Segmentation.** Clockwise from top left: definition of the trunk, background removal, intensity heterogeneity normalization, clustering segmentation and sub-classification.

*4.1.3 Brown Adipose Tissue: MRI Acquisition, Segmentation, Validation and Estimates of Repeatability/Reliability*




Fat protons resonate at a frequency 3.5 parts per million higher than water, enabling BAT to be spectroscopically(Hamilton, Smith, Bydder, Nayak, & Hu, 2011) differentiated from WAT. Multi-echo water-fat MRI takes advantage of the frequency difference, or chemical shift, by observing the contributions of differing phase on the overall signal(Glover, 1991; Ma, 2008; Y. Wang, Li, Haacke, & Brown, 1998). Multi-echo water-fat MRI has localized rodent interscapular BAT (iBAT)(Hu, Hines, Smith, & Reeder, 2012b; X. G. Peng, Ju, Fang, & Wang, 2013) and demonstrated increased water content between *in vivo* and *post mortem* states(Lunati et al., 1999). Rodent BAT volume quantification, derived from T2-weighted imaging with and without fat suppression, has further validated associations between iBAT and total weight(Y. I. Chen et al., 2012) and between fat fraction and total weight(Hu, Smith, Nayak, Goran, & Nagy, 2009). Collectively, these studies demonstrate that rodent BAT has an MR signature unique from WAT.

In direct opposition to its white counterpart, BAT is energy consuming via thermogenesis. During thermogenesis, the free flow of protons across the mitochondrial inner membrane results in a dissipation of heat. This metabolic process requires a capillary density capable of providing fuel in the form of glucose. It is the structural difference (namely capillary density) that allows for a signal contrast to differentiate between white and brown fat. That is, brown fat will have a signal that is a mixture of water and fat, whereas white fat signal will be fat dominated. This property is commonly expressed as a fat fraction (the ratio of fat signal to the sum of fat and water). The assessment of BAT via MRI then comes down to the problem of separating fat and water based signals.

Fatty acid chains cause localized chemical shifts due to electron shielding. The amount of shielding is position variant within the triglyceride but is dominated by bulk methylene protons. The main chemical shift in fat corresponds to 440 Hz in a magnetic field of 3 Tesla.

Because the water and fat protons are precessing at different frequencies, it is possible to choose echo times in which the constituents of water and fat are perfectly in phase with one another, or perfectly in phase with one another. The algebraic sum or difference then gives a signal composed entirely of either fat, or water (Figure 4.1.3a). This method of imaging is called Dixon MRI.

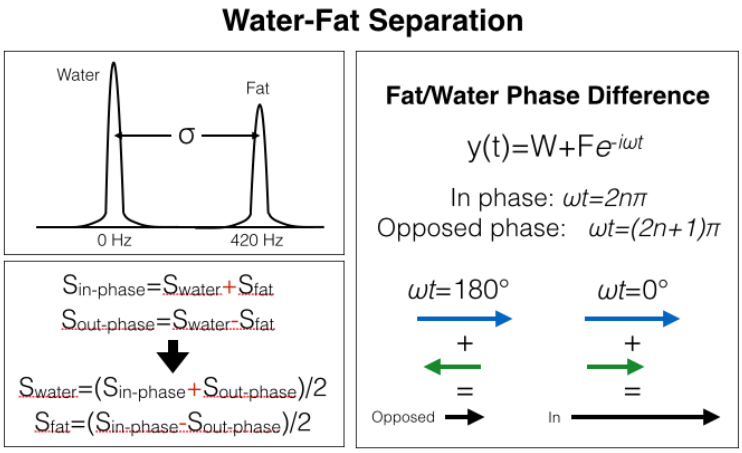



**Figure 4.1.3a. Water Fat Separation Using a Dual Echo Acquisition.** Water and fat precess at differing frequencies (upper left). The in-phase and opposed-phase signals can be linearly combined to calculate water and fat based signal intensities (lower left). Schematic of phase for corresponding echo time (right).

Once the MRI signal is decomposed into in-phase and opposed-phase images, it is a trivial matter to: 1) calculate the fat based image, 2) the water based image and 3) a fat fraction image defined as the ratio of fat to the sum of fat and water. An example of fat, water and calculated fat fraction is shown coronally in a newborn (Figure 4.1.3b).

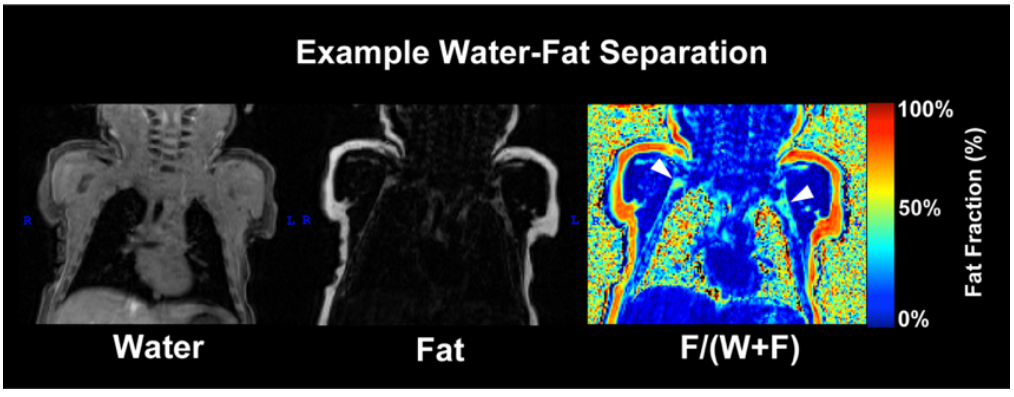



**Figure 4.1.3b. Example Water-Fat Separation in Neonate.** Fat fraction is far right panel and depicts BAT deposits with moderate fat fraction in the supraclavicular regions (white arrows).

The animal validation phase of the project was executed according to the recommendations found in the Guide for the Care and Use of Laboratory Animals of the National Institutes of Health. The protocol was approved by the Institutional Animal Care and Use Committee of the University of California at Irvine. Six two-month old Sprague-Dawley rats (250-275g) were imaged *post mortem* simultaneously in a sealed and decontaminated container. Deposits of iBAT were then excised from the interscapular region along with WAT deposits from the perirenal region. The excised tissue was placed in glass tubes and immediately imaged. All imaging occurred within a three-hour period of animal sacrifice to minimize *post mortem* effects on the tissue. MRI was performed on a Siemens 3T Tim Trio system (VB17 software) using a 12-channel head coil. Scans were conducted using a vendor-supplied chemical-shift two-point 3D gradient echo[20] Dixon method (TR=7.47ms, TE1/TE2=2.45/3.675ms, NA=16, BW/pixel=977Hz, FA=10, Matrix=512x320x160, 0.97x0.97x1mm, Scan Time=3min 2s).

Infant imaging was approved by the Institutional Review Board of the University of California at Irvine, and all parents provided informed, written consent. After feeding and soothing to the point of sleep, neonates were placed in a CIVCO beaded pillow (www.civco.com), covering body and head, that becomes rigid under vacuum providing a comforting swaddle, motion prevention and hearing protection when used in conjunction with standard foam earplugs. A pediatric specialist throughout the duration of scans observed neonates, monitoring for heart rate and oxygen saturation via a pulse oximeter attached to the foot. Scans were aborted in all cases of wakefulness within the neonate. The entire protocol included T1-weighted, T2-weighted, diffusion tensor and functional imaging of the brain. Of the 25 subjects who were initially imaged, 3 were excluded prior to analysis due to fat/water swapping arising from the ambiguity of phase greater than $2\pi$(Berglund, Johansson, Ahlström, & Kullberg, 2010; Ma, 2004) in the regions that contain BAT depots identified in this work (supraclavicular, axillary, spine), resulting in a final sample of 22 subjects (9 males and 13 females). All infants were from healthy pregnancies with no known obstetric, birth or current health complications. In terms of race/ethnicity approximately one half of the study sample was Non-Hispanic White (N=13), whereas the other infants were either Hispanic White (N=6) or Hispanic of other race (N=3). The mean infant age at assessment was 23.6 ± 11.7 (±SD) days and ranged from 11 to 56 days.

Subjects were imaged during natural sleep using a combination of a 12-channel head receive coil and a posterior neck coil. An anterior neck coil was added to increase the signal to noise ratio when infant size could accommodate it (N=17). The field of view was defined as just superior to the lower jaw down to the lower abdomen, with a fixed size. Imaging parameters were matched to the rodent imaging parameters, albeit with a single average resulting in a shorter scan time to minimize *in vivo* motion artifact.

Voxelwise fat fraction (FF) maps were created from water and fat separated volumes derived directly from the Siemens operating system, a feature readily available on most clinical platforms. The ratio of fat to the combined signal intensity from both fat and water used in this work is a fat signal fraction based on a two-point excitation incapable of accounting for the multiple peak resonances of fat and indirect dipole-dipole coupling. Hand drawn ROIs were used to extract FF from excised tissue samples and *post mortem* BAT regions. Thresholds for classifying BAT were determined based on a receiver operator characteristic analysis of the *ex vivo* samples. At an upper threshold of 60% FF, BAT was correctly classified 99% of the time with a WAT false positive of less than 10%. At a lower threshold of 20% FF, BAT was correctly classified 99.9% of the time.

Neonate BAT masks were created for visualization based on the following voxel attributes: 1) total signal greater than two standard deviations (SD) above the entire image mean (including background noise), 2) fat signal greater than one SD below the entire image mean, and 3) FF greater than 20% with no upper bound. Fat fraction values were overlaid on in-phase volumes to highlight individual differences in BAT depot volume, distribution and composition between subjects.

BAT and WAT deposits were segmented and quantified for depot volume and fat fraction in all subjects using a semi-automated intensity-based process(Yushkevich et al., 2006). BAT was segmented in ITK-SNAP (www.itksnap.org) by applying a threshold filter limiting FF values between 20% and 60%. Seed points for active contour segmentation were manually placed in deposits close to lateral processes along the spine and in supraclavicular, and axillary regions. Seed bubbles of 3mm were used to roughly cover these areas while avoiding any subcutaneous WAT partial volume regions. Supraclavicular ROIs were limited to four seed points per side, axillary to four seeds per side, and one seed per side on each vertebrae, ensuring consistent definition. Vertebral ROIs were limited to

the first five thoracic vertebrae (T1-T5) in order to maintain well-defined and consistent boundaries for definition between raters. The active contour evolution was iterated until the contours were visually covered by label, between 40 and 60 iterations. Iterations were constrained to 50 in the more heterogeneous supraclavicular and axillary regions to avoid bleeding into neighboring voxels. WAT was segmented using the fat-only image and thresholding for values above the lowest quartile. A single seed of 5mm was placed in the subcutaneous nuchal area of the neck to avoid regions contaminated by fat and water signal swap. The active contour evolution was iterated 100 times. Mean FF and total depot volume were computed for each of the three segmented BAT regions and one nuchal WAT region. An additional ROI mask containing the union of supraclavicular and axillary regions was also assessed to account for the occasionally ambiguous border between the supraclavicular and axillary regions.

The multi-echo water-fat MRI acquisition technique described was evaluated for test-retest reliability using a scan/re-scan approach examining voxelwise correlations between images of a single participant. Shim optimizations were run independently for each acquisition in order to reflect variation due to shim quality. The repeated acquisitions were separated only by the re-shim and default Siemens pre-scan preparations. The infant in-scanner position remained unchanged to maintain infant sleep state. There were no visually perceivable differences in position from the first to the second acquisition, although images were not co-registered to one another. Fat fraction quantitative and difference maps were made to assist the reader in visually assessing acquisition repeatability. After the image was masked for appreciable signal (as outlined above), voxelwise correlations were made and plotted for the union of all BAT segmentations, nuchal WAT and all remaining voxels.

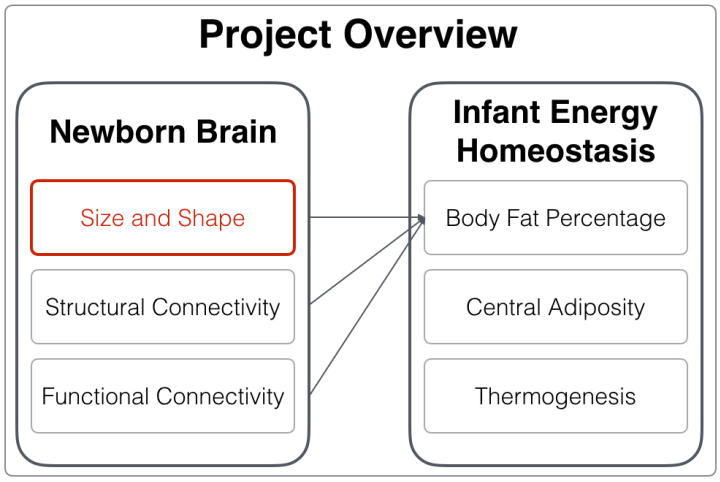
Inter- and intra-rater reliability measures were used to characterize the repeatability of the novel methods used here in segmenting BAT deposits. Two raters (raters 1 and 2) segmented BAT deposits using the semi-automated techniques described above, with one rater (rater 1) repeating the segmentations of all 22 scans after two weeks (rating 1a, rating 1b). Inter-rater reliability measure was then defined as the average intra-class correlation coefficient (ICC, the ratio of between-subject variance to total variance) between rating 1a vs. rating 2 and rating 1b vs. rating 2. The intra-rater reliability was

taken as the ICC between rating 1a vs. rating 1b. Similar metrics referred to here as within-subject correlation coefficients (WSC, the ratio of within-subject or between-rater variance to total variance) and noise (N, the ratio of unaccounted for variance to total variance) are reported(Y. Chen, Wang, & Detre, 2011; Jahng et al., 2005).

### 4.2 Quantifying Infant Brain Development

Despite recent technological and methodological advances in brain imaging (e.g., the Human Connectome Project(Van Essen, Smith, Barch, & Behrens, 2013)), measures of energy homeostasis brain circuitry have not yet been developed in newborns. Regional measures of GM/WM volume (anatomy) and structural/functional connectivity between key nodes of this circuitry were characterized using cutting-edge methods in acquisition and analysis. Due to the rapidly maturing infant brain, special consideration was given to modeling early life growth (Maturation Index) as outlined below.

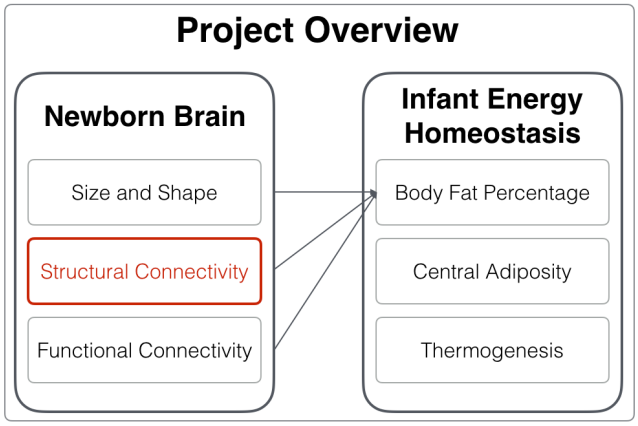
#### *4.2.1 Brain MRI Acquisition: Structure/Anatomy, Structural Connectivity, Functional Connectivity*




Anatomical MRI scans were acquired during natural sleep using a 12-channel head receive coil. High-resolution anatomical scans including T1-weighted (MPRAGE, TR/TE/TI=2400/3.16/1200ms, Flip Angle=8 degrees, Matrix=256x256x160, Resolution=1x1x1mm, 6m18s) and T2-weighted (TSE, TR/TE=3200/255ms, Matrix=256x256x160, Resolution=1x1x1mm, 4m18s) images were acquired. After feeding and soothing to the point of sleep, neonates were placed in a CIVCO beaded pillow (www.civco.com). The pillow covered the neonates' body and head, became rigid under vacuum, and provided a comforting swaddle, motion

prevention and hearing protection when used in conjunction with standard foam earplugs. A pediatric specialist observed the neonates throughout the duration of scans, monitoring for heart rate and oxygen saturation.

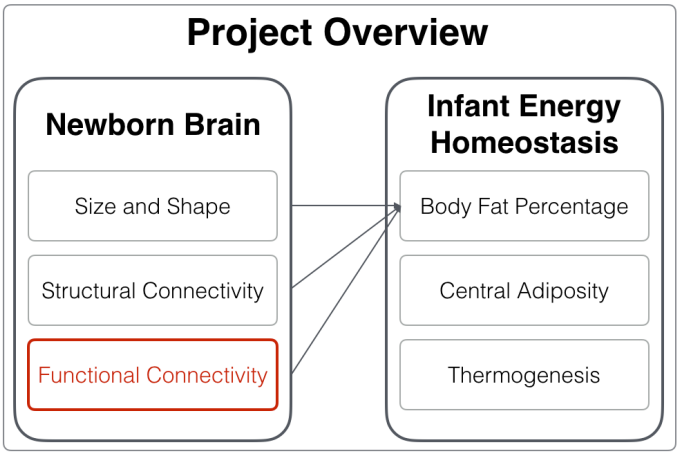
Brain compartments classified as either GM, WM, or cerebrospinal fluid using an automatic, atlas-moderated expectation maximization segmentation tool(Gilmore et al., 2007; Prastawa, Gilmore, Lin, & Gerig, 2005). ICV was defined as the sum of all three tissue-compartments. Cortical parcellation was used to define the insula using non-linear warping of a parcellation atlas template(Gilmore et al., 2007). Regional GM volume was defined as the intersection between the GM mask and region of interest. ICV was age-corrected in identical fashion to BF%, that is, residualized for gestational and postnatal age. In separate analyses, insula GM volume was either only corrected for GA and SA independent of ICV or additionally corrected for ICV. A simple geometric parcellation scheme was implemented by subdividing the insula along its long axis into 3 parcels of equal width.




Diffusion-weighted MRI scans were acquired during natural sleep using a 12-channel head receive coil. The 49-direction diffusion weighted protocol (EPI, TR/TE=8900/83ms, Matrix=256x256x75, Resolution=2x2x2mm, 42 unique directions at b=1000s/mm$^2$, 7 at b=0) was 7 minutes and 43 seconds in duration. After feeding and soothing to the point of sleep, neonates were placed in a CIVCO beaded pillow (www.civco.com). The pillow covered the neonates' body and head, became rigid under vacuum, and provided a comforting swaddle, motion prevention and hearing protection when used in conjunction with standard foam earplugs. A pediatric specialist observed the neonates throughout the duration of scans, monitoring for heart rate and oxygen saturation via a pulse-oximeter attached to the foot. The entire protocol included T1-weighted, T2-weighted, diffusion tensor and functional imaging of the brain.

Diffusion profile measurements were generated via the NA-MIC atlas based fiber analysis toolkit(Verde, 2014). In brief, diffusion datasets were first rigorously checked for appropriate quality. This was followed by weighted least square tensor estimation, skull

stripping via prior brain mask from co-registered structural T2 weighted images, and unbiased study specific DTI atlas building. Fiber tract streamline DTI tractography (Fillard, Gilmore, Piven, Lin, & Gerig, 2003) was performed via 3D Slicer (version 4.3.0) (http://www.slicer.org) in the DTI atlas space followed by fiber cleaning with FiberViewerLight (www.nitric.org/projects/fwlight). Tractography was performed for major fiber bundles: corpus callosum (genu, rostrum, tapetum, occipital, parietal), Left(L)/Right(R) cingulum, L/R fornix, L/R inferior fronto-occipital fasciculus (IFOF), L/R inferior longitudinal fasciculus (ILF), L/R superior longitudinal fasciculus (SLF), L/R uncinate fasciculus (UF), L/R motor, L/R pre-motor, L/R cortico-fugal parietal and L/R thalamo-cortical parietal and L/R optic tracts. Fiber profiles of FA, MD, AD, RD were extracted after fiber parameterization for profile analysis. DTI data was visually evaluated for appropriate mapping into the DTI atlas space via slice overlay. Visual inspection and quantitative quality assessment of the extracted fiber profiles were additionally performed by computing the cross-correlation coefficient between the FA tract profiles of the DTI atlas and of each subject case (minimal $r > 0.75$). For most tracts, all subjects passed quantitative profile QC. Few subjects were excluded for cingulum L (5), cingulum R (7), CST L (1), fornix L (2), and uncinate R (1). Brain compartment volumes were determined for gray matter, unmyelinated white matter, myelinated white matter, and cerebral spinal fluid using an automatic, atlas-moderated expectation maximization segmentation tool as previously described(Gilmore et al., 2007; Prastawa et al., 2005). Intracranial volume defined here is the sum of the four preceding compartment classes.




Functional connectivity methods will now be described. Respiratory and wakefulness were monitored throughout neonatal scans to ensure comfort and safety. EPI data were obtained using a gradient-echo approach sensitive to blood oxygen level-dependent (BOLD) contrast (TR = 2000 ms; TE = 30 ms; FOV = 220 × 220 × 160 mm; flip angle = 77◦). Full brain coverage was obtained with 32 ascending-

interleaved 4mm axial slices and a 1mm skip. The first four frames (8s total) were discarded to achieve steady state magnetization.

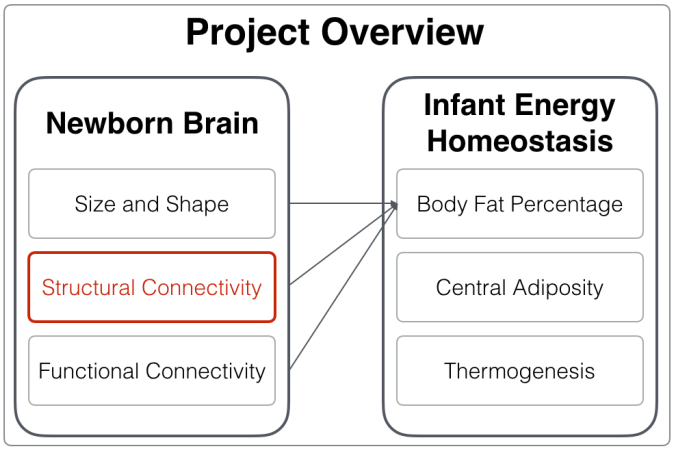
The Brain Extraction Tool from the FMRIB Software Library(Beckmann & Jenkinson, 2003; S. M. Smith, Jenkinson, Woolrich, & Beckmann, 2004) was used for brain extraction. Preprocessing steps included: (i) central spike removal, (ii) odd versus even slice intensity correction, (iii) motion correction, and (iv) intensity normalization to a whole brain mode value of 1000. The functional data was registered using a two-step registration. First, functional images were registered to their respective high-resolution T2 scan. Second, the high-resolution T2 scans were registered to a standard infant template (0- to 2-month age range; MRI Study of Normal Brain Development)(Fonov, Evans, McKinstry, & Almli, 2009). All analyses were performed on the native space volumetric time series and the two-step registration applied for statistical inference of group differences.

The removal of non-neuronal signal contribution was also performed(Fair, Nigg, Iyer, Bathula, & Mills, 2012; M. D. Fox & Raichle, 2007). Specifically, this included: temporal low-pass filtering (0 < 0.1 Hz), regression of rigid body head motion parameters in 6 directions, regression of the whole brain signal, regression of ventricular signal averaged from a ventricular region mask, regression of white matter signal averaged from a white matter mask and regression of first order derivative terms for the whole brain, ventricular, and white matter signals(Fair et al., 2012). Nuisance variables for regression were applied prior to low-pass filtering(Hallquist, Hwang, & Luna, 2013). FD (Power, Barnes, Snyder, Schlaggar, & Petersen, 2012) was used to examine movement of a given frame relative to the previous frame. Volumes with greater than 0.3 mm FD (and 1 preceding and 2 following volumes to account for temporal blurring) were censored. Only scans with greater than 4 min of data remaining after censoring were included. For the remaining infants (N = 88) remaining scan duration after censoring was approximately 5 and a half minutes (mean = 5.43, range = 4.00–6.50), and remaining FD was approximately 0.09 (mean = 0.089, range = 0.05–0.15). Post-hoc analyses adjusted for remaining FD to examine effects of remaining motion on findings.

A multi-modality, multi-template based semi-automatic method combining T1 and T2 weighted high-resolution images(L. Wang et al., 2013), followed by manual correction in

ITK-Snap(Yushkevich et al., 2006) was used for amygdala segmentation. The individualized amygdala ROIs were spatially warped to EPI space based on the atlas transform computed using the functional and high-resolution T2 scan. Individualized amygdala ROIs were used as seed regions for RS-fMRI analyses, based on observation of improved global maps relative to atlas-based group definition of amygdala as seeds. Residualized (see above regarding preprocessing) amygdala BOLD signal was averaged across the voxels within the invidualized ROI, and then correlated with the residualized time course for all other brain-masked voxels. Whole-brain voxel-wise connectivity maps for both the left and right amygdala were used as predictors of early life fat gain in regression models employing FSL RANDOMISE(Winkler, Ridgway, Webster, & Smith, 2014) to account for multiple comparisons.

*4.2.2 Maturation Index (MI) Defined*




Linear regression models were implemented using Matlab (www.mathworks.com) for the examination of predictive power using two separate models. Model 1 used PM as the only indicator of participant age at the time of the MRI scan and as the predictor of diffusion measures. Model 2 used GA and SA as separate independent variables representative of age at the MRI scan and as predictors of diffusion measures. Both model 1 and model 2 included ICV as a continuous covariate and sex as a binary covariate. For this study the dependent variables were FA, RD orAD (Y in below equations). This is shown below for the *i*th position along a fiber tract (models 1 and 2). In the case of *linear* maturation, growth rates before and after birth are equal ($\beta_{i,GA} = \beta_{i,SA}$). In this special linear case, model 2 is reduced to model 1, as PM is the sum of GA and SA, by definition. For this reason, the greater the difference between $\beta_{i,GA}$ and $\beta_{i,SA}$, the greater the inflection in growth rates at the time of birth.

$$Model\ 1:\ Y_i = \beta_{i,PM} \cdot PM + \beta_{i,BV} \cdot ICV + \beta_{i,Sex} \cdot Sex + \varepsilon \quad (1)$$

$$Model\ 2:\ Y_i = \beta_{i,GA} \cdot GA + \beta_{i,SA} \cdot SA + \beta_{i,BV} \cdot ICV + \beta_{i,Sex} \cdot Sex + \varepsilon \quad (2)$$

The gain in predictive power moving from model 1 to model 2 is descriptive of the divergence of $\beta_{i,GA}$ from $\beta_{i,SA}$ and therefore reflective of whether major maturational changes occur before or after birth. In order to justify the use of model 2, the gains from using the unrestricted model (model 2) were statistically characterized using an F-distribution. Here, $RSS_j$ is the residual sum-of-squares from the respective model *j*, n the number of observations and $p_j$ the number of model parameters. A p-value was then calculated along the tract using an F-test, $F(p_2\text{-}p_1, n\text{-}p_2)$. Because model 2 always has the potential to reduce to model 1 (when $\beta_{i,GA} = \beta_{i,SA}$), $RSS_1$ will always be larger than or equal to $RSS_2$. A large F-statistic is driven by a difference in the residual errors between the two models and is therefore indicative of an increase in the asymmetry of maturation ($\beta_{i,GA} \neq \beta_{i,SA}$) about the time of birth.

$$F = \frac{{}^{(RSS_1 - RSS_2)}/_{(p_2 - p_1)}}{{}^{RSS_2}/_{(n - p_2)}} \quad (3)$$

Three basic data sets were simulated to demonstrate the advantages of using the unrestricted second model. The three sets each consisted of 1,000 simulated observations, $Y_i = \beta_{i,GA} \cdot GA + \beta_{i,SA} \cdot SA$, with GA and SA randomized to a normal distribution and variance matched to our neonatal sample ($GA_{SIM}$=259+/-14 days; $SA_{SIM}$=28+/-14 days) whose dependent variable increased with GA only (set 1, *in utero* maturation only), GA and SA equally (set 2, linear maturation from the time of conception), or SA only (set 3, postnatal maturation only). Each set was then examined for correlations between the simulated dependent value and each of the three age variables individually: 1) GA, 2) SA and 3) PC. Explained variance of 1.0 (or 100%) occurs when the simulated data can be fully explained. The total variance explained by model 2 is given by the sum of $R_{GA}^2$ and $R_{SA}^2$.

MI values were defined using output from model 2. Specifically, MI is defined as the ratio of the *difference* in the squared slopes (*beta* value) of GA and SA, to the *sum* of squared slopes of GA and SA (Equation 4). The square of the slope was used to remove the sign dependence of the slope in the calculation. MI will tend towards +1 when the absolute rate of change during prenatal development is large relative to postnatal development, zero when the rates of change during pre- and postnatal development are equal and -1 when the postnatal rate of change is large relative to the rate of change during prenatal development.

$$MI = \frac{{\beta_{GA}}^2 - {\beta_{SA}}^2}{{\beta_{GA}}^2 + {\beta_{SA}}^2} \qquad (4)$$

MI was plotted against the increase in explanatory power from model 2 compared to model 1 (Equations 1 and 2). A large F-Ratio coupled with a large (non-zero) MI suggests a meaningful increase in power due to accounting for the non-linearity of developmental trajectories (using GA and SA, model 2) having an inflection point at the time of birth. The MI has two principal benefits over examining the slopes individually: 1) the dimensionality of the rates of change are reduced to a single number (an index), and 2) the magnitude of the slopes are effectively normalized so that the magnitude of the inflection becomes a dimensionless parameter, facilitating whole-brain characterization.

Infant neuroimaging was approved by the Institutional Review Board of the University of California at Irvine, and all parents provided informed, written consent. All of the 47 infants evaluated in this study were from healthy pregnancies with no major obstetric, birth or current health complications. Mother-child pairs were recruited for a research study of normative development. Gestational age was determined by best obstetric estimate with a combination of last menstrual period and early uterine size, and was confirmed by obstetric ultrasonographic biometry before 15 weeks using standard clinical criteria(O'Brien et al., 1981). The mean gestational age at birth was 39.1 ± 1.6 (±SD) weeks and ranged from 34.4 to 41.9 weeks. The mean postnatal infant age at assessment was 25.5 ± 12.2 (±SD) days and ranged from 5 to 56 days. Gestational age at birth and postnatal infant age at assessment were not correlated with one another ($R^2$=-2.8%,p=0.25).

A unique MI value for FA, RD and AD was calculated as described above for each point along the defined white matter fiber tracts. For the remainder of this work, each of these values will be denoted respectively as $MI_{FA}$, $MI_{RD}$, and $MI_{AD}$. $MI_{FA}$, $MI_{RD}$, and $MI_{AD}$ values were evaluated globally to test three basic hypotheses related to the developmental timeline of white matter microstructure: 1) the rate of change of AD is greatest during pre-myelination (see section 6.2.1), a process occurring prenatally before true-myelination, therefore average $MI_{AD}$ is expected to be greater than $MI_{FA}$ and $MI_{RD}$, 2) the rate of change of RD is *more* linear than those of AD and FA as it changes with both pre- and true-myelination (see section 6.2.1), therefore $MI_{RD}$ should have a mean between those of AD and FA, 3) FA changes are greatest after birth when true-myelination (see section 6.2.1) begins to increase globally and $MI_{FA}$ should, therefore, skew towards -1. Two-way paired t-tests between diffusion parameter MIs were used to test the above order in $MI_{FA}<MI_{RD}$, and $MI_{RD}<MI_{AD}$.

MI values along the fiber tracts used in this study were visualized in four groups: association (anterior-posterior connection), commissural (left-right connection), projection (superior-inferior connection) and limbic (those connecting limbic structures connection). Despite their anterior to posterior orientation, the cingulum and ILF(Latini, 2015) were assigned to the limbic group together with the UF and fornix. The fiber groups were compared for differences within the group (paired t-tests between diffusion parameter MIs within group) and $MI_{FA}$, $MI_{RD}$, and $MI_{AD}$ were compared across groups using independent two sample t-tests. The location, size and significance of the clusters with the largest magnitude MI are reported with a focus on $MI_{RD}$ as justified further below.

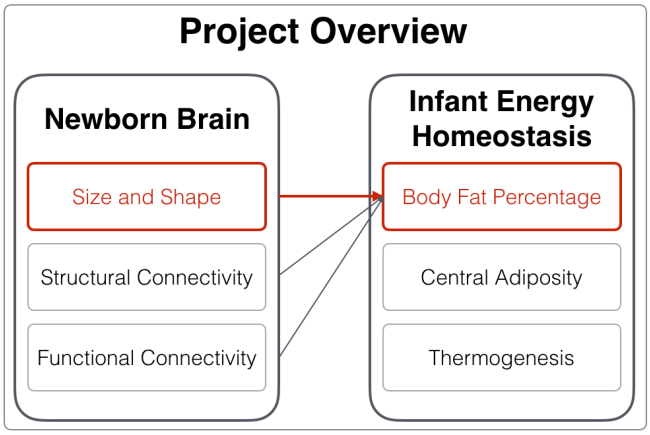
A *post-hoc* examination within a selected fiber tract was conducted in order to further elucidate the descriptive relationship between $MI_{FA}$, $MI_{RD}$, and $MI_{AD}$. The left pre-motor tract was chosen based on two criteria: 1) the projection fibers collectively showed the greatest amount of variability, each bisected by a region of large positive MI and large negative MI, and 2) the left sided projection fibers had the most negative MI values and have been shown to myelinate before right sided fibers(Dubois et al., 2009). ROIs were defined *post-hoc* as having a significant F-ratio between model 2 and model 1 (Equation 3) and were applied as a mask to the tract-based data extracting a mean slope for GA and SA from the model for comparison.

A post-hoc exploration of the relationship between $MI_{RD}$, $MI_{AD}$, and $MI_{FA}$ was made using a simple colored scatter plot depicting the three metrics together.

## 4.3 Prospective Associations Between Brain Phenotypes and Infant Adiposity: Modeling

The prospective association between brain phenotypes (anatomy, structural connectivity, functional connectivity) and early life fat gain (change in body fat percentage [BF%] from birth 'til six months) was the primary focus of this project. Below, I describe the models used in relating energy-homeostasis-relevant brain phenotypes to early life fat accumulation.

### *4.3.1 Newborn Insula Volume and Early Life Adiposity Gain*



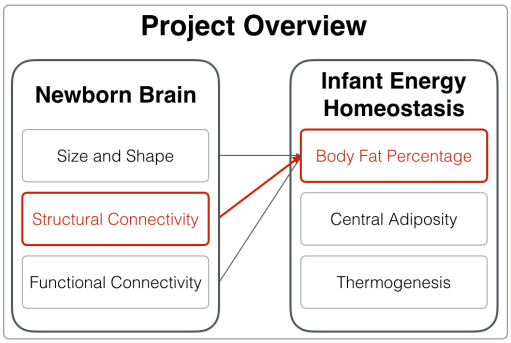

All statistical models tested without adjusting for potentially confounding variables used Pearson correlation analyses with gestational/postnatal age-corrected ΔBF% as the outcome, and either gestational and postnatal age-corrected insula GM volume or gestational/postnatal age *and* ICV-corrected insula GM volume as the predictor. The influence of potentially confounding variables was tested using multiple linear regression analyses with ΔBF% as the outcome and GM volume and the confounding factors (see below) as predictors. All statistical analyses employed Matlab R2014a using the statistics toolbox and anovan function.

As an indication of clinical value, Receiver Operating Characteristic (ROC)(Hanley & McNeil, 1982) analysis was conducted using a threshold of 75$^{th}$ percentile ΔBF% as proxy categorization of participants as either at-risk or not at-risk of future obesity. The summary statistic area-under-the-curve (AUC) is reported for the ROC. ROC analysis provides a quantitative measure of the utility of bi-lateral gray matter insula volume as an obesity-risk

screening tool by specifying a false positive rate for a given true positive rate of categorical risk identification.

Because maternal conditions during pregnancy may concurrently influence brain development and fat gain, the following variables were used as potential confounds: maternal insulin resistance index (HOMA-IR, proportional to the product of plasma insulin and glucose, averaged over three trimesters), sex (separate models for main effects and interaction), feeding practices (exclusive breastfeeding, exclusive formula feeding or mixed practices), maternal pre-pregnancy BMI, and newborn birth weight corrected for gestational age at birth. Maternal insulin and glucose were measured throughout pregnancy (first, second and third trimester) using standard enzyme-linked immunosorbent assay protocols. HOMA-IR was calculated based on these measures, and the average across pregnancy was used as an indicator of maternal metabolic function. Infant feeding practices were assessed *via* monthly maternal interviews. A composite measure of feeding practice categorized offspring with greater than 75% of the first six months of life spent exclusively breastfeeding as breastfed, less than 25% of the first six months of life spent exclusively breastfeeding as formula-fed and intermediate values as mixed feeding practice. Maternal pre-pregnancy BMI was based on maternal self-report and verified using height and weight measurements taken at the first pregnancy visit (self-reported pregnancy weight was highly correlated with measured weight on the first visit [$R^2$=0.94%, $p<0.001$]). Birth-weight was abstracted from the medical record, and gestational age was determined by best obstetric estimate with a combination of last menstrual period and early uterine size and was confirmed by obstetric ultrasonographic biometry before 15 weeks using standard clinical criteria(O'Brien et al., 1981).

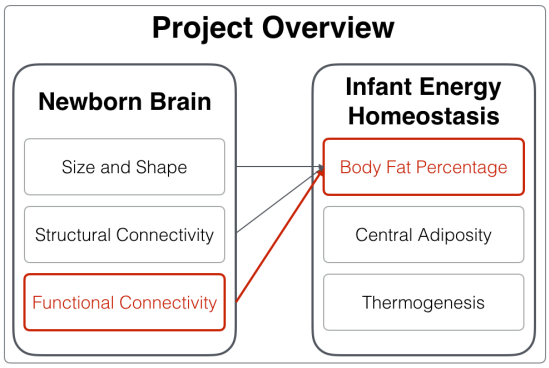
### *4.3.2 Newborn White Matter Properties and Early Life Adiposity Gain*




Prospective associations between structural connectivity and early life fat gain were assessed using tract-based statistics. Bivariate Pearson correlations were used at each unique point along the tract testing for associations

between early life fat gain and diffusion metrics residualized (linearly regressed out) for gestational age at birth and postnatal age at scan. All clusters were tested for multiple comparisons using a Monte Carlo simulation (N=10,000) to test the likelihood for a false positive at a given statistical threshold (minimum p-value) and cluster size. For each simulation, a normally distributed random variable was generated and tested for the false positive detection of a cluster at the defined significance threshold and cluster size.

*4.3.3 Newborn Functional Connectivity to the Amygdala and Early Life Adiposity Gain*




Prospective associations between functional connectivity to the amygdala (see section 3.3.3 for rationale) and early life fat gain were assessed using FSL's RANDOMISE(Winkler et al., 2014). After voxelwise whole brain maps of amygdala connectivity were defined at the individual level (in template space), voxelwise linear regressions were conducted considering ΔBF% over the first six months of life, gestational age at birth, and postnatal age at scan as predictors of amygdala functional connectedness. Multiple comparisons corrections were performed via a multiple permutation test of significance(Winkler et al., 2014).

The interconnectedness of various constituents (see figure 5.3.3d for the full list), and their prospective associations with early life fat gain, of homeostasis-related networks were considered post hoc. While all *components* of the network were a priori defined, a mix of anatomically and functionally defined ROIs were used to build the network graph. Anatomically defined regions were based on the anatomical segmentations while functional ROI definitions were defined based on amygdala connectivity greater than uncorrected significance at the $p<0.05$ level. It should be noted that by defining a portion of the regions based on functional connectivity to the amygdala, the centrality of the amygdala within the network is biased, making graph-based interrogation of the network challenging. As discussed above in section 4.3.2, future aims will use surface-based registration to increase the precision of anatomical definition and allow for a fully

anatomically defined network. For these reasons, the network based RS-fMRI findings should be considered descriptive in nature.

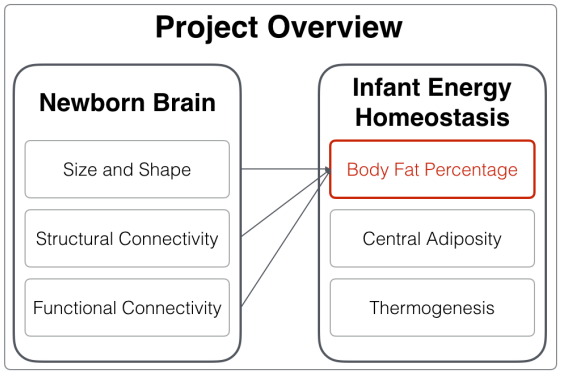
# 5 Results

The following section addresses experimental results relating to fat quantification in the human infant (DXA and MRI outcomes of brown and white adipose tissue), age models in early life brain development (Maturation Index), and prospective associations between newborn energy homeostasis relevant brain circuitry and early life fat accumulation.

## 5.1 Fat Quantification

Newborn DXA scans were available in a sample of 119 infants (64 male, 55 female). Six-month DXA scans were available in a sample of 91 infants (45 male, 46 female). Longitudinal DXA scans were available in a sample of 81 infants (40 male, 41 female). Mean gestational age at birth was 39.3 ± 1.4 [± SD] wks. Serial DXA assessments were obtained shortly after birth (11.4 ± 24.6 [± SD] days) and at six-months age (26.7 ± 3.3 [± SD] wks). N=42 neonates were available for assessment of abdominal fat depots using an MRI scan protocol T1-weighted for fat hyper-intensity, 38 of these participants also had newborn DXA assessments available for comparison. Dixon imaging was acquired in 22 participants and available for an assessment of inter- and intra-rater reliability in quantifying Brown Adipose Tissue depots.

### *5.1.1 Age, Sex and Breastfeeding Status: Associations with Newborn BF%, Six-month BF% and Six-month Change in BF%*




Four key infant characteristics were considered for a priori residualization of newborn and six-month BF%: gestational age at birth, age at scan, sex and breastfeeding status at six-months.

K-means (k=3) clustering of feeding practice resulted in 3 well-defined and evenly distributed groups (Figure 5.1.1a) that can qualitatively be described as follows: 1) the

breastfed group (N=45) remained almost entirely breastfed for the duration of six months (minimum 90% breastfed infants in the first month), 2) a mixed group (N=48) transitioning from some exclusive breastfeeding in the first two months to some exclusive formula feeding in months five and six, and 3) a formula group (N=52) transitioning from some mixed practices in the first month to predominantly formula exclusive by the second month of postnatal life (90%).

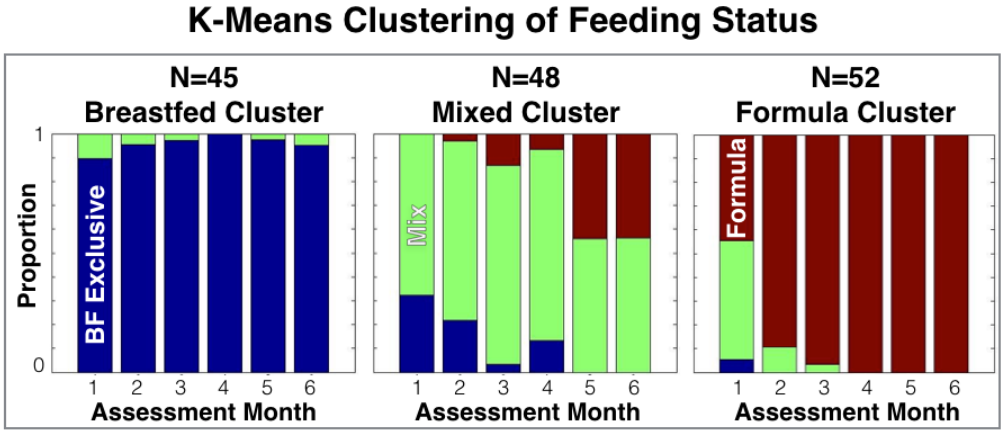



**Figure 5.1.1a. K-means Clustering of Feeding Status.** Infant feeding status (breast milk exclusive, formula exclusive and mixed practices) was clustered based on monthly maternal report across six months.

BF% at the newborn time point was significantly and positively associated with gestational age at birth ($p=0.017$, $R^2=4\%$), postnatal age at scan ($p<10^{-4}$, $R^2=26\%$) and females tended to have greater BF% ($p=0.081$, $R^2=2\%$). Associations between gestational age at birth and postnatal age at scan were not conditional upon infant sex ($p=0.028$ and $p<10^{-4}$ respectively, Figure 5.1.1b).

Only breastfeeding status was trend-associated with six-month BF% in the full model ($p=0.08$). When considering gestational age at birth and postnatal age at scan only, gestational age at scan was significantly associated with BF% (Figure 5.1.1c).

Age-corrected change in BF% from shortly after birth until six months was not associated with breastfeeding status or sex ($p>0.7$). Therefore, a priori correction of change in BF% was limited to age-correction (gestational age at birth and postnatal age at scan separately) with a recommendation for post-hoc hypothesis testing of sex and breastfeeding status effects.

The longitudinal ΔBF% was then defined as the change between age-corrected newborn and six-months time points. Newborn and six-months DXA BF% values were on average 13.8 ± 4.9% (±SD) and 31.9 ± 8.2% (±SD) respectively (Figure 5.1.1d). Notably, this is a 60% increase from birth to six months in BF% variability across subjects. Presumably, as a result, six-month BF% was a stronger predictor ($R^2$=69%) of ΔBF% than the newborn time-point ($R^2$=-5%) meaning this outcome is heavily weighted by a surrogate of peak BF%. The main outcome variable used here, ΔBF%, was +17.6 ± 7.8% (±SD) (i.e., an average increase of 0.75%/week).

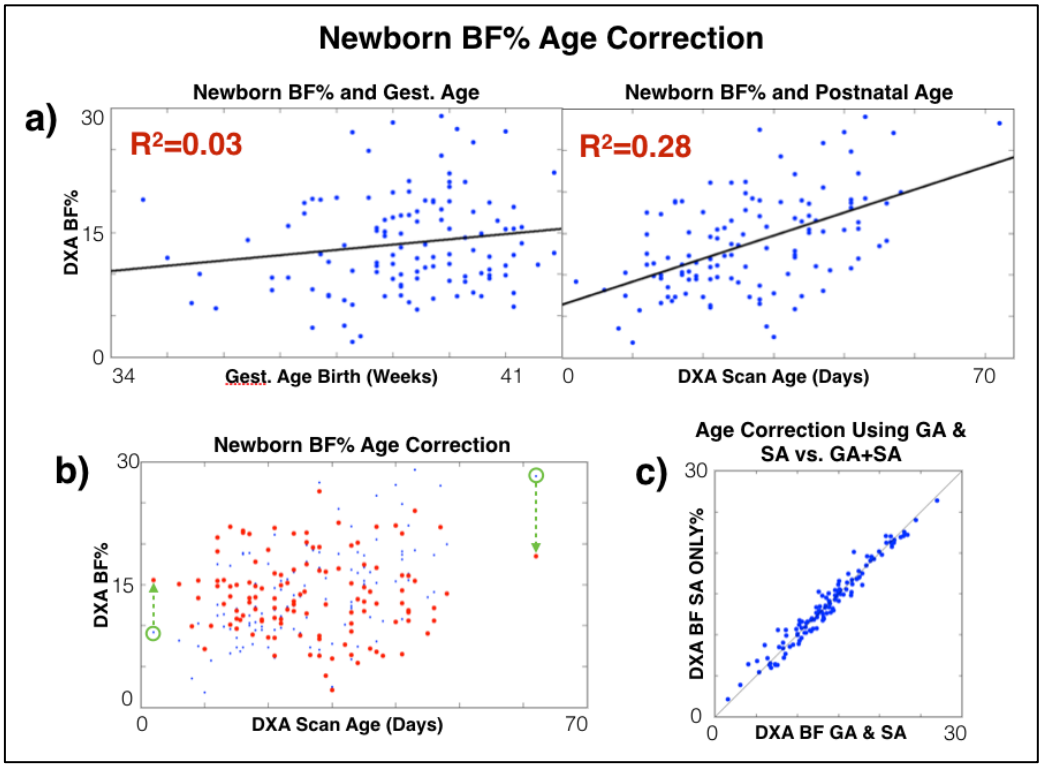



**Figure 5.1.1b. Newborn Age-correction of Global Body Fat Percentage (BF%).** Newborn BF% (N=118) is associated with gestational age at birth (left side, panel a, p=0.028) and postnatal age at scan (right side, panel a, $p<10^{-4}$). Resulting age-corrections are shown in panel b (red dots are corrected data, blue uncorrected, green arrows are example corrections). Panel c demonstrates the similarity in corrected values using postmenstrual age at scan (vertical axis) versus splitting into gestational age at birth and postnatal age at scan.

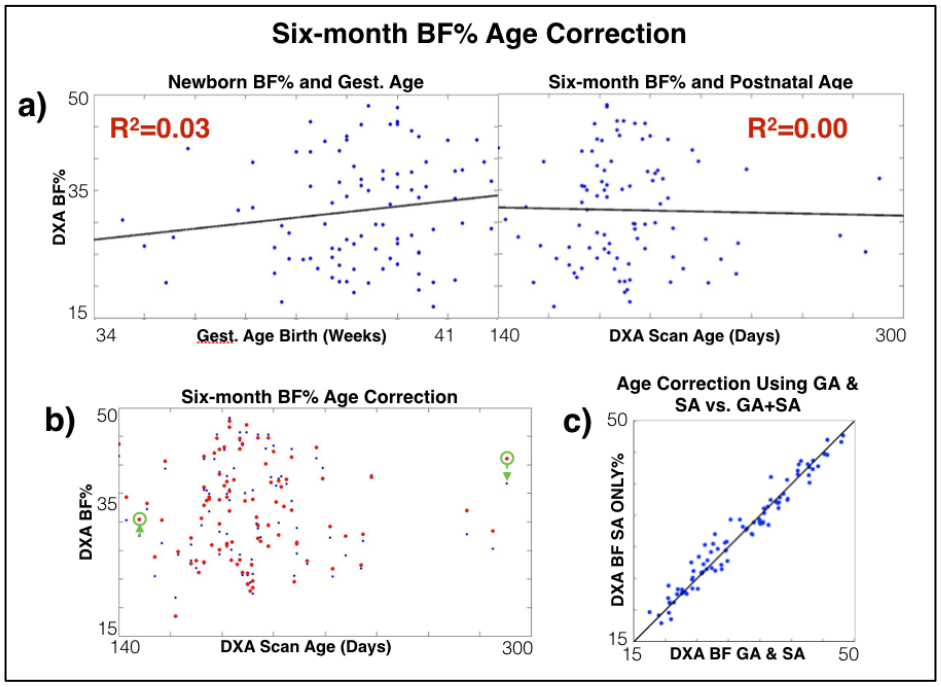



**Figure 5.1.1c. Six-month Age-correction of Global Body Fat Percentage (BF%).** Six-month BF% (N=90) is trend-associated with gestational age at birth (left side, panel a, p=0.061) but not postnatal age at scan (right side, panel a, p=0.23). Resulting age-corrections are shown in panel b (red dots are corrected data, blue uncorrected, green arrows are example corrections). Panel c demonstrates the similarity in corrected values using postmenstrual age at scan (vertical axis) versus splitting into gestational age at birth and postnatal age at scan.

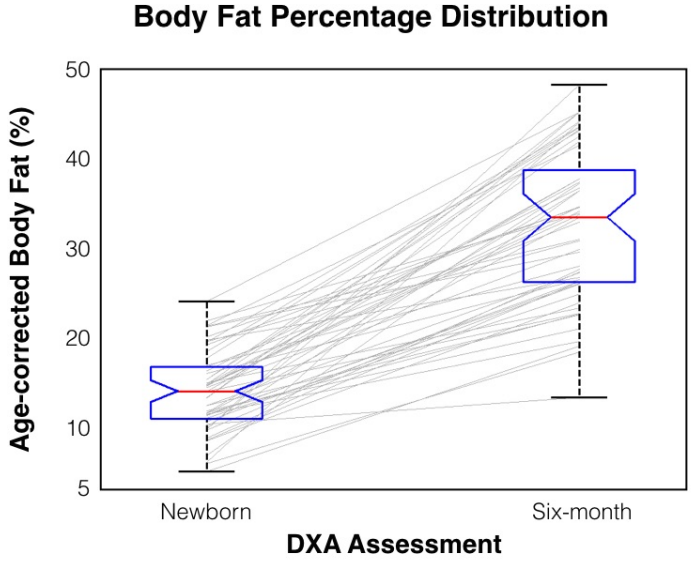
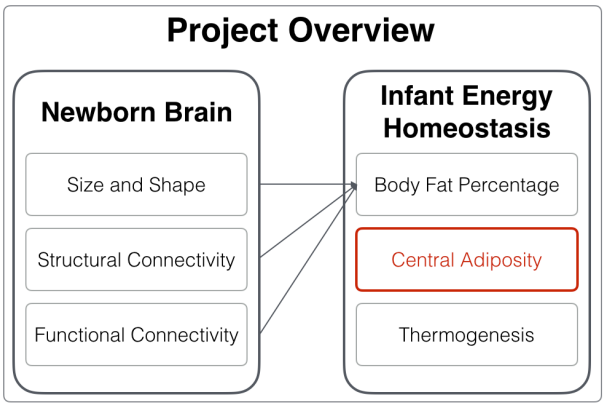



**Figure 5.1.1d. Inter-individual Variability in Body Fat Percentage Change in Early Life.** Box and whisker plots depict body fat percentage distributions in newborns and six-month old infants. Red lines, whiskers, boxes, and notches are medians, extreme values, quartiles (25/75) and confidence intervals (95%) respectively. The gray lines are individual trajectories of body fat percentage change, the main outcome variable considered in this project.

*5.1.2 Challenges in Visceral Adipose Tissue Segmentation and Quantification*

No gross errors in fat segmentation were evident in any of the 42 scans. Automatically defined fat compartments were manually subdivided into six distinct classes (Figure 5.1.2a): superficial subcutaneous fat, deep subcutaneous fat, visceral fat, retroperitoneal fat, paraspinal fat, and stomach fat (presumed to be recently consumed breast milk).



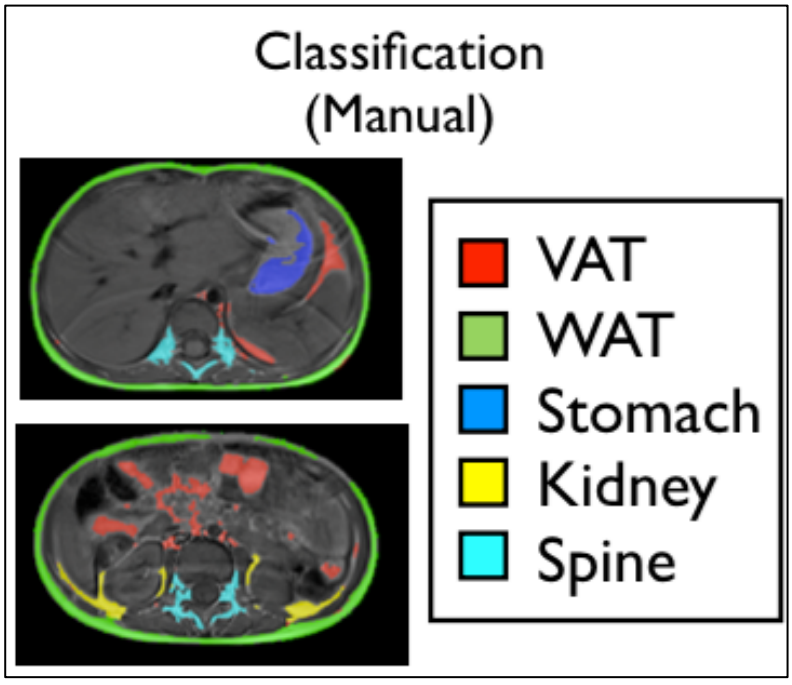




**Figure 5.1.2a. Example Regions Manually Sub-classified.** Subclasses of fat deposition were made following automatic segmentation of tissue class (fat/non-fat) on a voxel-wide basis. VAT=Visceral Adipose Tissue, WAT=White Adipose Tissue (superficial subcutaneous).

| Fat Depot | Absolute Fat Content (g) | Relative Percentage by Volume (%) |
|---|---|---|
| **Superficial Subcutaneous** | 44.0+/-16.8 | 55+/-12 |
| **Deep Subcutaneous** | 4.2+/-3.8 | 5+/-4 |
| **Visceral** | 10.2+/-6.2 | 13+/-7 |
| **Retroperitoneal** | 9.8+/-3.8 | 12+/-3 |
| **Paraspinal** | 4.0+/-1.9 | 5+/-2 |
| **Stomach** | 5.9+/-8.9 | 8+/-12 |
| **Total** | 79.9+/-25.3 | N/A |

**Table 5.1.2. Absolute and Relative Fat Compartment Size in the Newborn.** Superficial subcutaneous fat was the predominant compartment of fat in the human newborn torso.

Superficial subcutaneous fat mass (grams) in the torso was significantly associated with the newborn measure of BF% using DXA (p=0.003, N=38), suggesting a multi-modal validation of the measure. Neither visceral adipose tissue mass (p>0.9), nor deep subcutaneous fat (p>0.1) were associated with newborn BF%. In addition, total abdominal fat mass measured using MRI was only associated with newborn BF% at the trend-level (p=0.058), while subcutaneous fat mass was strongly, and unsurprisingly, associated with total abdominal fat mass. Together this suggests that measures of internal abdominal fat mass is independent of the fat measured using a gold standard technique (DXA).

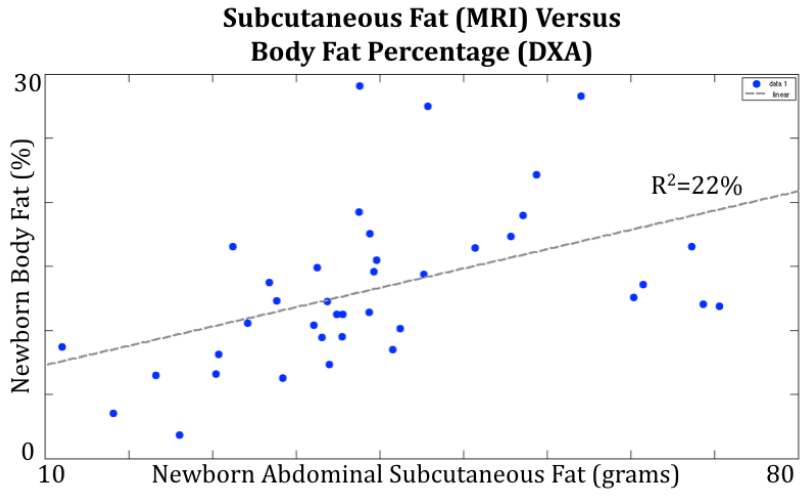
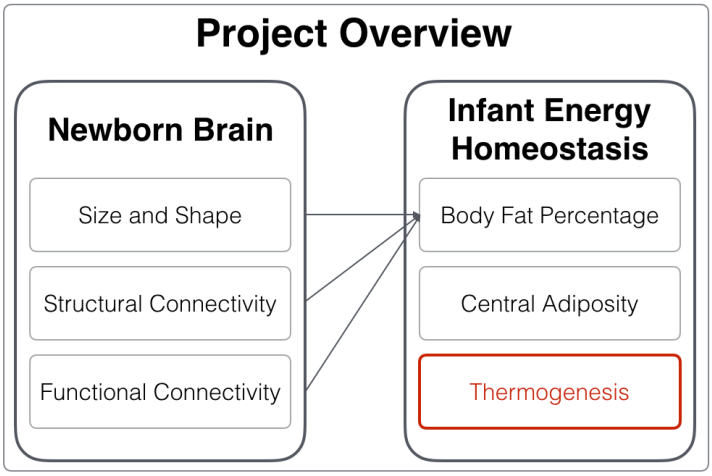



**Figure 5.1.2.b. MRI-Based Subcutaneous Fat Mass and DXA-Based Body Fat Percentage.** Fat mass measured in the newborn torso was associated with newborn DXA body fat percentage.

Breathing motion was a significant artifact in many of the participants, leading to poor quality data, particularly in the interior regions. In addition, because bowel status and milk in the gut can be attributed to signal hyper-intensity(Bauer, Noël, Vollhardt, Much, & Degirmenci, 2015), these factors represent a confounding signal contribution. Finally, newborns typically have, relative to adults, limited deposition of visceral adipose tissue(Tint, Fortier, Godfrey, & Shuter, 2016), and its location in neonates does not coincide with regions of intra-abdominal classically associated with metabolic dysfunction(Hung et al., 2014).

Because the premise, source and validation of visceral adipose tissue measured using MRI was in question, it was not pursued in further analysis.

### *5.1.3 Validation, Segmentation and Repeatability/Reliability of Imaging Brown Adipose Tissue (BAT)*




Validation of fat fraction values in BAT and WAT excised from rodents was assessed. In the rodents, mean excised BAT and WAT voxel FFs were significantly different ($p_{WAT\text{-}BAT}<10^{-5}$). *Ex vivo* $iBAT_{FF}$ (43.7±7.8% SD) was 30% lower than perirenal $WAT_{FF}$ (73.3±10.4%) (Figure 5.1.3a). Excised WAT tissue was found to have a larger spread in FF values as well as a relatively asymmetric distribution (skewness=-0.85) as compared to that of BAT tissue (skewness=-0.27). The distribution of WAT reflects its upper bound as it lies on the interval zero to one (e.g. beta distribution).

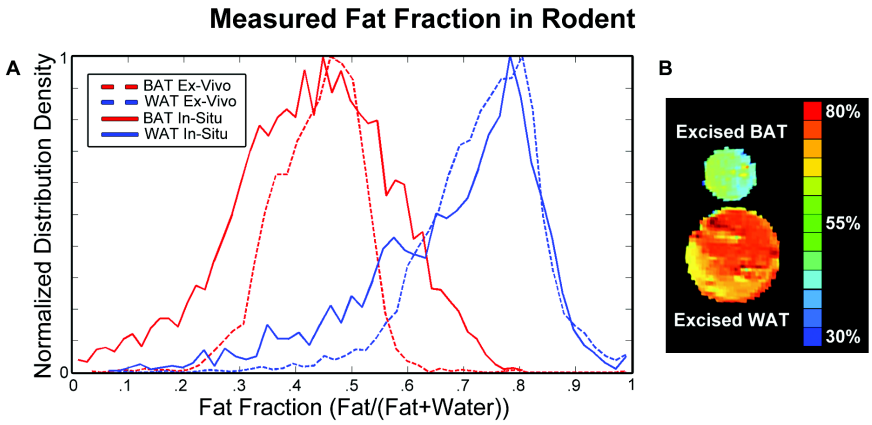



**Figure 5.1.3a. Fat Fraction in Rodent.** Measured fat fraction in rodent demonstrates differentiation in fat fraction between white and brown adipose tissues. (A) *In situ* and *ex vivo* samples of BAT (brown adipose tissue) and WAT (white adipose tissue). (B) Single slice fat fraction map of *ex vivo* tissues in glass vials.

Interscapular BAT (iBAT) regions were qualitatively identifiable between the scapulae in all 6 rodents imaged. Subcutaneous adipose tissue deposits were not accurately resolved due to the lower limit on spatial resolution for this protocol. The larger and more isotropic perirenal WAT deposits were easily identified. *In situ* relative to *ex vivo* FF differences were 0.8% and 5.4% in iBAT and WAT respectively ($p_{WAT-BAT}<10^{-5}$,iBAT$_{FF}$=43.0ATferences $_{FF}$=67.9ATferences were 0.*in situ* compared to ex vivo measurement of iBAT FF showed a nearly two-fold larger standard deviation ($SD_{in\ situ}/SD_{ex\ vivo}$=1.81).

All 22 human infants showed strong evidence for BAT deposits in spine, supraclavicular, and axillary regions (Figure 5.1.3b). Spine, supraclavicular, axillary and union BAT region (Figure 5.1.3c) fat fractions and depot volumes are reported in Table 5.1.3a. Depot volume was more variable than FF in all regions, with the greatest depot volume variability found in supraclavicular BAT. Subcutaneous nuchal WAT had a mean FF of 67.7±4.6%. BAT and WAT FF means were significantly differentiated, pairwise, *in vivo* ($\Delta_{WAT-BAT}$=38%, $p<10^{-4}$). In all four regions, FF was significantly positively correlated with depot volume ($R_{spine}^2$=71%, $p_{spine}<10^{-3}$; $R_{sc}^2$=25%, $p_{sc}<0.05$; $R_{axillary}^2$=49%, $p_{axillary}<10^{-3}$; $R_{union}^2$=31%, $p_{union}<0.05$).

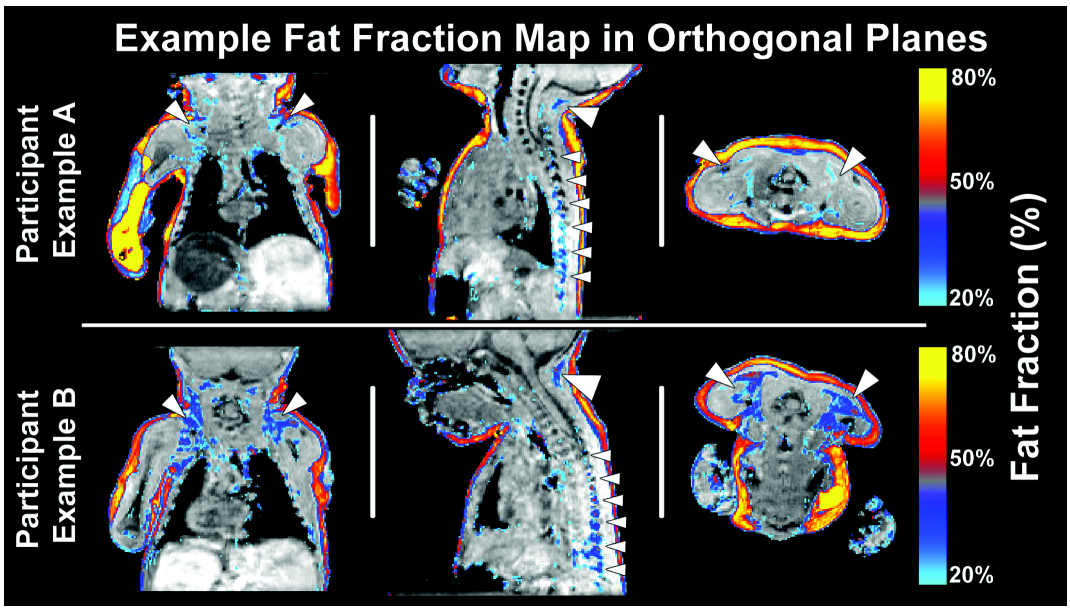



**Figure 5.1.3b. Fat Fraction In Three Planes.** Three-plane view of BAT (brown adipose tissue) in a participant with relatively large (bottom row) and small (top row) deposits. Arrows in the axial and coronal views indicate supraclavicular/axillary BAT. Arrows in the sagittal view indicate bilateral spinal BAT deposits. Underlay volume is the in-phase echo.

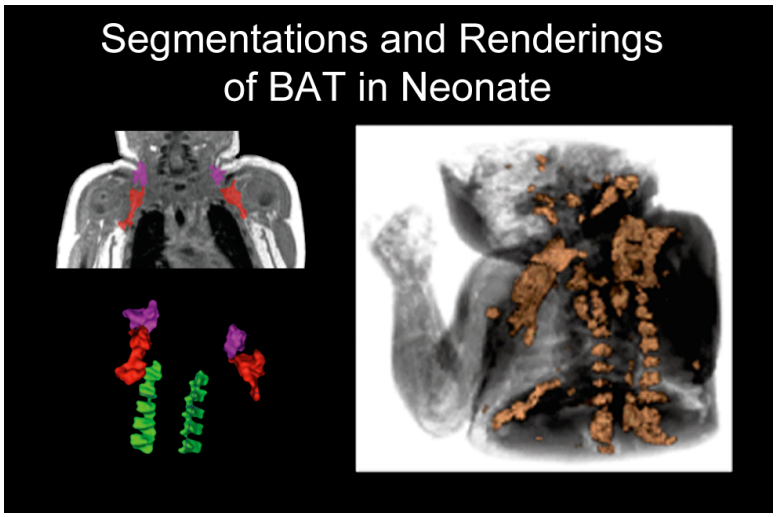



**Figure 5.1.3c. Neonatal Segmentations.** BAT (brown adipose tissue) segmentations in the neonate. From left to right: sagittal view of semi-automatic segmentations of spine T1-T5 (green), coronal view of supraclavicular (magenta) and axillary (red) ROIs, the 3-dimensional render of ROIs used in this manuscript, a 3-dimensional render of all voxels that fit the BAT criteria used in this manuscript for visualization (rust color).

| | Volume (cc) | | FF (%) | |
|---|---|---|---|---|
| | **Mean+/-SD** | **Range** | **Mean+/-SD** | **Range** |
| **Supraclavicular** | 2.95+/-1.32 | 0.53-6.13 | 28.9+/-4.0 | 21.9-40.0 |
| **Axillary** | 3.76+/-2.00 | 0.52-8.72 | 30.3+/-3.3 | 24.9-35.3 |
| **Union** | 6.50+/-3.10 | 1.05-14.60 | 29.5+/-3.7 | 22.9-35.2 |
| **Spine T1-T5** | 3.65+/-1.40 | 1.02-6.70 | 32.2+/-3.2 | 25.4-38.1 |

**Table 5.1.3a. Summary of Brown Adipose Tissue Depot Volume and Fat Fraction.** Fat fraction (FF) defined as the ratio of fat signal to the sum of fat and water signal on a voxelwise basis.

Fat fraction maps derived from two independent acquisitions of a single participant were visually indistinct from one another (Figure 5.1.3d). The highest intensities found in the fat fraction difference map were limited to the exterior border interface of fat/air and a small region within the hand containing a phase swap artifact. The mean residuals between scan and re-scan were 2.7% in BAT, 2.6% in WAT and 2.8% across the entire image. Voxelwise fat fractions were strongly correlated with one another (Figure 5.1.3e) in all segmented BAT voxels ($R_{BAT}^2$=88%), subcutaneous nuchal WAT voxels ($R_{WAT}^2$=78%) and all remaining voxels ($R_{ALL}^2$=99%). The mean fat fraction difference between BAT and WAT was 18-fold greater than the mean residual between scans, suggesting a high level of BAT/WAT tissue differentiation repeatability from scan to scan.

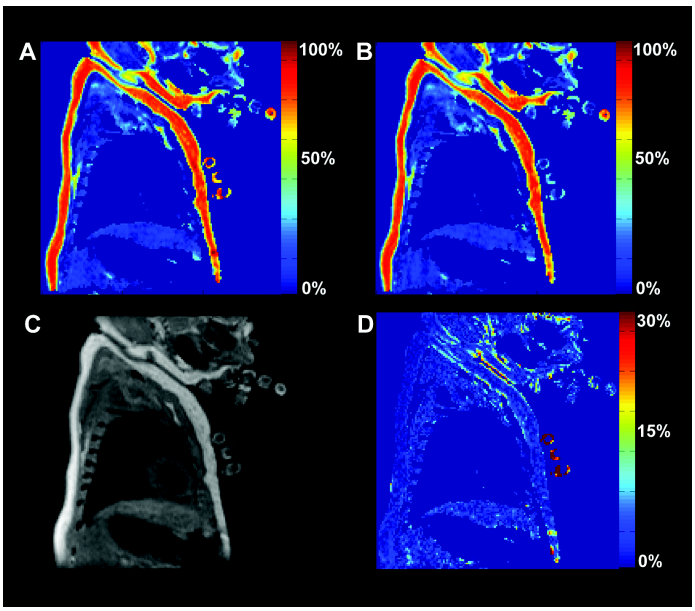



**Figure 5.1.3d. Acquisition Repeatability.** Sagittal view of scan/rescan comparison of Dixon based fat fraction maps in a single neonate. (A) First scan followed by (B) re-shimming and an identical repeat scan, hotter color denotes a higher fat fraction. (C) In-phase image depicting underlying anatomy. (D) Difference map in calculated fat fraction, note highest intensities are found at edges due to mis-registration between scans and an inhomogeneity artifact present in the fingers anterior to the chest.

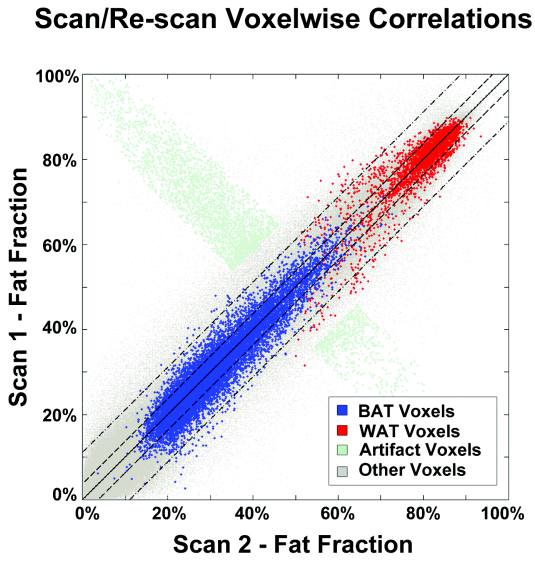



**Figure 5.1.3e. Voxelwise Repeatability.** Voxel by voxel fat fraction correlation between scans. Strong voxelwise correlations between scans were observed in BAT segmentations (blue, $R_{BAT}=^{2}88\%$), a WAT segmentation done in the nape of the neck (red, $R_{WAT}{}^{2}=78\%$) and all other voxels (gray, $R_{ALL}=99\%$). Artifact voxels are those identified in the hand.

Inter- and intra-rater measurements of regional BAT depot volume and FF showed a high degree of reliability for all four ROIs examined in this study (Table 5.1.3b). Spinal and supraclavicular/axillary union BAT depot volumes had the highest degree of between-rater reliability, followed by the supraclavicular region. Despite assessments being performed 2 weeks apart, intra-rater reliability was found to be slightly higher than inter-rater reliability. With the exception of axillary fat fraction, inter- and intra-rater performance of fat fraction characterization exceeded that of depot volume quantification. The supraclavicular/axillary union and bilateral spinal regions were seen to be the most robust to rater differences. The predominantly high intra-class correlations (Table 5.1.3b) demonstrate the ability of the applied segmentation method to reliably measure BAT FF and depot volume in infants.

| | **Depot Volume** | | | | | | **Fat Fraction** | | | | | |
|---|---|---|---|---|---|---|---|---|---|---|---|---|
| | **Inter-Rater** | | | **Intra-Rater** | | | **Inter-Rater** | | | **Intra-Rater** | | |
| | **ICC** | **WSC** | **N** | **ICC** | **WSC** | **N** | **ICC** | **WSC** | **N** | **ICC** | **WSC** | **N** |
| **Supraclavicular** | 0.61 | 0.11 | 0.28 | 0.74 | 0.04 | 0.22 | 0.83 | 0.00 | 0.18 | 0.89 | 0.00 | 0.11 |
| **Axillary** | 0.79 | 0.07 | 0.14 | 0.94 | 0.00 | 0.06 | 0.41 | 0.04 | 0.54 | 0.74 | 0.15 | 0.11 |
| **Union** | 0.86 | 0.00 | 0.14 | 0.93 | 0.00 | 0.07 | 0.91 | 0.00 | 0.09 | 0.93 | 0.02 | 0.06 |
| **Spine** | 0.87 | 0.00 | 0.13 | 0.89 | 0.01 | 0.10 | 0.96 | 0.01 | 0.04 | 0.97 | 0.00 | 0.03 |

Table **5.1.3b. Inter- and intra-rater reliability results.** Intraclass correlation coefficients (ICC) are given for inter- and intra-rater. WSC (ratio of within-subject or between-rater variance to total variance) and N (ratio of unaccounted for variance to total variance) are also given.

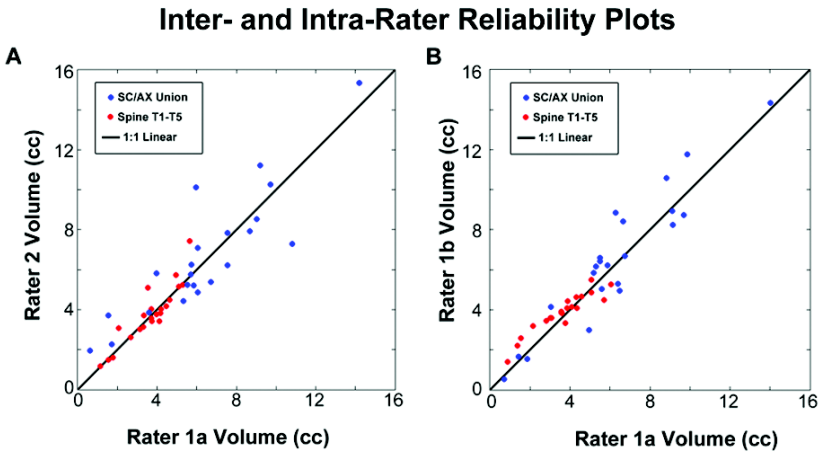
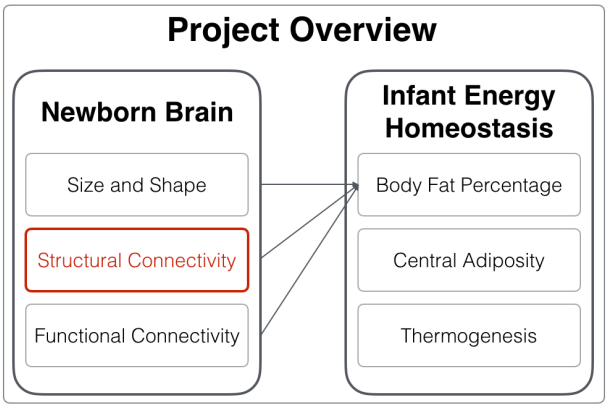



**Figure 5.1.3f. Segmentation Reliability.** (A) Segmentations repeated on 22 subjects by two different raters: supraclavicular/axillary union ROIs (blue, $R^2$=74%) and spinal (red, $R^2$=81%). (B) Segmentations repeated by a single rater separated by two weeks time (1a and 1b): supraclavicular/axillary ROIs (blue, $R^2$=88%) and spinal ROIs (red, $R^2$=88%).

## 5.2 Infant Brain Development

Cross-sectional observations of inter-individual variation in brain development require regressing out age as a covariate of non-interest. Typically this is done using either postmenstrual age or postmenstrual age while correcting for age at scan (or gestational age) in a linear model. Below, I discuss differences and limitations between these approaches as well as develop a novel index that leverages the differential estimated growth before and after birth, the MI. The MI is then applied to Diffusion Tensor Imaging (DTI) in newborns for characterizing typical white matter development in neonates. DTI was performed cross-sectionally in 47 neonates (gestational age at birth=39.1±1.6 weeks [GA], postnatal age at scan=25.5±12.2 days [SA]).

### *5.2.1 Maturation Index Reflects Typical Perinatal White Matter Development*




Three sets of simulated data were evaluated for illustrative purposes (Figure 5.2.1a). The two non-linear sets (prenatal-only or postnatal-only change) had predictably marked increases in explained variance ($R_{PM}^2$=50%; $R_{GA}^2$+$R_{SA}^2$=100%) when acknowledging the separate contribution of GA and SA to PM, while the linear set (equal increase in prenatal and postnatal periods) was fully predicted ($R_{PM}^2$=100%; $R_{GA}^2$+$R_{SA}^2$=100%) by both model 1 and model 2.

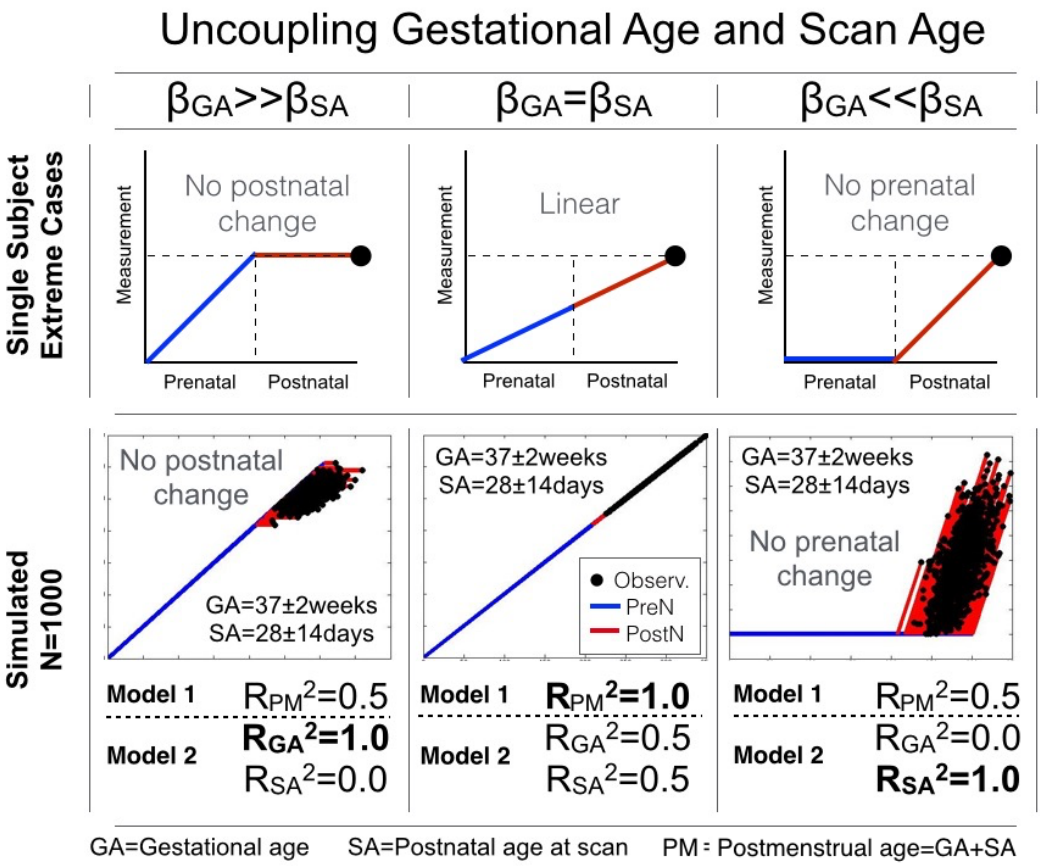



**Figure 5.2.1a. Splitting postmenstrual age (PM) into gestational age (GA) and age at scan (SA).** Top row: Cartoon depicting three distinct paths to the same outcome. Bottom row: Three sets ($\beta_{GA}>>\beta_{SA}$; $\beta_{GA}=\beta_{SA}$; $\beta_{GA}<<\beta_{SA}$) of outcomes (N=1,000) were generated using the model $Y=\beta_{GA}*GA+\beta_{SA}*SA$ with normally randomized GA (259+/-14 days) and SA (28+/-14 days). The PM age dependence (model 1) is significant in all three sets, however only the use of model 2 (GA and SA) is able to explain 100% of the variance in all three sets.

MI plotted against the F-Ratio comparing models 1 and 2 demonstrated increasing significance, and variability in significance, with increasing MI magnitude. Observations with large MI magnitude and high significance are driven by a sizeable relative difference between $\beta_{i,GA}$ and $\beta_{i,SA}$ that results in a significant increase in explanatory power. A parabolic upper limit was observed centered around an MI value of zero (the point at which $\beta_{i,GA} = \beta_{i,SA}$ and model 2 reduces to model 1, hence a null increase in power) (Figure 5.2.1b). The values contradicting this upper limit represent the points at which separating $\beta_{i,GA}$ and $\beta_{i,SA}$ allowed one of the other covariates (intracranial volume and/or sex) to significantly increase the explanatory power of model 2. These outlying points were limited to less than 0.1% of total observations. Points with large MI magnitude, but small F-Ratio,

suggest observations that had an optimized model with $\beta_{i,GA}$ unequal to $\beta_{i,SA}$. However, in these points, separating GA and SA resulted in little increase in explanatory power, likely due to the over-fitting of noise by the unrestricted variables GA and SA.

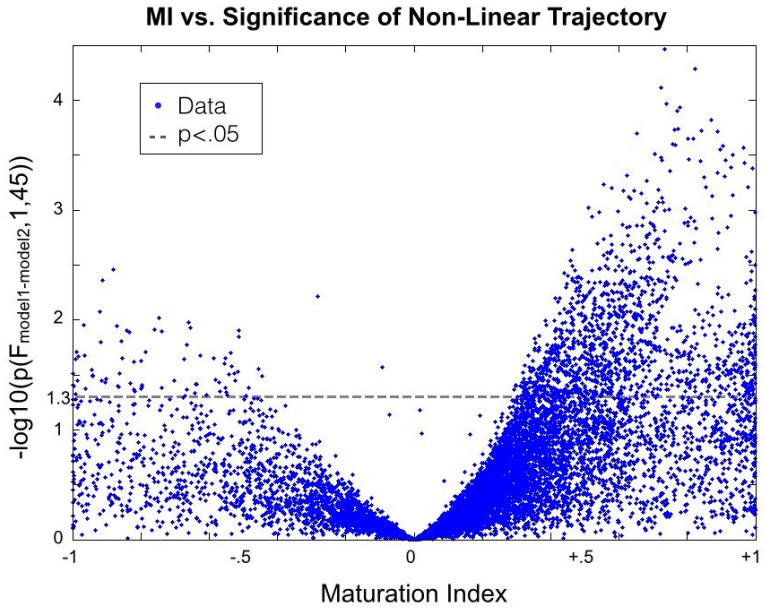



**Figure 5.2.1b. Explanatory Power Increase as a Function of Maturation Index.** The increase in explanatory power when separating PC into GA and SA is plotted against MI**.** MI reflects the change in estimated rates of change after birth relative to the estimated rate before birth. A large difference in slopes before and after birth results in a large magnitude MI and large increase in explanatory power when considering GA and SA as independent variables.

The MI across all fiber tracts revealed *global* differences in diffusion metrics (interquartile range, Q1/Q2/Q3: $MI_{FA}$=-0.12/+0.09/+0.26, $MI_{RD}$=0.05/0.25/0.40, $MI_{AD}$=0.09/0.34/0.59, Figure 5.2.1c). All MI measurement distributions were skewed with long tails in the negative MI region, a region indicating more rapid post-natal compared to prenatal fiber maturation. $MI_{AD}$ had the most skewed distribution of the three (skew[$MI_{FA}$]=-0.03, skew[$MI_{RD}$]=.09, skew[$MI_{AD}$]=-0.25), reflective of relatively early change in AD. The hypothesized order of MI values ($MI_{AD}$>$MI_{RD}$>$MI_{FA}$) was confirmed ($MI_{RD}$>$MI_{FA}$, $\Delta_{RD\text{-}FA}$=+0.17, 95% CI [.154 .195], $p_{RD\text{-}FA}<10^{-10}$; $MI_{AD}$>$MI_{RD}$, $\Delta_{AD\text{-}RD}$=+0.10, 95% CI [.074 0.112], $p_{AD\text{-}RD}<10^{-10}$).

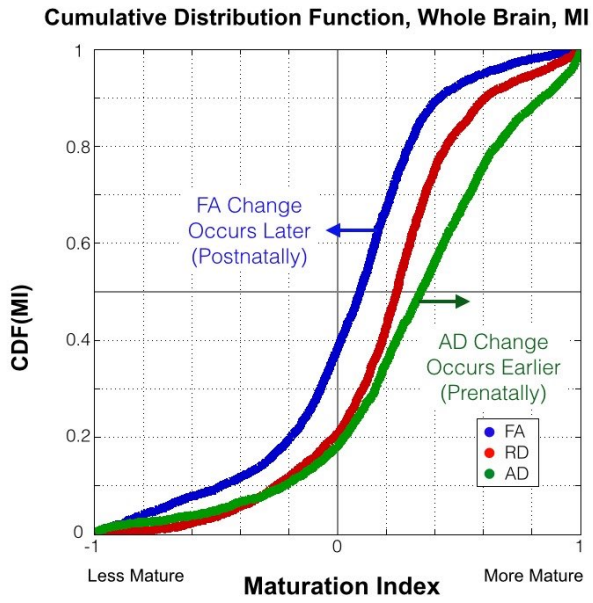



**Figure 5.2.1c. Cumulative Distribution Function of $MI_{FA}$, $MI_{RD}$, and $MI_{AD}$.** $MI_{FA}$ was significantly greater than $MI_{RD}$ ($p_{paired}<10^{-10}$) and $MI_{RD}$ was significantly greater than $MI_{AD}$ ($p_{paired}<10^{-10}$) across the whole brain. Large MI results from a greater estimated rate of change prenatally relative to postnatally.

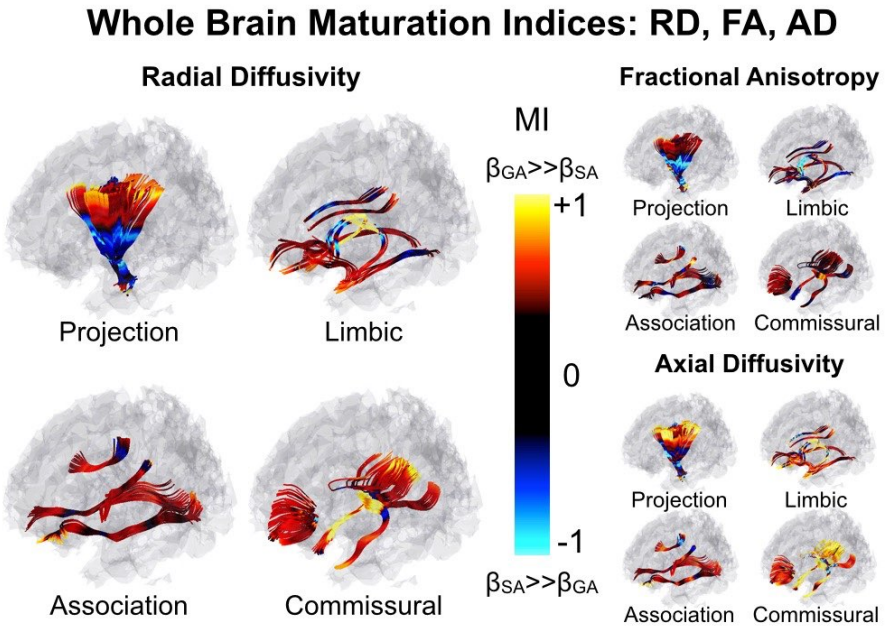



**Figure 5.2.1d. Whole Brain Maturation Index Map.** White matter tracts are separated by group: Projection (Inferior-Superior), limbic (limbic connections), association (anterior-posterior), and commissural (left-right). Note the large negative $MI_{RD}$ in the inferior projection fibers (internal capsule), and large positive $MI_{RD}$ in the more peripheral ends of the tract. $MI_{RD}$ is emphasized, here, as it is predictive of both $MI_{FA}$ and $MI_{RD}$.

A quantitative map of MI across the brain's white matter tracts can be seen in Figure 5.2.1e. In addition to the global differences in $MI_{FA}$, $MI_{RD}$ and $MI_{AD}$, there are apparent differences between fiber groups. Specifically, $MI_{FA}$, $MI_{RD}$ and $MI_{AD}$ were greatest in commissural fibers, lowest in projection fibers, and with moderate values in association and limbic fibers (Table 5.2.1a). While this is discussed in more detail below, these findings are reflective of large regions of negative MI bilaterally in the projection fibers, and large regions of positive MI bilaterally in the fornix and the tapetum of the corpus callosum.

| Fiber Group | $MI_{FA}$ | $MI_{RD}$ | $MI_{AD}$ |
|---|---|---|---|
| **Commissural**** | .01/.18/.32† | .20/.34/.49 | .23/.49/.73† |
| **Association*** | -.04/.14/.28† | .11/.21/.33† | .11/.23/.41 |
| **Limbic**** | -.15/.04/.19 | .10/.25/.44† | .17/.39/.60† |
| **Projection**** | -.42/-.03/.20 | -.26/.03/.27 | -.18/.16/.47 |

**Table 5.2.1a. Interquartile values of $MI_{FA}$, $MI_{RD}$ and $MI_{AD}$ by fiber group.** The statistics for MI are shown using the interquartile range, 25/50/75. Commissural fibers had the largest MI and projection fibers had the lowest, with association and limbic fibers in the middle. The order of microstructural MI is retained in all fiber groups. *, ** denote fiber group retained $MI_{FA}<MI_{RD}<MI_{AD}$ within the fiber group at a minimum pairwise significance of $p<0.005$, or $p<10^{-10}$, respectively. Each microstructure MI had a pair of fiber groups that were *not* significantly different (two sample t-test, $p>.05$), these pairs are denoted with a †. All other pairs were significant at $p<0.05$.

All 27 tracts assessed in this study had at least one cluster with significantly ($p<0.05$, Equation 3) positive $MI_{RD}$. The top ten (by significance) positive $MI_{RD}$ clusters are shown below (Table 5.2.1b). Only 4 of the 27 tracts assessed had significant clusters of negative $MI_{RD}$. All 4 of the significant clusters were located in the *left* sided projection fibers. At the trend level ($p<0.1$), three of the four *right* sided projection fibers and the left optic tract were also significant (Table 5.2.1c) suggesting left-right asymmetric development.

| Tract | Cluster Extent (%) | Loc. | Coord. MNI | $\beta_{RD,GA}$ (%/week) | $\beta_{RD,SA}$ (%/week) | $\Delta\beta_{RD}$ (%) | $MI_{RD}$ | $p(F)_{min}$ |
|---|---|---|---|---|---|---|---|---|
| L Par. Post. CF | 10 | SPG | -16,-55,56 | -5.4 | -2.5 | +54 | 0.65 | <0.001 |
| CC Parietal | 8 | SPG | 13,-62,49 | -5.3 | -2.6 | +51 | 0.62 | 0.002 |
| R Premotor CT | 6 | SFG | 11,6,59 | -5.3 | -1.9 | +64 | 0.77 | <0.001 |
| R Par. Post. CF | 5 | SPG | 17,-37,56 | -5.1 | -2.8 | +44 | 0.53 | <0.001 |
| CC Occipital | 4 | SOG | 23,-86,31 | -5.1 | -2.4 | +53 | 0.64 | 0.002 |
| L SLF | 3 | SPG | -28,-44,61 | -4.4 | -1.5 | +67 | 0.80 | <0.001 |
| R Cingulum | 3 | SPG | 12,-53,48 | -5.6 | -3.0 | +46 | 0.54 | 0.003 |
| R Fornix | 3 | ITG | 35,2,-35 | -5.0 | -2.0 | +60 | 0.78 | 0.003 |
| R ILF | 2 | STG | 49,8,-17 | -4.4 | -1.9 | +58 | 0.69 | 0.002 |
| R IFOF | 1 | MOG | 18,-101,-5 | -4.8 | -2.5 | +47 | 0.55 | 0.004 |

**Table 5.2.1b. Estimated rates of change for, and coordinates of, significant clusters of *positive* $MI_{RD}$.** Top ten clusters identified as having a significant ($p<0.05$) increase in explained variance when splitting up postmenstrual age into gestational age and age at scan. All metrics are averaged across clusters unless otherwise specified. Cluster extent is expressed in percentage of length relative to the tract. TC=Thalamocortical, CF=Corticofugal, CT=Corticothalamic, SLF=Superior Longitudinal Fasciculus, ILF=Inferior Longitudinal Fasciculus, IFOF=Inferior Fronto-Occipital Fasciculus, SPG=Superior Parietal Gyrus, SFG=Superior Frontal Gyrus, SOG=Superior Occipital Gyrus, MOG=Medial Occipital Gyrus, STG=Superior Temporal Gyrus, MTG=Medial Temporal Gyrus, ITG=Inferior Temporal Gyrus.

| Tract | Cluster Extent (%) | Loc. | Coord. MNI | $\beta_{RD,GA}$ (%/week) | $\beta_{RD,SA}$ (%/week) | $\Delta\beta_{RD}$ (%) | $MI_{RD}$ | $p(F)_{min}$ |
|---|---|---|---|---|---|---|---|---|
| L Motor CT | 13 | PLIC | -25,-15,23 | -1.6 | -2.9 | -84 | -.54 | 0.02 |
| L Par. Post. TC | 11 | PLIC | -25,-21,21 | -1.1 | -2.4 | -127 | -.68 | <0.01 |
| L Par. Post. CF | 10 | CP | -15,-22,-12 | -1.1 | -2.7 | -142 | -.68 | 0.01 |
| L Premotor CT | 9 | PLIC | -22,-7,17 | -1.6 | -2.9 | -81 | -.53 | 0.02 |
| R Par. Post. TC | 9 | PLIC | 24,-20,17 | -1.3 | -2.0 | -62 | -.45 | 0.05 |
| R Motor CT | 9 | PLIC | 24,-15,17 | -1.0 | -2.0 | -102 | -.58 | 0.06 |
| L Optic | 3 | ST | -29,-25,-2 | -1.2 | -2.3 | -89 | -.55 | 0.08 |
| R Premotor CT | 3 | PLIC | 21,-6,15 | -1.0 | -2.1 | -104 | -.61 | 0.09 |

**Table 5.2.1c. Estimated rates of change for, and coordinates of, significant clusters of *negative* $MI_{RD}$.** Four clusters were identified as having a significant ($p<0.05$) increase in explained variance when splitting up post-conceptional age into gestational age and age at scan. Four additional clusters are listed at the trend level ($p<0.1$). All metrics are averaged across clusters unless otherwise specified. Cluster extent is expressed in percentage of length relative to the tract. PLIC=Posterior Limb Internal Capsule, ST=Stria Terminalis, CP=Cerebral Peduncle.

Diffusivity measures, MI and fitted slope values are shown for the left premotor corticospinal tract in Figure 5.2.1e. As seen in the figure, the tract can be considered as two distinct regions (peripheral and central) bisected by the switch in sign of MI and changing microstructural properties (FA, RD, AD), reflective of the anatomical transition into the internal capsule. The peripheral portion can be described as having: 1) small FA, large RD and moderate to high AD, 2) large positive $MI_{AD}$ and $MI_{RD}$, and 3) large differences in AD and RD *beta* values with $\beta_{GA}>\beta_{SA}$. Conversely, the central portion can be qualitatively described as having: 1) large FA, small RD and moderate to low AD, 2) large negative $MI_{FA}$ and $MI_{RD}$, and 3) large differences in *beta* values with $\beta_{SA}>\beta_{GA}$. Percent differences in rates of change before and after birth for FA, RD and AD in the peripheral portion were +32%, +62% and +107%, respectively. For the central portion the same changes in FA, RD and AD were -43%, -41% and -27%.

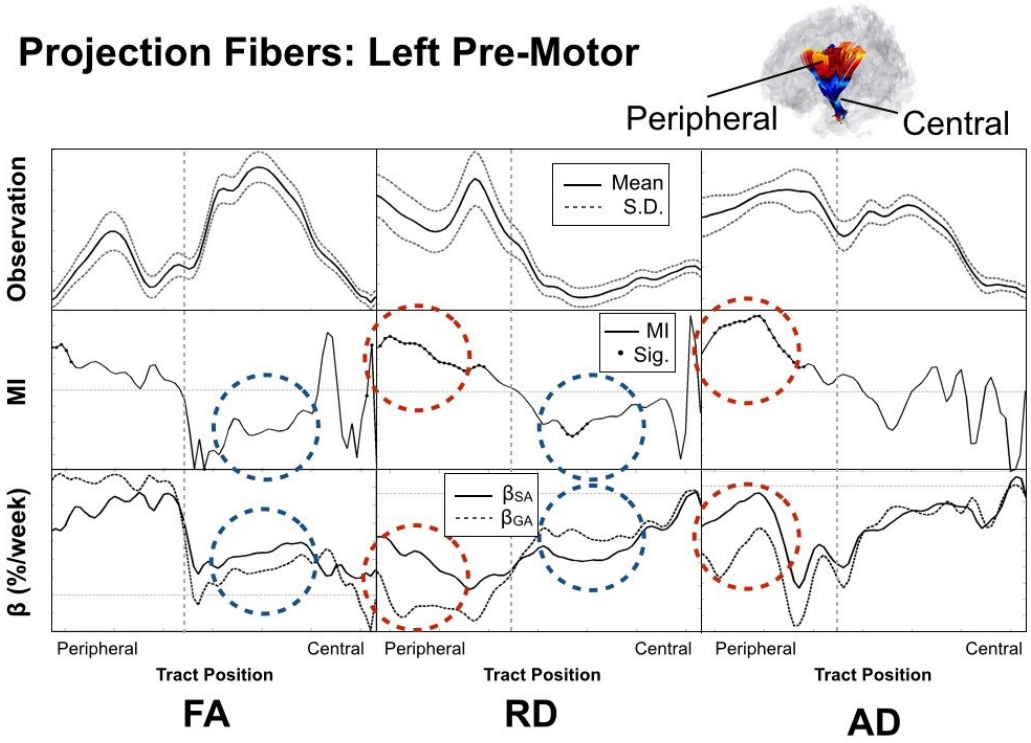
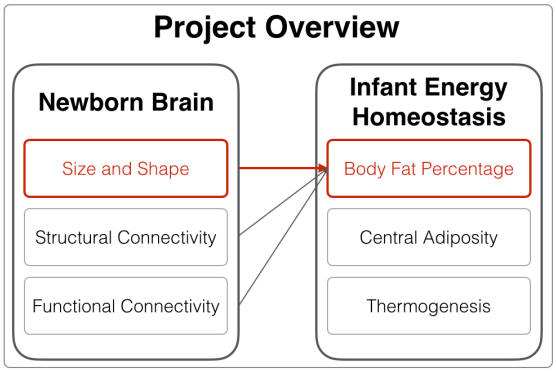



**Figure 5.2.1e. Detailed Features Along the Left Premotor Tract.** Top row: microstructural value (FA, RD, AD); Middle row: Maturation index; Bottom row: estimated rate of change (GA dashed line, SA solid line). Note the clear delineation between inferior and superior regions (marked by vertical dashed lines) reflected in the anatomy, MI and rate of change. Red dashed circles highlight a peripheral region with large positive $MI_{RD}$ and $MI_{AD}$, reflective of premyelination and blue dashed circles highlight a central region with large negative $MI_{RD}$ and large negative $MI_{FA}$ reflective of true myelination. The sign of $MI_{RD}$ indicates rapid premyelination prior to birth and an acceleration of true myelination following birth.

## 5.3 Prospective Associations Between Newborn Brain MRI-Phenotypes and Early Life Adiposity Gain

The prospective associations between newborn gray matter volume in the insula, structural connectivity near the amygdala/thalamus and functional amygdala connectivity with early life fat gain are given below.

### *5.3.1 Newborn Insula Volume and Early Life Adiposity Gain*




The project obtained complete data in a sample of 52 infants (29 male, 23 female). Mean gestational age at birth was 39.5 ± 1.4 [± SD] wks. Neonatal T1- and T2-weighted MR brain imaging was obtained at 25.9 ± 12.2 [± SD] days after birth. Serial DXA assessments were obtained shortly after birth (11.4 ± 24.6 [± SD] days) and at six-months age (26.7 ± 3.3 [± SD] wks).

Newborn and six-month body fat percentages were adjusted for the expected (and observed; see below) effects of gestational age at birth and postnatal age at scan using a General Linear Model (GLM). The longitudinal change in ΔBF% was then defined as the change between newborn and six-months time points. Newborn and six-months DXA BF% values were on average 13.4 ± 6.0% (±SD) and 32.1 ± 8.4% (±SD) respectively. The main outcome variable used here, ΔBF%, was +18.4 ± 8.3% (±SD) (i.e., an average increase of 0.80%/week).

Mean ICV, and whole brain GM values were 479±56 $cm^3$ (±SD), and 258±31 $cm^3$ (±SD), respectively. ICV and whole brain GM were significantly associated with gestational age at birth ($p_{ICV}<10^{-3}$, $\hat{\beta}_{ICV}=0.58$; $p_{GM}<10^{-5}$, $\hat{\beta}_{GM}=0.69$) and postnatal age at scan ($p_{ICV}<10^{-3}$, $\hat{\beta}_{ICV}=0.49$; $p_{GM}<10^{-5}$, $\hat{\beta}_{GM}=0.56$). Left and right insula GM volumes were on average 1378±296$mm^3$ (±SD) and 1320±292$mm^3$ (±SD), respectively. As anticipated, left and right insula GM volumes were correlated ($R^2=44\%$,$p<10^{-5}$). Insula GM volumes were associated

with ICV ($\eta^2_{Left}$=31%, $p_{Left}<10^{-5}$; $\eta^2_{Right}$=28%, $p_{Right}<10^{-5}$) but were not associated with gestational age at birth ($p_{Left}>0.1$; $p_{Right}>0.1$) or postnatal age at scan ($p_{Left}>0.1$; $p_{Right}>0.1$).

Left/right averaged insula volume was negatively associated with ΔBF% after correcting for gestational and postnatal age at scan (Figure 5.3.1a; $\beta_{insula}$=-3.6%/S.D., $R^2_{insula}$=18.6%, $p_{insula}$=0.001). The left and right insula were roughly equal contributors to this association ($\beta_{Left}$ =-3.4%/S.D., $R^2_{Left}$=16.7%, $p_{Left}$ =0.002; $\beta_{Right}$ =-3.1%/S.D., $R^2_{Right}$=14.4%, $p_{Right}$ =0.005). Because there was a tendency for a negative association between ICV and ΔBF% ($\beta_{ICV}$ =-2.0%/S.D., $R^2_{ICV}$=5.7%, $p_{ICV}$ =0.086), the analyses were repeated including ICV as a covariate. Although the magnitude of the effect was attenuated, the effect of average insula volume remained significant upon controlling for ICV ($\beta_{insula,ICV}$=-2.4%/S.D., $R^2_{insula,ICV}$=8.2%, $p_{insula,ICV}$=0.038). Receiver Operating Characteristic (ROC) analysis was performed to assess the true positive rate as a function of the false positive rate of classifying an obesity risk proxy measure (>75$^{th}$ percentile ΔBF%) using bilateral gray matter insula volume. The results indicate significant stratification of high- (>75$^{th}$ percentile ΔBF%) and moderate to low-percentile (<75$^{th}$ percentile ΔBF%) participants by insula GM volume (Figure 5.3.1b, AUC=0.74 [95% CI: 0.57-0.91]).

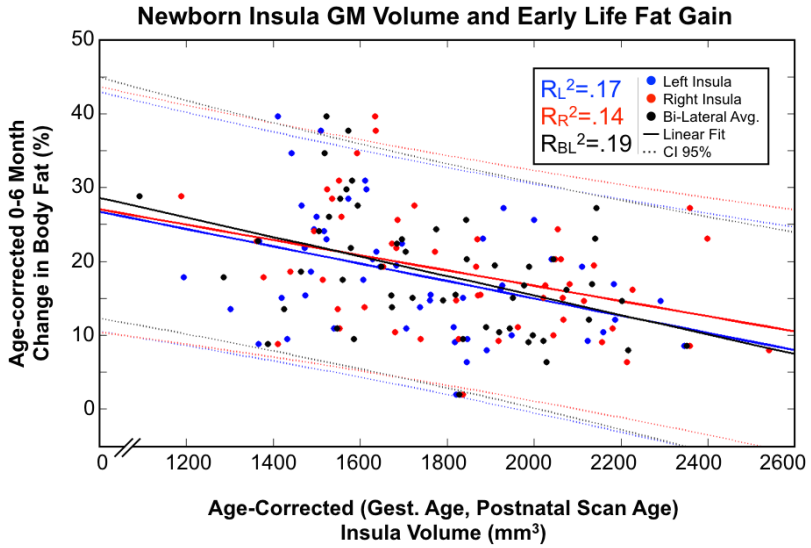



**Figure 5.3.1a. Insula Gray Matter Volume Predicts Adiposity Change in the First Six Months of Life.** Bilateral insula volume at birth is negatively associated with change in body fat percentage.

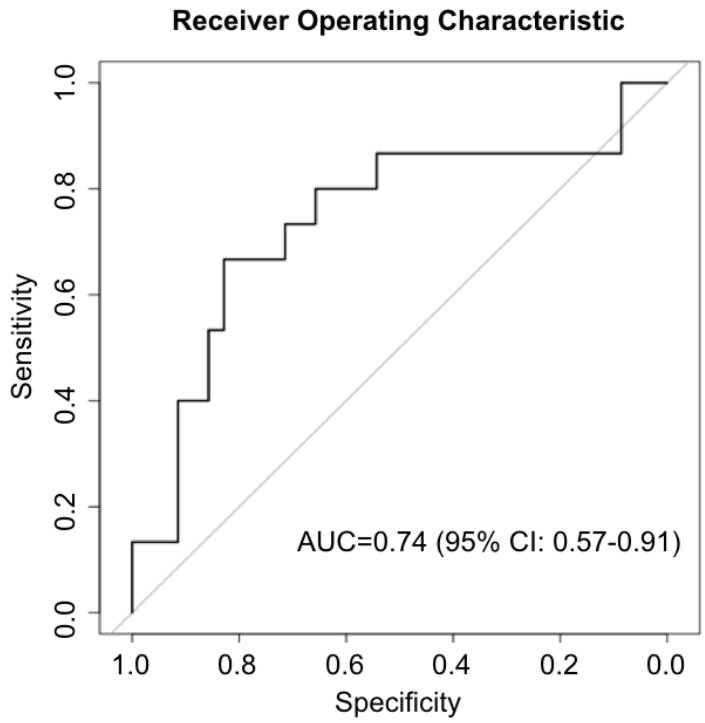



**Figure 5.3.1b. Receiver Operating Characteristic Curve.** The sensitivity and specificity of correct classification (i.e., plot of the true positive rate against the false positive rate) of an obesity risk proxy (>75$^{th}$ percentile ΔBF%) using newborn bi-lateral average insula GM volume. An AUC of 0.74 reflects the utility of insula GM volume to discriminate at-risk individuals (>75$^{th}$ percentile ΔBF%).

Left and right insula were individually parcellated using a tri-sectioning geometric scheme for a post hoc analysis of regional effects within the insula that predict infant adiposity. Regional associations between GM volume and ΔBF% (Figure 5.3.1c) revealed a central-posterior pattern of significance. These findings are spatially consistent with cortical representations of gustation and interoception as defined by electrocortical stimulation (27), magnetoencephalography (28) and functional MRI in humans (26, 29). The effect of the posterior section of the trisected parcellation was the most significant one in both left and right insula ($\beta_{Left,posterior}$=-3.5%/S.D., $p_{Left,posterior}$=0.005; $\beta_{Right,posterior}$=-3.3%/S.D., $p_{Right,posterior}$=0.009;).

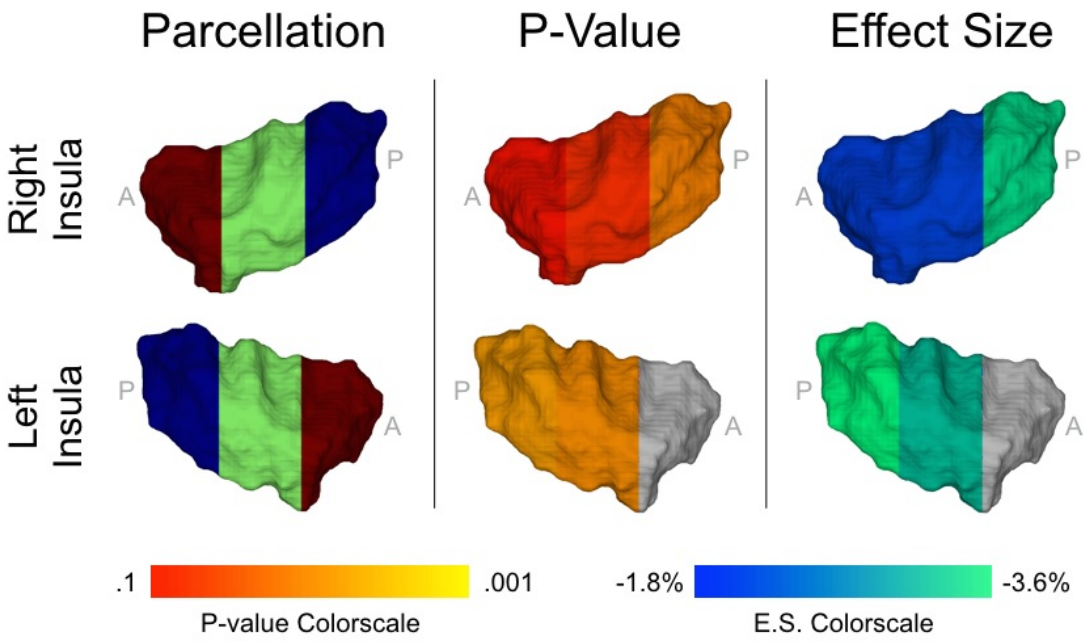
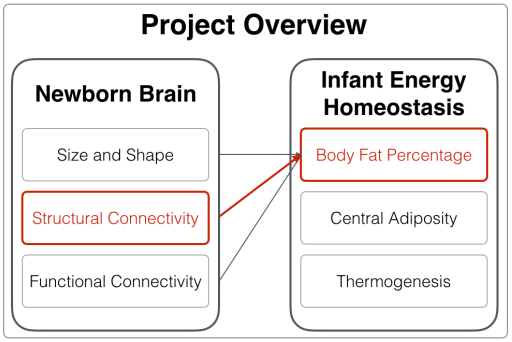



**Figure 5.3.1c. Sub-parcellation of the Insula Suggests a Central-Posterior Pattern of Association between Insula GM Volume and Infant Adiposity.** The insula was geometrically parcellated using a three-region scheme. Central-posterior insula GM volume showed the strongest prediction of early life fat gain. The effect size (E.S.) illustrated here is estimated slope from the General Linear Model, ΔBF% per standard deviation in volume. Left-most row: Dark Blue=Posterior, Green=Central, Dark Red=Anterior.

Post hoc analyses testing for possible confounding effects was performed using the following variables: maternal insulin resistance index (HOMA-IR averaged over three trimesters), sex (separate models for main effects and sex by insula volume interaction), feeding practices (exclusive breastfeeding, exclusive formula feeding or mixed practices), maternal pre-pregnancy BMI, and infant birth weight percentile (i.e., birth weight corrected for gestational age at birth). Bilateral insula GM volume remained significantly ($p<0.01$) associated with ΔBF% when including these covariates. While in stratified analyses the main association between average insula volume and infant adiposity gain appeared weaker in boys ($\beta_{GM,Volume-\Delta BF\%}=3.2\%/S.D.$, $p_{GM,Volume-\Delta BF\%}=0.045$) than in girls ($\beta_{GM,Volume-\Delta BF\%}=4.1\%/S.D.$, $p_{GM,Volume-\Delta BF\%}=0.008$), there was no main effect of sex or interaction effect of sex and insula volume in a full model ($p>0.1$).

*5.3.2 Newborn White Matter Properties and Early Life Adiposity Gain*




The neonatal atlas constructed for section 4.2.1 was used to define FA, AD and RD in 27 major tracts. N=54 neonates were available for correlational analyses considering available diffusion metrics measured along the tract and prospective newborn change in BF%. BF% and diffusion metrics were age-corrected as outlined in above sections 4.1.1 and 4.2.2, respectively.

FA in the left Fornix was negatively associated with early life weight gain in a cluster proximal to the left amygdala (Figure 5.3.2a, $p<10^{-3}$, $R^2=22\%$). This region was also more strongly associated with gestational age at birth than postnatal age-at-scan, suggesting a phenotype largely programmed in utero. The fornix is a major fronto-limbic white matter connection beginning in the septal nuclei and terminating in the temporal lobe.

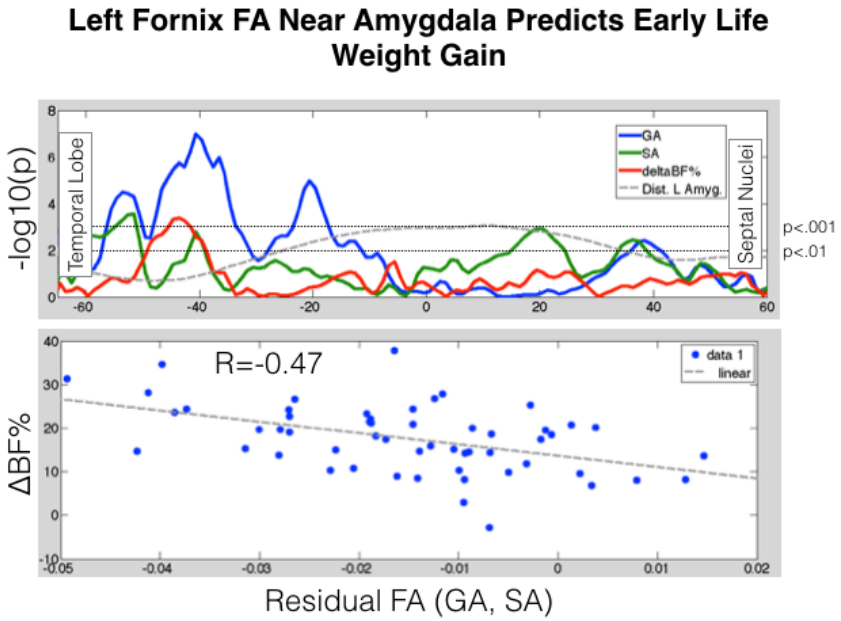



**Figure 5.3.2a. Tract-Based Statistics of Association Between DTI Diffusion Properties and Gestational Age at Birth, Postnatal Age at Scan, and Early Life Fat Gain in the Left Fornix.** Fractional Anisotropy (FA) was negatively associated with early life fat gain in a cluster in the left Fornix close to the left amygdala. GA=Gestational age at birth, SA=Postnatal age at scan, ΔBF%=change in body fat percentage from near birth until six months of age.

FA was also negatively associated with early life weight gain in a cluster proximal to the right thalamus ($p=0.008$, $R^2=15\%$) found in the anterior thalamic radiations. The thalamus is a central hub within the brain and is a major part of relaying gustatory signals from taste receptors in the tongue to the insula.

A cluster inferior to the thalamus (Figure 5.3.2b, $p=0.012$, $R^2=12\%$) and proximal to the NST (Figure 5.3.2b, $p<10^{-3}$, $R^2=24\%$) in projection fibers demonstrated a strong positive association between axial diffusivity and early life fat gain (including moderate associated with FA, $p<0.05$).

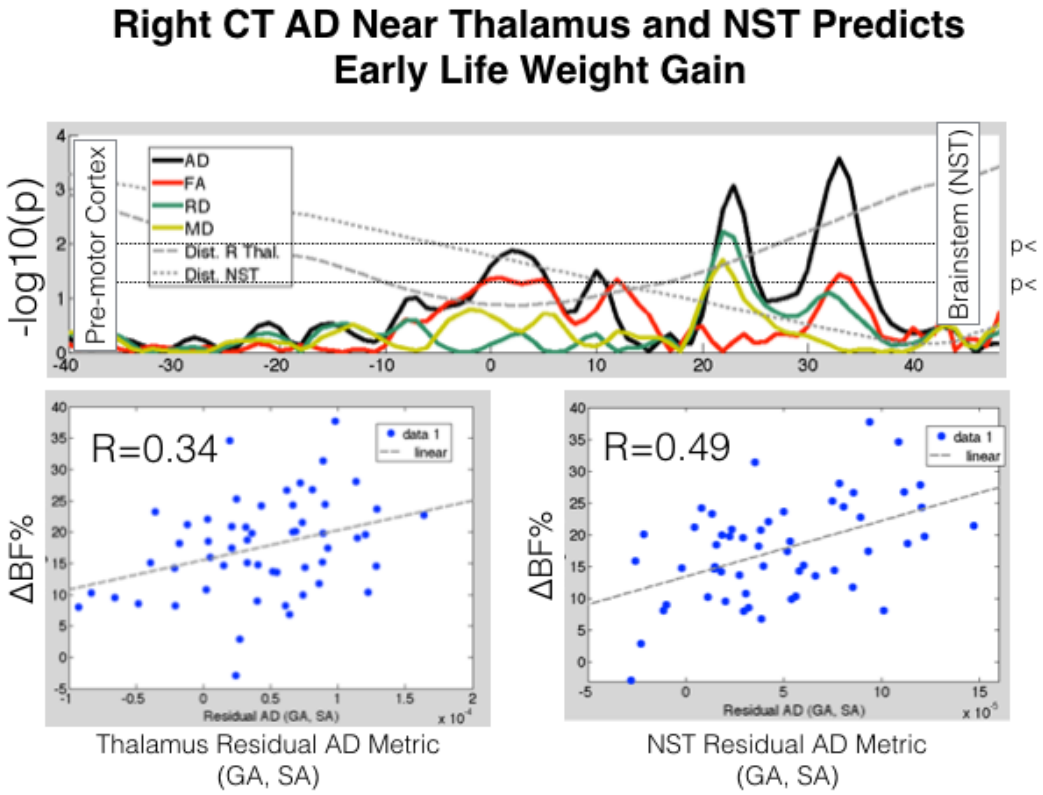
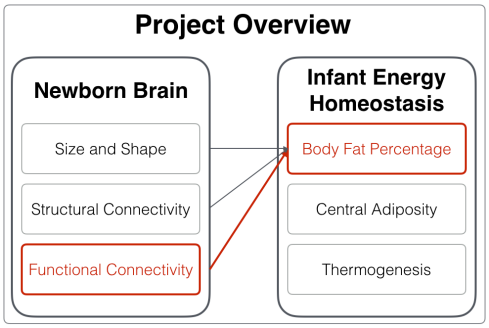



**Figure 5.3.2b. Tract-Based Statistics of Association Between DTI Diffusion Properties and Gestational Age at Birth, Postnatal Age at Scan, and Early Life Fat Gain in the Gustatory Pathway.** Axial Diffusivity (AD) was positively associated with early life fat gain in a cluster in the gustatory pathway near the nucleus of the solitary tract (NST) and thalamus. GA=Gestational age at birth, SA=Postnatal age at scan, ΔBF%=change in body fat percentage from near birth until six months of age.

All clusters identified above were significant at the $p<0.05$ level in a Monte Carlo simulation accounting for multiple comparisons across the tracts. Collectively, these regions correspond to the portions of the gustatory pathway inferior to the thalamus.

*5.3.3 Newborn Functional Connectivity to the Amygdala and Early Life Adiposity Gain*

N=48 participants were available for associations between early life fat gain and functional connectivity to the amygdala.




Associations between functional connectivity and early life fat gain were assessed using amygdala as a seed for connectivity. Both right and left amygdala demonstrated widespread bilateral positive functional connectivity on average ($p<0.005$) in central regions of the brain including basal ganglia, thalamus, brainstem and insula. The posterior cingulate cortex, lateral parietal and medial/lateral frontal cortex were negatively associated with low frequency fluctuations in the amygdala. The whole brain connectivity map can be seen in Figure 5.3.3a.

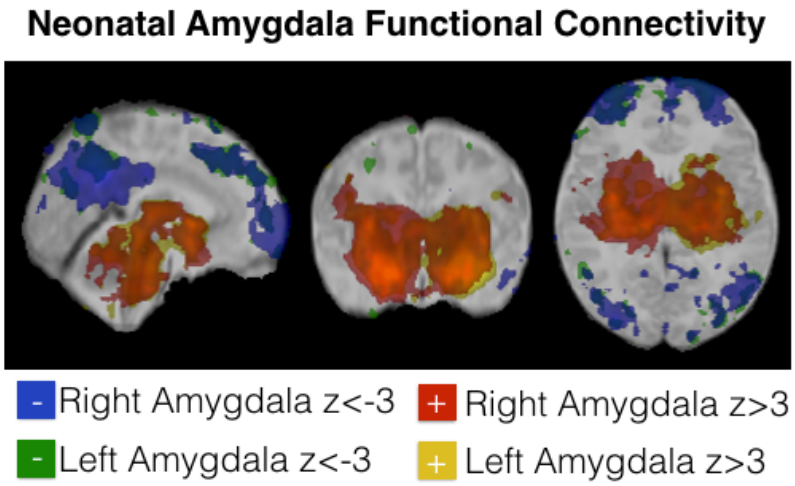



**Figure 5.3.3a. Whole Brain Amygdala Connectivity Map.** Whole brain map of functional connectivity between the right (blue [negative] and red [positive]) and left amygdala (green [negative] and yellow [positive]) is shown. Positive values reflect temporally correlated BOLD signal fluctuation with the amygdala at rest. Negative values reflect temporally *anti*-correlated BOLD signal fluctuation with the amygdala at rest. Right and left amygdala demonstrated similar patterns of connectivity across the brain.

Left amygdala connectivity with bilateral thalamus ($z_{left}$=3.9, $z_{right}$=4.5, p-corrected<0.05), bilateral insula ($z_{left}$=3.5, $z_{right}$=4.3, p-corrected<0.05) and brainstem ($z_{right}$=3.7, p-corrected<0.05) demonstrated effect modification by gestational age at birth in a positive direction (Figure 5.3.3b). That is, neonates born at a later gestational age demonstrated a more positive functional connectivity to the amygdala (for example, thalamus/amygdala connectivity). Right amygdala connectivity exhibited similar, yet attenuated, associations with bilateral thalamus ($z_{left}$=3.8, $z_{right}$=4.3, p-corrected<0.05). No significant associations between left and right amygdala connectivity and postnatal age at scan were detected.

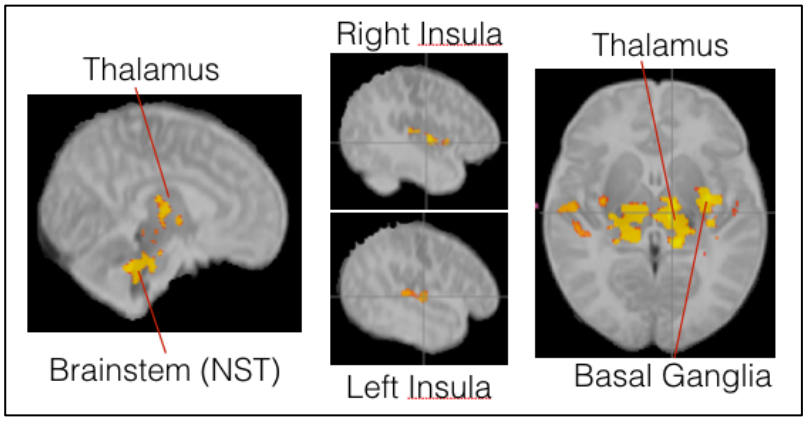



**Figure 5.3.3b. Whole Brain Left Amygdala Connectivity Associations with Gestational Age at Birth.** Left amygdala gestational age associations are shown using a multiple comparisons corrected threshold (p<0.05).

Prospective associations between early life fat gain and functional connectivity to the amygdala were centered on the thalamus and insula (Figure 5.3.3c). Specifically, bilateral thalamus (p-uncorrected$_{left}$=0.018, $z_{left}$=3.3; p-uncorrected$_{right}$=0.026, $z_{right}$=2.9), and right putamen (p-uncorrected$_{right}$<0.01, $z_{right}$=3.0) connections with left amygdala demonstrated positive associations, and right amygdala connectivity between left thalamus (p-uncorrected$_{left}$<0.01, $z_{left}$=2.9;), and bilateral insula (p-uncorrected$_{left}$=0.012, $z_{left}$=4.2; p-uncorrected$_{right}$=0.026, $z_{right}$=3.1), were prospectively associated with early life fat gain. A negative association between right amygdala (only) and ventromedial prefrontal cortex functional connectivity and early life fat gain was also observed (p-uncorrected$_{right}$=<$10^{-3}$, $z_{right}$=-4.3). Note that, despite effect sizes (z-scores) comparable in magnitude to gestational

age associations, the prospective associations with early life fat gain clusters are more spatially disperse, resulting in a more stringent multiple comparisons criteria. Therefore, uncorrected p-values are provided here as the multiple comparisons correction criteria removed the significance ($p<0.1$) from the above clusters.

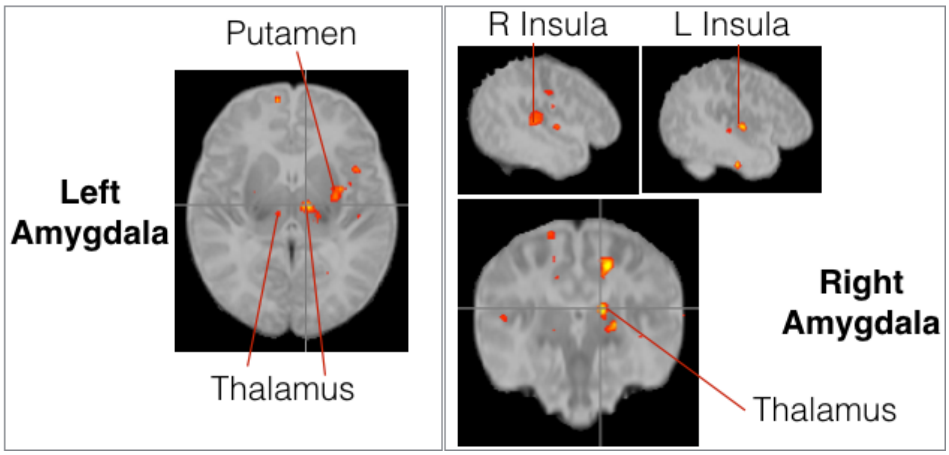



**Figure 5.3.3c. Whole Brain Amygdala Connectivity Associations with Early Life Fat Gain.** Right and left amygdala early life fat gain associations are shown using an uncorrected threshold ($p<0.005$).

A descriptive (preliminary, see section 4.3.3) characterization of within-network connectedness was performed using a mix of functionally (insula, putamen, thalamus and NST) and anatomically (hypothalamus, nucleus accumbens, amygdala, hippocampus) defined ROIs. This approach considers all pairwise connections within the defined network (as opposed to amygdala connections only). As expected, all pairwise ROIs were significantly and positively bivariate functionally connected across participants on average ($p<0.05$). Figure 5.3.3d depicts gestational age at birth as a within-network effect modifier, while Figure 5.3.3e reflects early life functional connections that were prospectively associated with early life weight gain within the energy homeostasis-related network.

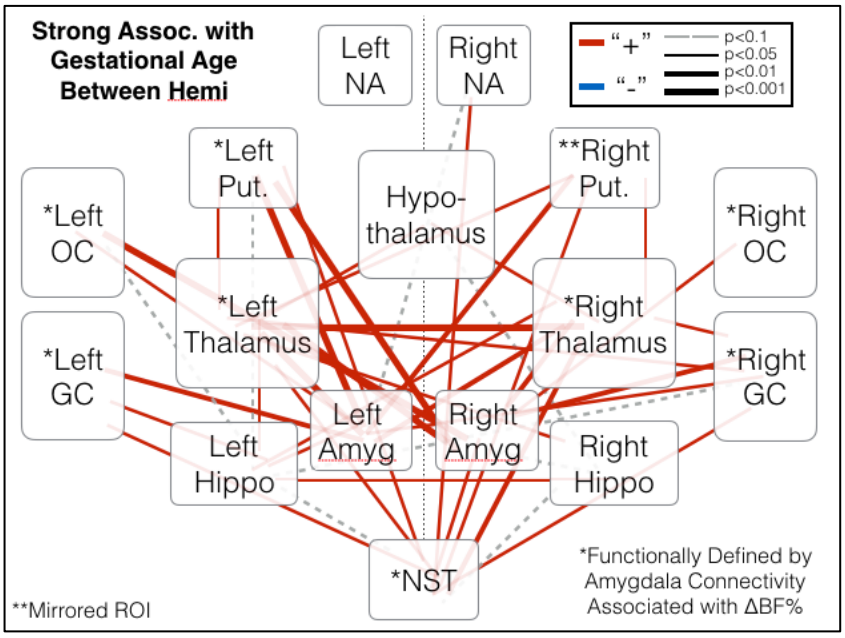



**Figure 5.3.3d. Graph Representation of Feeding-Relevant Functional Connections Modified by Gestational Age at Birth.** Widespread effect modification by gestational age-at-birth on functional connections within feeding-relevant regions is evident. GC=Gustatory Cortex, Hippo=Hippocampus, Put=Putamen, OC=Olfactory Cortex, Amyg=Amygdala, NA=Nucleus Accumbens.

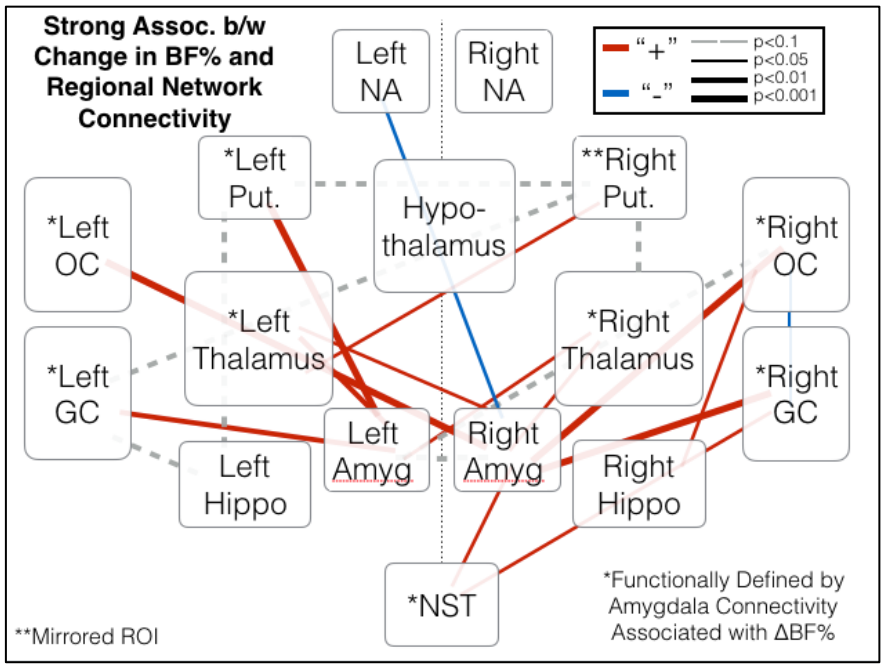



**Figure 5.3.3e. Graph Representation of Feeding-Relevant Functional Connections Prospectively Associated with Early Life Fat Gain.** All prospective associations of early life fat gain by functional connections are positive with the exception of right amygdala to left nucleus accumbens. GC=Gustatory Cortex, Hippo=Hippocampus, Put=Putamen, OC=Olfactory Cortex, Amyg=Amygdala, NA=Nucleus Accumbens.

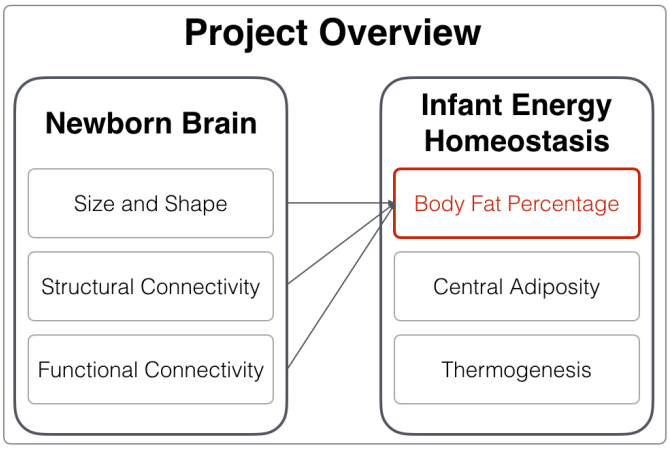
Collectively, these functional connectivity findings reflect widespread feeding-network relevant inter-hemispheric functional connections susceptible to effect modification by gestational age at birth. Multiple connections including amygdala-insula, amygdala-thalamus and amygdala-putamen as well as right-lateralized connections between NST and amygdala/gustatory cortex are prospectively associated with early life fat gain.

# 6 Discussion

Experimental results pertaining to quantification of early life fat accumulation, age models in infant brain development and prospective associations between newborn homeostasis relevant brain circuitry and early life fat gain are discussed below.

## 6.1 Fat Quantification

### *6.1.1 Gestational and Postnatal Age at Birth are Important Covariates of Non-Interest in Quantification of Six-month Change in BF%*

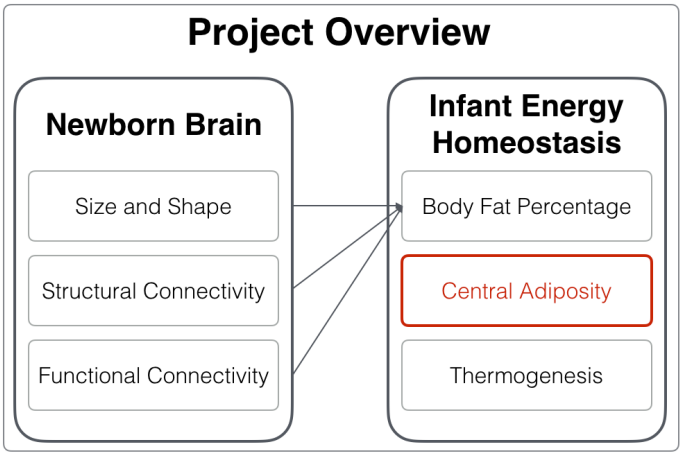



Gestational age at birth and postnatal age at scan were regressed out of newborn and six-month BF% variables prior to determining relative change in BF%. This is well supported in early infancy by data suggesting that BF% increases rapidly in the first few months of life. Conversely, increase in BF% is greatly retarded as it approaches peak-BMI near six months postnatal life. Because of this minimal growth near six months, age-correction at the six-month time point is minimal yet allows for an age independent relative change between the newborn time point and that at six months of age. For this reason, age effects (gestational and postnatal) were a priori regressed out of BF% measurements at birth and six months of age.

Categorical feeding practice status (exclusive breast milk, exclusive formula, exclusive mix) effect on BF% showed a tendency for exclusively breastfed infants to have higher BF% at six months of age, but no effect in relative change in BF%. This result is well supported in current literature. One recent meta-analysis of 15 studies considering body fat percentage in the first year of life demonstrated increased BF% at 6 months of age in exclusively breastfed babies(Gale, Logan, & Santhakumaran, 2012). However, this analysis did not consider relative change in BF%. Another large cohort study including over 5,000 infants

found conditional increases in *weight* from birth until 1 month, but a decrease in weight from 1 month to six months of age in breastfed infants(de Beer, Vrijkotte, & Fall, 2015). Because this study did not consider BF% or fat/lean compartments it is unclear what these gains may be attributed to. A second recent meta-analysis of feeding method on body composition concluded "because of the limited number of studies available, larger studies are needed to clarify the differences in body composition between exclusively/predominantly breastfed and exclusively formula-fed infants."(Gianni et al., 2012) Finally, in a recent cohort study (N=158) of *change* found no effect of feeding status on relative change in FM from birth until 4 months of age(Giannì, Roggero, & Morlacchi, 2014). Collectively, because our results support the concept that absolute but not relative change are effected by breastfeeding status, and because the change in fat mass is the primary outcome variable of interest in this project, it was decided that breastfeeding status would not be a priori regressed out, but would be considered as a post hoc confounding variable in all formal prospective association analyses. Similarly, sex showed a tendency for greater BF% in females in early infancy, but not at six months of age or in relative change in BF% in early life. Therefore, sex was not a priori regressed out of change in BF% but also considered as a post hoc confounding variable in all prospective associations.

### *6.1.2 MRI-Based Visceral Adipose Tissue Quantification Is Questionable*

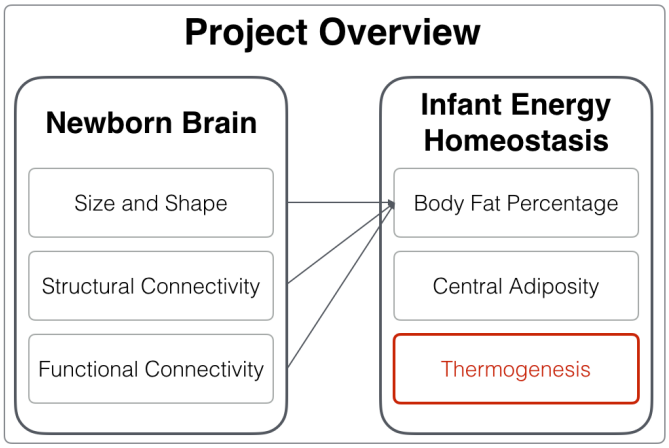



As outlined in above section 5.1.2, motion, bowel status, milk in the gut, and a general lack of visceral adipose tissue at birth suggests that, as implemented, visceral adipose tissue mass in the human neonate is not reliably estimated(Bauer et al., 2015; Hung et al., 2014; Tint et al., 2016). However, future aims should attempt to minimize motion using faster acquisition schemes and milk/bowel confounds may be

addressed using water saturated sampling schemes and/or expert segmentation of the bowels and gut. A more precise and reliable measure of visceral adipose tissue may reduce noise and enable a more meaningful phenotype to be used in observational studies despite the limited abundance in human newborn visceral adipose tissue.

**Insight 1:** The quantification of visceral fat in the human newborn, as measured here using MRI, is not recommended due to confounding signal from milk fat in the gut and stomach and the limited amount of metabolically active visceral adipose tissue present in the neonate.

### *6.1.3 Brown Adipose Tissue (BAT) Composition Quantification Using MRI is Reliable and Repeatable*




The reliability of a non-invasive method for infant BAT imaging based on imaging in rodents and a relatively large cohort of neonates was considered. Previous findings were replicated by demonstrating that multi-echo water-fat MRI-based BAT FF is significantly lower than WAT FF in both rodents ($\Delta_{WAT\text{-}BAT}$ 30%) and neonates ($\Delta_{WAT\text{-}BAT}$ 38%). Neonatal BAT deposit fat fraction and depot volume were quantified using MRI in supraclavicular regions, axillary regions, and bilaterally along the spine. The study findings show high BAT scan/re-scan and segmentation (fat fraction and BAT depot volume) reliability.

The BAT imaging protocol used in this study was validated in rodents by demonstrating that WAT and BAT tissues significantly differ in FF. Recent studies have established, albeit with limited data, that FF in BAT deposits are comparable between rodents and humans. The measured rodent BAT FF in our study (43%) is in tight concordance with previous observations(Hu et al., 2010). To the best of our knowledge, only 3 published reports exist of human neonate BAT FF: the first was a *post mortem* infant with a measured fat fraction of 42%(Hu, Tovar, Pavlova, Smith, & Gilsanz, 2012), the second was limited to two neonate

subjects with fat fractions of 39% and 52%(Hu, Perkins, Chia, & Gilsanz, 2013a), and the third had an infant age range from birth of up to six month with an average of 38.2% BAT fat fraction(Hu et al., 2013b). Closer inspection of infants of similar age in the third report suggests a range of FF from 20-40% (with an average of approximately 30%). These numbers overlap with the means and ranges observed in our report ($BAT_{FF,Range}$=22-40%, $BAT_{FF}$=30.2%). Finally, one study(Lunati et al., 1999) reported a 10% increase in FF from the *in vivo* to *post mortem* state in rodents. Our findings support this observation, with supraclavicular BAT deposits for *in vivo* neonates having an average fat fraction of 29% compared to the post mortem fat fraction of 43% observed here in rats. The significant decrease in FF from the *in vivo* to the *ex vivo* state might be a physiological consequence of the perfusion that occurs in functioning BAT(Rutkowski, Davis, & Scherer, 2009), contributing to the overall water content in BAT FF measurements.

Fat fraction as a relative measure is less susceptible to rater interpretation than volume measurements. BAT deposits are surrounded by a number of soft tissues, making their borders difficult to consistently define without a standardized protocol. Only 2 of the 4 previously published neonatal BAT MRI studies provide quantitative data on BAT depot volume. The first identified a unique interscapular BAT deposit in 8 post-mortem infants with a mean (SD) of 3.6mL (2.4). The second quantified a supraclavicular BAT volume of 17.4ml in a single *post mortem* neonate. While this value is greater than the highest value observed here, the difference might easily be accounted for by a difference in age at scan (roughly 10 weeks on average). It should also be noted that current fat fraction methods fail to account for potential partial voluming of WAT interspersed into BAT depots, introducing an ambiguity to the true volume of BAT available for thermogenesis. Assuming uniform function and distribution of BAT, volume is important in the calculation of overall energy demand by the tissue. That means, more BAT volume equates to more available tissue for thermogenesis and consequently energy expenditure.

Prior literature has focused only on the supraclavicular/axillary regions of BAT in the human neonate. Our work measures other BAT deposition sites based on prior evidence from PET/CT and/or post mortem dissections. BAT deposition was consistently observed in three areas roughly corresponding to medial shoulder (supraclavicular), an area connecting the axilla to the inner shoulder (axillary), and bilaterally along the spine. The

borders between the distribution in the axillary regions and those within supraclavicular regions were difficult to differentiate in some subjects. The spinal deposits along the transverse and articular processes in the spinal column were often accompanied by deposition around the vertebral body and the spinous process. For consistency, only the deposits along the transverse and articular processes were segmented in this study and limited to vertebrae T1-T5. The BAT regions described here were sometimes accompanied by a bilateral distribution extending up the neck, but were not segmented due to their inconsistent presence.

All neonate BAT regions identified in this study are concordant with regions identified in adult PET studies(Cypess et al., 2009; Saito et al., 2009; van Marken Lichtenbelt et al., 2009; Virtanen et al., 2009). Recent documentation of *in vivo* BAT in infants(Hu et al., 2013b) more fully characterizes the fat fraction in the supraclavicular fossa and describes the low fat fraction region extending into the nape of the arm. A clinical report more fully describes the axillary deposit seen in the neonate(Carter & Schucany, 2008). In early reports the spinal region is discussed as the predominant site of heat production in the neonate(Aherne & Hull, 1964; Dawkins & Scopes, 1965). All of these regions are visible in PET/CT studies, with more pronounced signs of metabolic activity in the supraclavicular regions. It is not known to what extent the regions examined in these studies overlap, and what influence *post mortem* effects may have had on previous attempts at detecting BAT throughout the torso.

An assessment of various aspects of reliability was performed in order to validate the consistency of the methodology used here. Spinal adipose deposits present with clearly delineated borders resulting in a high degree of measurement reliability within and between raters. Supraclavicular regions posed a more significant challenge for segmentation routines due to the presence of other soft tissues and a relatively ambiguous border between the supraclavicular and axillary areas. Each of these regions on their own showed a high degree of reliability within a rater, but was found to be more rater dependent when compared to the union of supraclavicular and axillary regions. In order to minimize rater bias it is our recommendation based on these observations that in the absence of clear definable anatomical boundaries the combined region including the axillary be used in association studies.

As is the case for any newly developing field, there is more to be done in the area of neonatal BAT imaging. I have demonstrated reliable methods that are readily available to researchers. More sophisticated, but less clinically accessible, methods of quantifying the proton density fat fraction are capable of accurate quantification of water and fat by using multiple echoes (3+) to model multiple fat peaks, T1/T2/T2* relaxation and other potential confounds(Hu, Börnert, & Hernando, 2012a). Despite the increased accuracy extra echoes affords in water-fat separation, multiple methods have demonstrated the capability of dual-echo methods in discriminating BAT from WAT in humans(Holstila, Virtanen, Grönroos, & Laine, 2013; Lidell et al., 2013). Because PET/CT presents unnecessary risks to healthy pediatric populations, water-fat MRI is currently the most viable solution for *in vivo* quantification of BAT composition.

MRI methods, however, have yet to provide a direct measurement of BAT activity and thermogenesis in neonates as do PET/CT and thermography, respectively. Furthermore, multi-echo water-fat MRI does not differentiate between active and inactive BAT, a potential confound when considering the biological importance of BAT activity. Current MRI modalities capable of this may include imaging the perfusion associated with BAT activation using Arterial Spin Labeling or applying methods established for Blood-Oxygen-Level-Dependent changes in rodents(Khanna & Branca, 2012) under norepinephrine administration or humans under cold exposure(van Rooijen, van der Lans, & Brans, 2013). Two major obstacles prevent temperature challenges in assessing BAT function in neonates: 1) safely and reliably exposing neonates to standardized cold conditions, and 2) detecting small *in vivo* signal changes induced by BAT activation brought on by cold condition administration. Diffusion Tensor Imaging may also present an interesting avenue for descriptive work due to its known ability to demonstrate diffusion in adipose tissue(Steidle, Eibofner, & Schick, 2011) as well as the ability to co-locate the nerve endings needed for norepinephrine innervation of BAT(Bartness, Vaughan, & Song, 2010). Finally, hyperpolarized $^{13}C$ imaging has recently been used to monitor BAT activation in rodents under norepinephrine injection by measuring the metabolic conversion of pre-polarized [1-$^{13}C$] pyruvate(Lau, Chen, & Gu, 2014) and shows great promise in BAT activity detection.

This study imaged, identified, quantified and examined the reliability of BAT composition in neonates. Currently, little is known in humans about the developmental

determinants of BAT and the changes in BAT mass during the first years of life. Given the suggestion that early reductions in BAT deposition may continue throughout life(Symonds, Pope, Sharkey, & Budge, 2012) and may be related to the onset of obesity, localizing and quantifying BAT depot volume and fat fraction in newborns and infants may help us arrive at a better understanding of the underlying early developmental risk factors for obesity and metabolic dysfunction. The application of these methods holds promise towards this goal and therefore has important implications for health and disease risk over the individual lifespan.

**Insight 2:** Brown Adipose Tissue composition can be reliably and repeatably quantified using water-fat separated MRI acquisition schemes and semi-automatic segmenting procedures.

## 6.2 Infant Brain Development

MR-based measures of infant brain anatomy, structural connectivity and functional connectivity all demonstrated expected relationships with gestational and postnatal age at development. The principal finding with respect to age and early life brain development was focused on the Maturation Index as an indicator of perinatal white matter development.

### *6.2.1 Maturation Index Reflects Typical Perinatal White Matter Development*

By devising a model of development that considers the rates of perinatal maturational change of white matter fiber tracts, this work has demonstrated three principal findings: 1) group level information about pre- versus post-natal developmental changes of white matter fiber tracts can be retrieved based on a cross-sectional sample of healthy newborns with similarly varying gestational age at birth and postnatal age at scan; 2) when evaluating imaging associations with age in neonates, separating postmenstrual age into gestational age and age at scan (postnatal age) results in a significantly more powerful model, as compared to using postmenstrual age as a predictor, because it accounts for an

inflection in maturational changes at the time of birth; 3) the prenatal and postnatal rates of change can be cast as a unit-less index (MI), the value of which is reflective of relatively increasing or decreasing maturational processes after birth.

Two additional postulations based on adopted(Dubois et al., 2008) DTI models of myelination (see below paragraph for complete discussion), the application of the proposed MI and deductive reasoning are made below: 1) shortly before birth, the developing brain is primarily in a state of pre-myelination which appears to slow at birth; and 2) more mature central regions are increasing the process of true myelination near the time of birth.

Neonatal white matter microstructural development across the brain has been characterized *indirectly* via DTI(Dubois et al., 2014; Yoshida, Oishi, Faria, & Mori, 2013) measures of diffusivity (FA, AD, and RD). We are here adopting the model used by Dubois et al.(Beaulieu, 2002; Dubois et al., 2008) for inferences on myelin development based on observed DTI properties. RD measures diffusivity perpendicular to the axon and monotonically decreases during the three identified stages of axonal development: axonal organization, oligodendrocyte proliferation (premyelination) and myelin deposition (true myelination). AD measures water diffusion along the axis of the axon and increases during axonal organization as the axons become more coherently arranged along the main axis, decreases along with RD during premyelination due to isotropic reduction in water content and, unlike RD, is largely stable during true myelination as the hydrophobic myelin sheathing restricts diffusion in the perpendicular direction. FA is a relative measure of AD and RD and is therefore reflective of the difference between the two. Axonal organization is characterized by an increase in AD and decrease in RD resulting in increased FA. Premyelination has a concomitant decrease in AD and RD and therefore results in no change in FA. FA increases during true myelination are driven by a decrease in RD. While axonal organization, or fascicle coherence, will be discussed further below, it is thought that the majority of fascicles are already organized by the late prenatal stages due to an abundance of extracellular matrix and guidance molecules(Kostović & Jovanov-Milošević, 2006). Consequently, the primary mechanisms discussed here are restricted to pre-myelination (RD decrease, AD decrease, FA no change) and true myelination (RD decrease,

AD no change, FA increase), the major maturational processes that occur around the time of birth.

Signs of rapid *in utero* premyelination (based on adopted models) followed by a decreasing rate of premyelination after birth were present throughout a relatively large percentage of the observed white matter fiber tracts (16% at $p(F_{(+MI,RD)})<0.05$, 25% at $p<0.1$). All 27 of the tracts included in the analyses had at least one significant cluster suggestive of slowing premyelination at birth. Among those, commissural tracts showed the greatest propensity towards this pattern as manifested by large positive $MI_{RD}$ and $MI_{AD}$, on average. Because the premyelination process is observed to be slowing at birth (positive MI), it is reasonable to assume it is largely being completed near term. Certainly, oligodendrocyte proliferation continues through childhood, yet this finding is consistent with typical oligodendrocyte lineage(Barateiro & Fernandes, 2014) and the window of vulnerability (23-32 postmenstrual weeks) for perinatal white matter injury(Back, Luo, & Borenstein, 2001).

As expected, only a small percentage of fiber tracts in the neonatal brain suggested signs of true myelination (1% at $p(F_{(-MI,RD)})<0.05$, 2% at $p<0.1$). These observations are consistent with the adopted model of true myelination (FA, RD changes) occurring postnatally (negative MI) within tightly bound regions of the tract (internal capsule). The tracts that did show evidence of true myelination at the time of birth were those that based on postmortem studies are known to be myelinated early (around the time of birth)(Kinney, 2014). Specifically, the portion of corticospinal tracts running through the posterior limb of the internal capsule (PLIC) extending down into the cerebral peduncle as well as a portion of the left optic tract showed significant signs of true myelination (large negative $MI_{RD}$ and $MI_{FA}$). Postmortem analysis in 40 postmenstrual week old infants has detected microscopic traces of myelin at birth in these regions(Kinney, 2014). In addition, these sites have been identified *in utero* (Zanin et al., 2012) and in preterm cohorts(Kersbergen et al., 2010; Partridge et al., 2004) as early myelination sites and in *in vivo* neonates as being one of the earliest maturing tracts when using adults as normative measures(Dubois et al., 2008). Finally, PLIC is the first region detectable by myelin water fraction (MWF) mapping as early as 107 postnatal days(Deoni et al., 2011).

The concept that large *positive* $MI_{RD}$ is associated with large magnitude $MI_{AD}$ and, conversely, large *negative* $MI_{RD}$ is associated with large magnitude $MI_{FA}$ is introduced using a simple scatter plot. In order to further emphasize the relationship between $MI_{FA}$, $MI_{RD}$, and $MI_{AD}$, the three metrics are shown together alongside a cartoon depiction of the hypothesized mechanisms (Figure 6.2.1, left panels) leading to the observed relationship between $MI_{RD}$ and the magnitude of $MI_{AD}$ or $MI_{FA}$ (Figure 6.2.1, right panels). A larger *positive* $MI_{RD}$ resulted in a large positive $MI_{AD}$ and null $MI_{FA}$. These findings are consistent with the adopted(Dubois et al., 2008) model of pre-myelination occurring more rapidly *prior* to birth. Alternatively, a larger *negative* $MI_{RD}$ indicated a large negative $MI_{FA}$ and relatively null $MI_{AD}$. These data points are consistent with the adopted model of true myelination occurring more rapidly *after* birth. Using this framework, $MI_{RD}$ is the most informative measure of diffusivity as its sign appears to be reflective of simple models of either pre-myelination or true myelination.

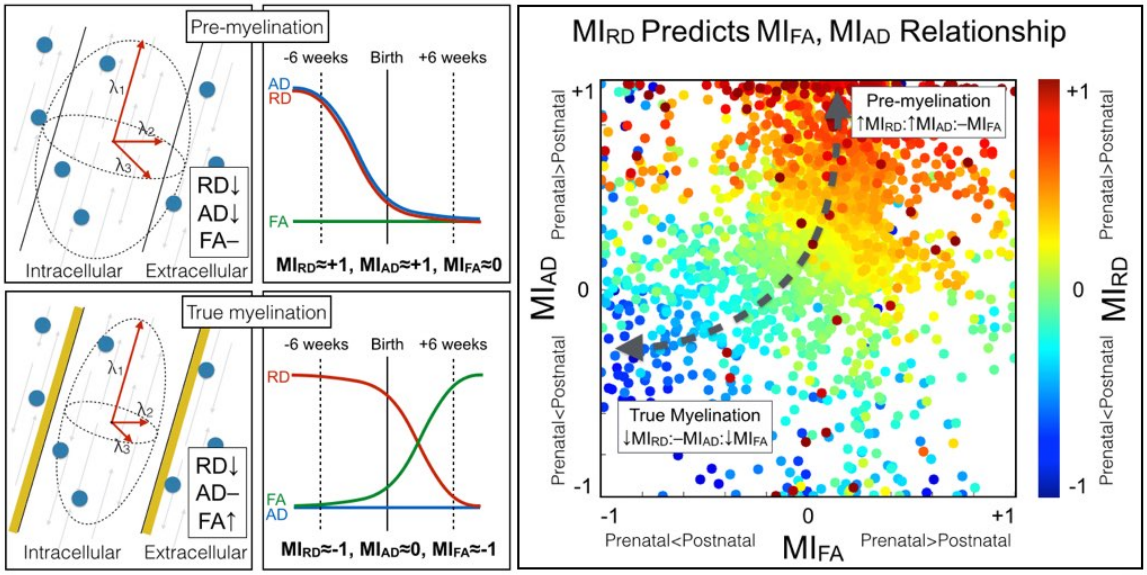



**Figure 6.2.1. The sign of $MI_{RD}$ Predicts $MI_{AD}$ and $MI_{FA}$.** Left panel set: DTI model of pre- and true myelination (far left panels) and a cartoon depiction of pre-myelination occurring before birth and true myelination occurring after birth (middle two panels). Note the process-dependence of FA, RD and AD (far left) as well as the expected values for $MI_{FA}$, $MI_{RD}$, and $MI_{AD}$ (middle). Far right panel: $MI_{RD}$ predicts the relationship between $MI_{FA}$ and $MI_{AD}$. As expected, the majority of data points are found to have a large positive $MI_{RD}$, large positive $MI_{AD}$ and null $MI_{FA}$, possibly reflective of pre-myelination before birth. A large cluster of data points with large negative $MI_{RD}$, large negative $MI_{FA}$ and roughly null $MI_{AD}$, suggestive of true myelination, were found in regions known to show early signs of myelin.

One common criticism of the conventional DTI techniques applied here is the lack of specificity. Indeed, all common measures of diffusion (RD, AD, FA) may be confounded by a number of concomitant attributes including axonal diameter, compaction, water content and fiber coherence(Jones et al., 2013). While these confounds cannot and should not be dismissed in whole, I believe that because the calculation of MI is relative (comparison of rates of change before and after birth), all *static* confounds will be controlled for. As such, many of the inherent weaknesses of using absolute measures of FA, RD and AD are uniquely avoided using this technique. It should also be noted that alternatives to conventional diffusion imaging, while considered at the onset of the current study, were deemed to be either too long of an acquisition time (High Angular Resolution Diffusion Imaging)(Zhan et al., 2012) with the available hardware or potentially not sensitive enough to myelin (MWF) at less than 48 postmenstrual weeks(Deoni et al., 2011).

This study focused on two primary stages of axonal development: premyelination and true myelination. A third developmental stage often considered in neonates is axonal organization. During this stage, one would expect FA and AD to increase with a concomitant decrease in RD. Only one small cluster was found to have significant MI values for all three diffusion parameters in the far superior portion of the right premotor tract. While this may be a reasonable site for such a process, rates of change of both AD and RD were negative, a finding not likely in the event of increasing fiber coherence. Furthermore, the majority of axonal organization is thought to be largely concluding in the human fetus during the late preterm phase of development(Kostović & Jovanov-Milošević, 2006).

While we believe the observed MI patterns are reflective of the myelination process, it is worth considering non-myelin-specific contributions to the diffusion measurements used here. Spatial resolution is limited in the growing brain and because the brain is rapidly increasing in size, partial voluming of the fiber tracts may cause brain size dependent variation(Yoshida et al., 2013). To help account for this, intracranial volume was used in both model 1 and model 2. Similarly, the DTI acquisition methods employed in this work are susceptible to ambiguity caused by crossing fibers. While these voxels may obfuscate developmental changes, causing false negatives, it is unlikely that they would induce false positives, as the measures used here are relative, requiring the nature of the fiber crossings

themselves to change as a result of birth. In addition, reductions in FA(Dubois et al., 2014) are expected when the amount, diameter or integrity of crossing fibers is increased, and such values were not observed in this study. Finally, it should be stated that the interpretation of observed effects made here is predicated on the DTI model of maturation provided by Dubois et al.(Dubois et al., 2008), and is therefore not an unequivocal observation of pre- or true-myelination patterns in the perinatal period.

While the aim of this study was to apply the MI method to perinatal diffusion data, this framework may extend to other dynamic processes with temporally well-defined events including maturation during pubertal onset, and neurodegeneration surrounding the onset of Alzheimer's disease. The MI can be generalized as the change in slope after a well-defined "event" (i.e., birth). A known "initiation" and measurement at an "observation" time point following the "event" are also required. The event, initiation and observation in the current context are birth, conception and postnatal age at MRI, respectively. The changes used in the calculation of MI are always considered using the event (birth) as the frame of reference. The variation in time separating initiation (conception) and observation (scan age) ought to be comparable in order to give equal weighting in explanatory power between the relative exposure times. While the resultant change in slope at the time of the event (birth) implies causation driven by the event, in the context of this work, the knee of an exponentially increasing or decreasing maturation curve such as those found in logistic function models of growth(Dean et al., 2014) would also drive similar results as they have a non-zero first derivative. Logistic growth has also been previously modeled as being either biphasic or monophasic linear growth and would be consistent with significant MI in this study(Ball, Srinivasan, & Aljabar, 2013). It seems plausible from a developmental perspective that the inflection point in maturation curves be in sync with birth given the abrupt transition to the extrauterine environment. In this study, this was interpreted as rapid premyelination (large RD and FA change) before birth across large regions of the brain and rapid true myelination (large RD and AD change) in areas known to have trace amounts of myelin at birth followed by mature myelin within 28 weeks after birth(Deoni et al., 2011).

Because the developmental trajectories suggested by the MI are in concordance with our understanding of perinatal maturation of white matter fiber tracts based on

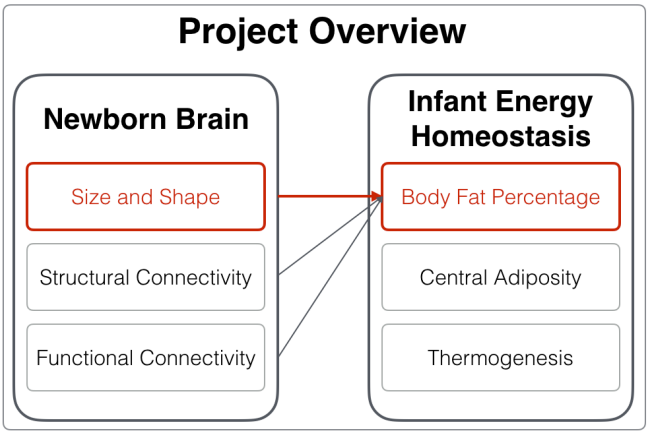
histological postmortem studies, the novel MI approach used here seems to be informative about prenatal relative to postnatal maturational change using a cross-sectional design of healthy late preterm and full-term newborns. By considering three diffusion parameters and their role in different stages of white matter development, we have constructed a plausible model of the ontogeny of early life white matter. While the MI described here has been shown to be useful for characterizing average group patterns, it is not designed to probabilistically identify differences in individuals or between groups. Future efforts will focus on developing between-group tests to identify deviations from normal brain development and to better understand environmental conditions that are associated with such deviations that may be amenable to intervention.

**Insight 3:** Separating postmenstrual age into gestational age and postnatal age at scan: a) provides optimal control of age effects in the rapidly developing newborn brain, and b) may yield insight into perinatal rates of developmental change.

## 6.3 Prospective Associations Between Newborn Brain MRI-Phenotypes and Early Life Adiposity Gain

The insula, amygdala and thalamus were identified as a priori regions relevant to energy homeostasis relevant brain circuitry and had prospective, cross modality, associations with early life fat gain.

### *6.3.1 Newborn Insula Volume is Prospectively Associated with Early Life Adiposity Gain*




This finding represents, to the best of my knowledge, the first report prospectively relating newborn brain structure with infant fat gain over the first six months of postnatal life, a key risk factor for childhood obesity. Using a hypothesis-based and focused approach, a negative association between

newborn insula GM volume and subsequent infant fat mass accretion was evident. The direction of this effect is consistent with previous findings relating insula GM volume and obesity in adults, and spatially consistent with region-specificity of the insular cortex involved in gustation and interoception. Furthermore, the observed effect remained significant after controlling for a number of important covariates. Thus, these findings support the hypothesis that a smaller insula at birth is associated with greater fat gain in early life, and it, therefore, has promising potential as a novel biomarker of childhood obesity risk.

The insula is implicated in an array of complex human processes driving feeding behavior, including somatosensation, interoception, gustation, olfaction, reward/addiction and emotion(Kurth, Zilles, Fox, Laird, & Eickhoff, 2010). The region-specific associations identified here suggest that the central-posterior region of the insula – the region where gustatory and interoception functionality overlap(Avery et al., 2015) - is the primary driver of the observed effect. In this context, it then suggests that reduced GM volume in regions functionally responsible for sensing fullness and qualities of food intake (e.g., nutritional content and viscosity) may be reflective of an attenuated ability to integrate internal and environmental cues necessary for the normal cessation of eating, resulting in abnormal regulation of intake and homeostasis in infancy.

Perhaps the most salient point of this study is that insula GM volume was measured in newborns, a time point when postnatal environmental exposures cannot yet have exerted an influence. This, then, raises the question of the origin(s) of its inter-individual variation at birth. Indeed, a number of prenatal conditions, including variation in maternal-placental-fetal endocrine(Gillman et al., 2006), immune/inflammatory(Radaelli et al., 2006), metabolic(Daraki, Georgiou, Papavasiliou, & Chalkiadaki, 2015), and lipid biology(Gademan, Vermeulen, & Oostvogels, 2014), have been associated with offspring obesity. These same prenatal environmental conditions have the potential to program the developing fetal brain(Buss, Entringer, & Wadhwa, 2012), which may represent one of the pathways mediating the link between the *in utero* environment and adiposity (obesity) risk. Thus, it is plausible that these environmental conditions interact with genotypic variation in producing a phenotype (integrity of insula circuitry) that is associated with an altered propensity for obesity.

In the context of obesity the role of the insula in modulating complex feeding behaviors is well established(Morton et al., 2014; Y. Peng et al., 2015; Simon et al., 2006; Volkow et al., 2013). This is evidenced by differential insula activation in obese relative to non-obese individuals when presented with a gastric distension(Tomasi, Wang, Wang, Backus, & Geliebter, 2009), food-related visual(Martin et al., 2010; Rothemund et al., 2007; Stoeckel et al., 2008) and gustatory stimuli(DelParigi et al., 2005). Functional activation of the insula has also been associated with ghrelin administration(Malik et al., 2008), stomach extension(Vandenbergh et al., 2005; G. J. Wang, Tomasi, Backus, Wang, & Telang, 2008), and leptin replacement(Baicy et al. 2007). Structurally, obesity-related reductions in insula GM volume have been reported in multiple, large population-based studies(Carnell et al., 2011; Janowitz et al., 2015; Kurth et al., 2013; Pannacciulli et al., 2006). More nuanced structural obesity-insula findings include negative associations between frontal operculum GM volume and blood leptin concentration(Pannacciulli et al., 2007), positive associations between insula GM volume and aerobic capacity(J. Peters et al., 2009), and reduced brain metabolism coupled with insula GM atrophy in obese individuals(Jauch-Chara et al., 2016). Finally, reduced insula GM in individuals identified as obese-prone relative to those categorized as obese-resistant supports the notion that reduced insula volume is itself a risk factor for future weight gain(Smucny et al., 2012).

Strengths of the study include the prospective longitudinal research design, MRI-based measures of brain anatomy shortly after birth, and direct ascertainment of infant adiposity by serial DXA-based measures of percent body fat. As mentioned earlier, there is considerable evidence suggesting child size and growth velocity (particularly during the period of early infancy) represent among the most reliable, valid, and strongest predictors of childhood obesity risk. Increased size or rapid weight or fat gain during this phase is associated with increased infant cardiovascular risk factors(McCloskey et al., 2016), increased childhood (and adult) obesity risk(Baird et al., 2005; Druet et al., 2012; Koontz et al., 2014; Kruithof et al., 2016; Magnus et al., 2015; Ong, Emmett, & Northstone, 2009) and related outcomes including type 1 diabetes(Magnus et al., 2015), metabolic disorders(Ekelund et al., 2007), hypertension(Huxley et al., 2000), and asthma(Sonnenschein-van der Voort et al., 2014) in later life. A recent study reported that change in infant fat mass during early infancy was a much stronger predictor of childhood

obesity risk than weight gain alone(Koontz et al., 2014). These findings support the critical importance of longitudinal assessments of body composition particularly during the period of early infancy and the validity of their use as outcomes in the context of the current work.

Limitations of this study include the lack of assessment of physical activity as a potential postnatal covariate and limited spatial resolution due to the constraints of imaging newborn participants. Early life physical activity levels (PAL) appear to be only weakly associated with adiposity at six months of age(R. Li, O'Connor, Buckley, & Specker, 1995). Furthermore, because the insula is thought to impact processing of feeding cues as opposed to energy expenditure, it is expected that inclusion of PAL as a confounding variable would only remove variance in ΔBF% unrelated to insula volume. Lastly, due to effectively low resolution (the newborn brain is roughly one-third the size of an adult brain) and low tissue contrast in the newborn brain, the estimates of the insula used here were limited to lobar volume and a relatively simple parcellation scheme that is not wholly reflective of fine grained insula neuroanatomy(Morel, Gallay, Baechler, Wyss, & Gallay, 2013).

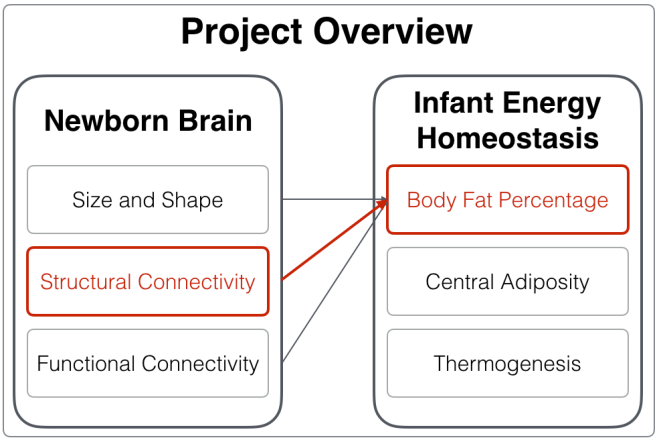
An important expansion of this work would include assessment of the determinants of newborn insula GM volume, including offspring genetic risk for obesity, prenatal environmental conditions such as variation in maternal-placental-fetal endocrine, immune/inflammatory, metabolic and lipid biology, and longer-term characterization of adiposity trajectories in order to determine if the observed effects persist into childhood and thereafter. Furthermore, future studies could benefit from imaging the newborn insula at a higher resolution(Van Leemput, Maes, Vandermeulen, & Suetens, 1999) (allowing for reliable estimates of cortical thickness), considering appetitive characteristics as a mediator of the observed insula-fat gain association, and expanding brain predictors of adiposity change to functional and structural connectivity measures.

The current study has demonstrated that reduced insula GM volume is *prospectively* associated with increased change in body fat percentage in the first six months of life. This relationship is moderately large in effect size(Lakens, 2013) and relatively larger than those reported for physical activity(R. Li et al., 1995) and genetic-adult obesity associations using a combination of single nucleotide polymorphisms(Locke et al., 2015). While future work is needed to establish the persistence of excess fat in individuals born with smaller

insula GM volume, this work may have identified a novel biomarker that reflects a neurobehavioral foundation for future adiposity gain and obesity risk.

**Insight 4:** Newborn insula gray matter volume, a structure central to interoception, is prospectively associated with early life fat accumulation.

*6.3.2 Newborn White Matter Microstructure Proximal to the Amygdala and Thalamus are Prospectively Associated with Early Life Adiposity Gain*




Analyses of white matter diffusion properties found a prospective negative association between infant fat mass accretion and newborn fractional anisotropy (FA) in the fornix and anterior thalamic radiations near the amygdala and thalamus, respectively. The direction of this effect is supported by previous findings demonstrating reduced FA in similar tracts/regions of obese adults(Kullmann et al., 2015). Conversely, a significant and positive association between early life fat gain and axial diffusivity in the corticospinal tract near the thalamus and nucleus of the solitary tract was also identified. While these are regions and diffusion parameters with an established relevance to the obese state(Kullmann, Callaghan, Heni, & Weiskopf, 2016; van Bloemendaal, Ijzerman, & Jennifer, 2016), the effect observed here is in an opposite direction to that observed in adults.

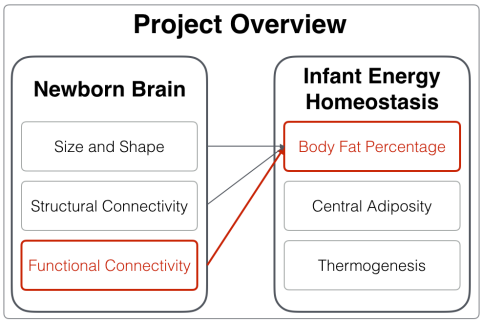
While it is common (though discouraged(Jones et al., 2013)) to cite myelination as the underlying biological component driving differences found in adults, it is unlikely that myelination would play a significant role in the observations highlighted here as they are regions not expected to be substantially myelinated at this age. In the context of the Maturation Index findings highlighted above, it is likely that axial diffusivity effects in the presence of attenuated radial diffusivity suggests axonal organization as the underlying

biological mechanism in these regions. However, reduced oligodendrocyte proliferation in those prone to obesity would be consistent with a relative increase in AD and the positive association with weight gain observed here. Finally, fractional anisotropy effects are likely not strongly reflective of oligodendrocyte proliferation as it is a mostly isotropic mechanism. Collectively, these findings suggest dysmaturation of white matter fibers found in the gustatory pathway and fronto-limbic circuits are prospectively related to early life fat gain.

**Insight 5:** Newborn white matter diffusion properties near structures involved in gustatory sensation and reward processing are prospectively associated with early life fat accumulation.

The tract-based analytical approach used here is centered on major white matter tracts defined using a neonatal, sample-based, brain atlas and warped back into native space. While this approach leverages a sample-based average to afford an optimal signal-to-noise ratio during the definition of the tracts themselves, it fails to: 1) define tracts based on individual data, and 2) define tracts based on a priori connections (e.g. amygdala to insula). Therefore, employing the atlas-based approach used here lacks some degree of specificity in the results and, while future aims will attempt to define these tracts using improved registration methods(H. Kim, Lepage, Maheshwary, Jeon, & Evans, 2016), the current interpretation of results should be considered preliminary.

### *6.3.3 Newborn Amygdala Functional Connectivity to the Insula, Thalamus and Putamen are Prospectively Associated with Early Life Adiposity Gain*




Greater neonatal amygdala connectivity to several cortical and subcortical regions, regions central to food-related signaling, were prospectively associated with an increase in fat accretion. Specifically, insula, thalamus and putamen functional connectivity with

amygdala were prospectively associated with early life fat gain. In addition, many of these regions also appeared to be associated with gestational age at birth, suggesting connections that are in rapid flux during early life.

While preterm birth is known to alter functional connectivity at term-equivalent age and beyond(Doria, Beckmann, & Arichi, 2010; D. J. Kim, Davis, Sandman, & Sporns, 2014), to my knowledge this is the first evidence that near term variation in gestational age at birth is associated with early life functional connectivity. The whole brain observed effect of gestational age at birth was fairly symmetric for laterality of amygdala seed region ($R^2$=82%). Amygdala connections demonstrating a significant and positive effect modification by gestational age at birth included bilateral insula, basal ganglia, and thalamus. A longer period of gestation was positively associated with a higher degree of connectivity.

Existing literature of amygdala functional connectivity differences in obese adults can be summarized by: decreased connectivity to the ventromedial prefrontal cortex(Wijngaarden et al., 2015), increased connectivity to the insula(Lips & Wijngaarden, 2014), and a U-shaped pattern of connectivity to the basal ganglia(Dietrich, Hollmann, Mathar, & Villringer, 2016). The amygdala-insula connectivity observed here was consistent with the hypothesized direction of effect based on adult literature. That is, a greater level of functional coupling between the amygdala and insula reflected a greater gain in fat over the first six months of life. Because the insula reflects interoception, it is possible that variation in amygdala connectivity is reflective of reward(Baxter & Murray, 2002) modulation in the context of hunger. Because both the amygdala and the vmPFC are associated with reward and feeding(Baxter & Murray, 2002; Y. Lee, Chong, Liu, & Libedinsky, 2013; J. Peters & Büchel, 2010; Sescousse, Caldú, Segura, & Dreher, 2013), it is hypothesized that the observed amygdala-vmPFC connectivity negative association with fat gain (also consistent in direction with adult literature) is reflective of a dysregulation of reward behavior in those gaining more fat on average. Finally, while the direction of basal ganglia-amygdala connectivity effect (positive and linear) on early life fat gain is inconsistent with adult literature in direction of effect (U-shaped association with BMI), amygdala-basal ganglia connections are also consistent with reward circuitry(Sesack &

Grace, 2010). Collectively, these findings reflect alterations to reward and interoception brain circuitry at birth that are prospectively associated with early life fat accumulation.

**Insight 6:** Newborn functional connectivity status between the amygdala and structures involved in gustatory sensation, reward processing and interoception are prospectively associated with early life fat accumulation.

The descriptive network-based (pairwise associations within a priori ROIs) functional connectivity associations with gestational age at birth and future weight gain were consistent with the amygdala connectivity findings. However, future aims ought to focus on the connectivity within and between the nodes of homeostasis systems by building an MxM homeostasis specific connectivity matrix (connectome) that is naïve to any pairwise connection (e.g. to the amygdala). Where M is the collective number of structures involved in interoception, satiety, salience, reward and default networks. In combination with more sophisticated methods of tissue(H. Kim et al., 2016) and anatomical(Alcauter, Lin, Smith, & Gilmore, 2015) segmentation, this would allow for the construction of a rigorously defined homeostasis-specific connectome and the use of graph-based analytical methods of interrogation.

## 7. Conclusion/Summary

The research contained within this thesis relates to the public health problem of childhood obesity, with a specific focus on the characterization and role of energy homeostasis-related brain circuitry in the human newborn. Obesity is a complex, multi-factorial phenotype. Among these factors, energy homeostasis and the critical importance of the hypothalamic-limbic-cortical brain circuitry that regulates energy homeostasis is well established. In adults, MRI-based measures of energy homeostasis-related brain circuits have been associated with obesity. However, it is unclear whether the observed differences in these brain regions and circuitry in obese relative to normal-weight individuals are a cause, consequence, or both, of the obese state. Moreover, relatively little is known about the developmental ontogeny of these brain regions and circuitry and their prospective role in shaping propensity for childhood obesity. This work has addressed this fundamental knowledge gap through a deep characterization of infant adiposity, newborn brain anatomy/connectivity and the prospective association between the energy homeostasis-related brain circuitry in the human newborn and early life fat gain in a population of ~100 mother-infant dyads followed from early gestation through birth till 6 months age.

Converging evidence suggests growth velocity during the period of early infancy represents among the most reliable, valid, and strongest predictors of childhood obesity risk. As a result, serial changes in infant adiposity, specifically from birth to six-months of age have been chosen as the operationalized outcome variable for quantifying infant adiposity. A detailed consideration of demographic predictors (age, sex, feeding status) has been made in order to yield insight into their proper adjustment for analysis. This work has concluded that a priori age regression and post hoc hypothesis testing of sex specific effects and breastfeeding status as a confounder was the optimal analytical approach. In addition, a comprehensive description of the acquisition, segmentation and quantification reliability/repeatability of human newborn Brown Adipose Tissue composition has been made.

Within this project, measures of energy homeostasis brain circuitry using anatomical, diffusion and functional MRI have been developed. Because such measures have not yet

been established in the context of newborn homeostasis circuitry, this work has fulfilled an important and as yet unmet need in terms of not only scientific knowledge but also technical capability. Furthermore, because it is necessary to regress out effects of age on the rapidly developing brain, detailed considerations on how to properly do this have been documented. An unexpected outcome of this work resulted in a novel Maturation Index that has been posited to reflect typical perinatal white matter maturation in the human brain. Specifically, it has been proposed that the developing brain is primarily in a state of oligodendrocyte proliferation prior to birth followed by a shift towards true myelination in regions known to myelinate early.

Converging evidence suggests that inter-individual variation in the propensity for obesity is already present at birth and is an indicator of future health risks. Here, I have identified a collection of neurophenotypes assessed at birth - insula gray matter volume, white matter diffusion properties proximal to reward/gustatory pathways, and functional connectivity between amygdala and reward/interoception brain structures – and have described, in detail, their prospective association with the rate of fat accrual in early postnatal life.

The identification of plausible brain-related biomarkers of childhood obesity risk that predate the influence of the postnatal obesogenic environment may contribute to an improved understanding of our inter-individual variation in propensity for obesity, early identification of at-risk individuals, and intervention targets for primary prevention.

## References


Adair, L. S. (2007). Size at birth and growth trajectories to young adulthood. *American Journal of Human Biology*, *19*(3), 327–337. http://doi.org/10.1002/ajhb.20587

Aherne, W., & Hull, D. (1964). The Site of Heat Production in the Newborn Infant. *Proc R Soc Med*, *57*, 1172–1173.

Alcauter, S., Lin, W., Smith, J. K., & Gilmore, J. H. (2015). Consistent anterior–posterior segregation of the insula during the first 2 years of life. *Cerebral Cortex*. 25(5):1176-87. doi: 10.1093/cercor/bht312.

Alfonzo-González, G., Doucet, E., Alméras, N., Bouchard, C., & Tremblay, A. (2004). Estimation of daily energy needs with the FAO/WHO/UNU 1985 procedures in adults: comparison to whole-body indirect calorimetry measurements. *European Journal of Clinical Nutrition*, *58*(8), 1125–1131. http://doi.org/10.1038/sj.ejcn.1601940

Allison, D. B., Mentore, J. L., & Heo, M. (1999). Antipsychotic-induced weight gain: a comprehensive research synthesis. *Am J Psychiatry,* 156(11):1686-96.

Alosco, M. L., Stanek, K. M., Galioto, R., Korgaonkar, M. S., Grieve, S. M., Brickman, A. M., et al. (2014). Body mass index and brain structure in healthy children and adolescents. *The International Journal of Neuroscience*, *124*(1), 49–55. http://doi.org/10.3109/00207454.2013.817408

Anderson, A. K., & Phelps, E. A. (2001). Lesions of the human amygdala impair enhanced perception of emotionally salient events. *Nature*, *411*(6835), 305–309. http://doi.org/10.1038/35077083

Andres, A., Casey, P. H., Cleves, M. A., & Badger, T. M. (2013). Body fat and bone mineral content of infants fed breast milk, cow's milk formula, or soy formula during the first year of life. *The Journal of Pediatrics*, *163*(1), 49–54. http://doi.org/10.1016/j.jpeds.2012.12.067

Arndt, T. L., Stodgell, C. J., & Rodier, P. M. (2005). The teratology of autism. *International Journal of Developmental Neuroscience*, *23*(2-3), 189–199. http://doi.org/10.1016/j.ijdevneu.2004.11.001

Avery, J. A., Kerr, K. L., Ingeholm, J. E., Burrows, K., Bodurka, J., & Simmons, W. K. (2015). A common gustatory and interoceptive representation in the human mid-insula. *Human Brain Mapping*, *36*(8), 2996–3006. http://doi.org/10.1002/hbm.22823

Back, S. A., Luo, N. L., & Borenstein, N. S. (2001). Late oligodendrocyte progenitors coincide with the developmental window of vulnerability for human perinatal white matter injury. *The Journal of Neuroscience,* 21(4), 1302-1312.

Baicy, K., London, E. D., Monterosso, J., Wong, M. L., Delibasi, T., Sharma, A., & Licinio, J. (2007). Leptin replacement alters brain response to food cues in genetically leptin-deficient adults. *Proceedings of the National Academy of Sciences*, *104*(46), 18276-18279.

Baird, J., Fisher, D., Lucas, P., Kleijnen, J., & Roberts, H. (2005). Being big or growing fast: systematic review of size and growth in infancy and later obesity. *Bmj,* 331.7522 929.

Ball, G., Srinivasan, L., Aljabar, P., Counsell, S. J., Durighel, G., Hajnal, J. V., ... & Edwards, A. D. (2013). Development of cortical microstructure in the preterm human brain. *Proceedings of the National Academy of Sciences*, *110*(23), 9541-9546.

Barateiro, A., & Fernandes, A. (2014). Temporal oligodendrocyte lineage progression: in vitro models of proliferation, differentiation and myelination. *Biochimica Et Biophysica Acta (BBA)-Molecular,* 1843(9), 1917-1929.

Bartness, T. J., Vaughan, C. H., & Song, C. K. (2010). Sympathetic and sensory innervation of brown adipose tissue. *International Journal of Obesity, 34*, pp.S36-S42.
Bassareo, V., & Di Chiara, G. (1999). Differential responsiveness of dopamine transmission to food-stimuli in nucleus accumbens shell/core compartments. *Neuroscience*, *89*(3), 637–641.
Bauer, J. S., Noël, P. B., Vollhardt, C., Much, D., & Degirmenci, S. (2015). Accuracy and reproducibility of adipose tissue measurements in young infants by whole body magnetic resonance imaging. *PLoS One,*10(2):e0117127.
Baxter, M. G., & Murray, E. A. (2002). The amygdala and reward. *Nature Reviews Neuroscience,* 3(7):563-73.
Beaulieu, C. (2002). The basis of anisotropic water diffusion in the nervous system - a technical review. *NMR in Biomedicine*, *15*(7-8), 435–455. http://doi.org/10.1002/nbm.782
Beckmann, C., & Jenkinson, M. (2003). General multilevel linear modeling for group analysis in FMRI. *Neuroimage,* 20(2):1052-63..
Berglund, J., Johansson, L., Ahlström, H., & Kullberg, J. (2010). Three-point dixon method enables whole-body water and fat imaging of obese subjects. *Magnetic Resonance in Medicine*, *63*(6), 1659–1668. http://doi.org/10.1002/mrm.22385
Bhadelia, R. A., Price, L. L., Tedesco, K. L., Scott, T., & Qiu, W. Q. (2009). Diffusion tensor imaging, white matter lesions, the corpus callosum, and gait in the elderly. *Stroke,* 40(12):3816-20. doi: 10.1161/STROKEAHA.109.564765.
Brennan, D. D., Whelan, P. F., & Robinson, K. (2005). Rapid automated measurement of body fat distribution from whole-body MRI. *American Journal of Radiology,* 185(2):418-23.
Bruce, A. S., Bruce, J. M., & Black, W. R. (2014). Branding and a child's brain: an fMRI study of neural responses to logos. *Social Cognitive Neuroscience,* 9(1):118-22. doi: 10.1093/scan/nss109
Buss, C., Entringer, S., & Wadhwa, P. D. (2012). Fetal programming of brain development: intrauterine stress and susceptibility to psychopathology. *Science Signaling,* 5(245):pt7.
Carnell, S., Gibson, C., Benson, L., Ochner, C. N., & Geliebter, A. (2011). Neuroimaging and obesity: current knowledge and future directions. *Obesity Reviews*, *13*(1), 43–56. http://doi.org/10.1111/j.1467-789X.2011.00927.x
Carter, B. W., & Schucany, W. G. (2008). Brown adipose tissue in a newborn. *Proc (Bayl Univ Med Cent)*, *21*(3), 328–330.
Chen, Y. I., Cypess, A. M., Sass, C. A., Brownell, A.-L., Jokivarsi, K. T., Kahn, C. R., & Kwong, K. K. (2012). Anatomical and Functional Assessment of Brown Adipose Tissue by Magnetic Resonance Imaging. *Obesity*. http://doi.org/10.1038/oby.2012.22
Chen, Y., Wang, D. J. J., & Detre, J. A. (2011). Test-retest reliability of arterial spin labeling with common labeling strategies. *Journal of Magnetic Resonance Imaging : JMRI*, *33*(4), 940–949. http://doi.org/10.1002/jmri.22345
Coman, I., Barbin, G., Charles, P., & Zalc, B. (2005). Axonal signals in central nervous system myelination, demyelination and remyelination. *Journal of the Neurological Science,* 233(1-2):67-71.
Corbetta, M., Patel, G., & Shulman, G. L. (2008). The reorienting system of the human brain: from environment to theory of mind. *Neuron*, *58*(3), 306–324. http://doi.org/10.1016/j.neuron.2008.04.017
Counsell, S. J. A. R. M. A. (2002). Magnetic resonance imaging of the newborn brain, 1–13.

http://doi.org/10.1054/ycupe.0318
Coutinho, J. F., Fernandesl, S. V., Soares, J. M., Maia, L., Gonçalves, Ó. F., & Sampaio, A. (2015). Default mode network dissociation in depressive and anxiety states. *Brain Imaging and Behavior*. http://doi.org/10.1007/s11682-015-9375-7
Cummings, D. E., Purnell, J. Q., Frayo, R. S., Schmidova, K., Wisse, B. E., & Weigle, D. S. (2001). A preprandial rise in plasma ghrelin levels suggests a role in meal initiation in humans. *Diabetes*, *50*(8), 1714–1719.
Cypess, A. M., Lehman, S., Williams, G., Tal, I., Rodman, D., Goldfine, A. B., et al. (2009). Identification and importance of brown adipose tissue in adult humans. *N Engl J Med*, *360*(15), 1509–1517. http://doi.org/10.1056/NEJMoa0810780
Dabelea, D., & Harrod, C. S. (2013). Role of developmental overnutrition in pediatric obesity and type 2 diabetes. *Nutrition Reviews*, *71 Suppl 1*, S62–7. http://doi.org/10.1111/nure.12061
Daghestani, M. H., Ozand, P. T., Al-Himadi, A. R., & Al-Odaib, A. N. (2007). Hormonal levels of leptin, insulin, ghrelin, and neuropeptide Y in lean, overweight, and obese Saudi females. *Saudi Medical Journal*, *28*(8), 1191–1197.
Dallman, M. F., Pecoraro, N. C., & la Fleur, S. E. (2005). Chronic stress and comfort foods: self-medication and abdominal obesity ☆ . *Brain, Behavior, and Immunity*, *19*(4), 275–280. http://doi.org/10.1016/j.bbi.2004.11.004
Dallman, M. F., Pecoraro, N., & Akana, S. F. (2003). Chronic stress and obesity: a new view of "comfort food." *Proceedings of the National Academy of Sciences*, *100*(20), pp.11696-11701.
Daraki, V., Georgiou, V., Papavasiliou, S., & Chalkiadaki, G. (2015). Metabolic profile in early pregnancy is associated with offspring adiposity at 4 years of age: the Rhea pregnancy cohort. *PLoS One*. http://dx.doi.org/10.1371/journal.pone.0126327
Dawkins, M., & Scopes, J. (1965). Non-shivering thermogenesis and brown adipose tissue in the human new-born infant. *Nature*, 206(980):201-2.
de Araujo, I. E., Geha, P., & Small, D. M. (2012). Orosensory and homeostatic functions of the insular taste cortex. *Chemosensory Perception*. **DOI**: 10.1007/s12078-012-9117-9.
de Beer, M., Vrijkotte, T., & Fall, C. (2015). Associations of infant feeding and timing of linear growth and relative weight gain during early life with childhood body composition. *International Journal of Obesity,* 39(4):586-92. doi: 10.1038/ijo.2014.200.
Dean, D. C., O'Muircheartaigh, J., Dirks, H., Waskiewicz, N., Lehman, K., Walker, L., et al. (2014). Modeling healthy male white matter and myelin development: 3 through 60months of age. *Neuroimage*, *84*, 742–752. http://doi.org/10.1016/j.neuroimage.2013.09.058
DelParigi, A., Chen, K., Salbe, A. D., Reiman, E. M., & Tataranni, P. A. (2005). Sensory experience of food and obesity: a positron emission tomography study of the brain regions affected by tasting a liquid meal after a prolonged fast. *Neuroimage*, *24*(2), 436–443. http://doi.org/10.1016/j.neuroimage.2004.08.035
Deoni, S. C. L., Dean, D. C., III, O'Muircheartaigh, J., Dirks, H., & Jerskey, B. A. (2012). Investigating white matter development in infancy and early childhood using myelin water faction and relaxation time mapping. *Neuroimage*, *63*(3), 1038–1053. http://doi.org/10.1016/j.neuroimage.2012.07.037
Deoni, S. C. L., Mercure, E., Blasi, A., Gasston, D., Thomson, A., Johnson, M., et al. (2011).

Mapping Infant Brain Myelination with Magnetic Resonance Imaging. *Journal of Neuroscience*, *31*(2), 784–791. http://doi.org/10.1523/JNEUROSCI.2106-10.2011
Deurenberg-Yap, M., & Schmidt, G. (2000). The paradox of low body mass index and high body fat percentage among Chinese, Malays and Indians in Singapore. *International Journal of Obesity*, 24(8):1011-7.
Di Martino, A., Ross, K., Uddin, L. Q., Sklar, A. B., Castellanos, F. X., & Milham, M. P. (2009). Functional brain correlates of social and nonsocial processes in autism spectrum disorders: an activation likelihood estimation meta-analysis. *Biological Psychiatry*, *65*(1), 63–74. http://doi.org/10.1016/j.biopsych.2008.09.022
Dietrich, A., Hollmann, M., Mathar, D., & Villringer, A. (2016). Brain regulation of food craving: relationships with weight status and eating behavior. *International Journal of Obesity,* 40(6):982-9. doi: 10.1038/ijo.2016.28.
Doak, C. M., Visscher, T., & Renders, C. M. (2006). The prevention of overweight and obesity in children and adolescents: a review of interventions and programmes. *Obesity*, 7(1):111-36.
Donahue, R. P., Bloom, E., Abbott, R. D., Reed, D., & Yano, K. (1987). Central obesity and coronary heart disease in men. *The Lancet,* 1(8537):821-4.
Doria, V., Beckmann, C. F., & Arichi, T. (2010). Emergence of resting state networks in the preterm human brain. *Proceedings of the National Academy of Sciences*, 20015-20020.
Druet, C., Stettler, N., Sharp, S., Simmons, R. K., Cooper, C., Smith, G. D., et al. (2012). Prediction of childhood obesity by infancy weight gain: an individual-level meta-analysis. *Paediatric and Perinatal Epidemiology*, *26*(1), 19–26. http://doi.org/10.1111/j.1365-3016.2011.01213.x
Dubois, J., Dehaene-Lambertz, G., Kulikova, S., Poupon, C., Hüppi, P. S., & Hertz-Pannier, L. (2014). The **early development of brain white matter: a review of imaging studies in fetuses**, **newborns and infants**. *Neuroscience*, 1–24. http://doi.org/10.1016/j.neuroscience.2013.12.044
Dubois, J., Dehaene-Lambertz, G., Soarès, C., Cointepas, Y., Le Bihan, D., & Hertz-Pannier, L. (2008). Microstructural correlates of infant functional development: example of the visual pathways. *Journal of Neuroscience*, *28*(8), 1943–1948. http://doi.org/10.1523/JNEUROSCI.5145-07.2008
Dubois, J., Dehaene-Lambertz, G., Perrin, M., Mangin, J. F., Cointepas, Y., Duchesnay, E., ... & Hertz-Pannier, L. (2008). Asynchrony of the early maturation of white matter bundles in healthy infants: quantitative landmarks revealed noninvasively by diffusion tensor imaging. *Human brain mapping*, *29*(1), 14-27.
Dubois, J., Hertz-Pannier, L., Cachia, A., Mangin, J. F., Le Bihan, D., & Dehaene-Lambertz, G. (2009). Structural Asymmetries in the Infant Language and Sensori-Motor Networks. *Cerebral Cortex*, *19*(2), 414–423. http://doi.org/10.1093/cercor/bhn097
Ekelund, U., Ong, K. K., Linné, Y., Neovius, M., Brage, S., Dunger, D. B., et al. (2007). Association of weight gain in infancy and early childhood with metabolic risk in young adults. *Journal of Clinical Endocrinology & Metabolism*, *92*(1), 98–103. http://doi.org/10.1210/jc.2006-1071
Ellison-Wright, I., & Bullmore, E. (2009). Meta-analysis of diffusion tensor imaging studies in schizophrenia. *Schizophrenia Research,* 108(1-3):3-10. doi: 10.1016/j.schres.2008.11.021..
Engelson, E. S., Kotler, D. P., Tan, Y. X., & Agin, D. (1999). Fat distribution in HIV-infected

patients reporting truncal enlargement quantified by whole-body magnetic resonance imaging. *The American Journal of Clinical Nutrition,* 69(6):1162-9..

Fair, D. A., Cohen, A. L., Dosenbach, N. U. F., Church, J. A., Miezin, F. M., Barch, D. M., et al. (2008). The maturing architecture of the brain's default network. *Proceedings of the National Academy of Sciences of the United States of America*, *105*(10), 4028–4032. http://doi.org/10.1073/pnas.0800376105

Fair, D. A., Cohen, A. L., Power, J. D., Dosenbach, N. U. F., Church, J. A., Miezin, F. M., et al. (2009). Functional brain networks develop from a "local to distributed" organization. *PLoS Computational Biology*, *5*(5), e1000381. http://doi.org/10.1371/journal.pcbi.1000381

Fair, D. A., Dosenbach, N. U. F., Church, J. A., Cohen, A. L., Brahmbhatt, S., Miezin, F. M., et al. (2007). Development of distinct control networks through segregation and integration. *Proceedings of the National Academy of Sciences of the United States of America*, *104*(33), 13507–13512. http://doi.org/10.1073/pnas.0705843104

Fair, D. A., Nigg, J. T., Iyer, S., Bathula, D., & Mills, K. L. (2012). Distinct neural signatures detected for ADHD subtypes after controlling for micro-movements in resting state functional connectivity MRI data. Frontier Systems Neuroscience, 6:80. doi: 10.3389/fnsys.2012.00080.

Fan, Y., Shi, F., Smith, J. K., Lin, W., Gilmore, J. H., & Shen, D. (2011). Brain anatomical networks in early human brain development. *Neuroimage*, *54*(3), 1862–1871. http://doi.org/10.1016/j.neuroimage.2010.07.025

Fang, Z., Spaeth, A. M., Ma, N., Zhu, S., Hu, S., Goel, N., et al. (2015). Altered salience network connectivity predicts macronutrient intake after sleep deprivation. *Scientific Reports*, *5*, 8215. http://doi.org/10.1038/srep08215

Farooqi, S., & O'Rahilly, S. (2006). Genetics of obesity in humans. *Endocrine Reviews*, *27*(7), 710–718. http://doi.org/10.1210/er.2006-0040

Fillard, P., Gilmore, J., Piven, J., Lin, W., & Gerig, G. (2003). Quantitative analysis of white matter fiber properties along geodesic paths. *International Conference on Medical Image Computing and Computer-Assisted Intervention* (pp. 16-23). Springer Berlin Heidelberg.

Finegood, D. T., Merth, T. D. N., & Rutter, H. (2010). Implications of the foresight obesity system map for solutions to childhood obesity. *Obesity*, *18 Suppl 1*, S13–6. http://doi.org/10.1038/oby.2009.426

Flegal, K. M., Shepherd, J. A., Looker, A. C., Graubard, B. I., Borrud, L. G., Ogden, C. L., et al. (2009). Comparisons of percentage body fat, body mass index, waist circumference, and waist-stature ratio in adults. *The American Journal of Clinical Nutrition*, *89*(2), 500–508. http://doi.org/10.3945/ajcn.2008.26847

Fonov, V. S., Evans, A. C., McKinstry, R. C., & Almli, C. R. (2009). Unbiased nonlinear average age-appropriate brain templates from birth to adulthood. *NeuroImage*, *54*(1), pp.313-327.

Forgat-Campagna, A., & Narayan, K. V. (2001). Type-2 diabetes in children: Exemplifies the growing problem of chronic diseases. *BMJ*, 322(7283): 377–378..

Fox, M. D., & Raichle, M. E. (2007). Spontaneous fluctuations in brain activity observed with functional magnetic resonance imaging. *Nature Reviews Neuroscience,* 8(9):700-11..

Frederich, R. C., Hamann, A., Anderson, S., Löllmann, B., Lowell, B. B., & Flier, J. S. (1995). Leptin levels reflect body lipid content in mice: evidence for diet-induced resistance to leptin action. *Nature Medicine*, *1*(12), 1311–1314.

Freedman, D. S., Khan, L. K., Dietz, W. H., Srinivasan, S. R., & Berenson, G. S. (2001). Relationship of childhood obesity to coronary heart disease risk factors in adulthood: the Bogalusa Heart Study. *Pediatrics*, *108*(3), 712–718.

Functional connectivity in the resting brain:A network analysis of the defaultmode hypothesis. (2002). Functional connectivity in the resting brain:A network analysis of the defaultmode hypothesis, 1–6.

Gademan, M., Vermeulen, M., & Oostvogels, A. (2014). Maternal prepregancy BMI and lipid profile during early pregnancy are independently associated with offspring's body composition at age 5–6 years. *PLoS One,* 9(4):e94594. doi: 10.1371/journal.pone.0094594..

Gale, C., Logan, K. M., & Santhakumaran, S. (2012). Effect of breastfeeding compared with formula feeding on infant body composition: a systematic review and meta-analysis. *The American journal of clinical nutrition*, pp.ajcn-027284.

Gao, W., Alcauter, S., Smith, J. K., Gilmore, J. H., & Lin, W. (2015). Development of human brain cortical network architecture during infancy. *Brain Structure and Function*, *220*(2), 1173–1186. http://doi.org/10.1007/s00429-014-0710-3

Gao, W., Gilmore, J. H., Giovanello, K. S., Smith, J. K., Shen, D., Zhu, H., & Lin, W. (2011). Temporal and spatial evolution of brain network topology during the first two years of life. *PLoS One*, *6*(9), e25278. http://doi.org/10.1371/journal.pone.0025278

Gao, W., Gilmore, J. H., Shen, D., Smith, J. K., Zhu, H., & Lin, W. (2013). The synchronization within and interaction between the default and dorsal attention networks in early infancy. *Cerebral Cortex*, *23*(3), 594–603. http://doi.org/10.1093/cercor/bhs043

Gao, W., Lin, W., Chen, Y., Gerig, G., Smith, J. K., Jewells, V., & Gilmore, J. H. (2008). Temporal and Spatial Development of Axonal Maturation and Myelination of White Matter in the Developing Brain. *American Journal of Neuroradiology*, *30*(2), 290–296. http://doi.org/10.3174/ajnr.A1363

Gao, W., Zhu, H., Giovanello, K. S., Smith, J. K., Shen, D., Gilmore, J. H., & Lin, W. (2009). Evidence on the emergence of the brain's default network from 2-week-old to 2-year-old healthy pediatric subjects. *Proceedings of the National Academy of Sciences of the United States of America*, *106*(16), 6790–6795. http://doi.org/10.1073/pnas.0811221106

García-García, I., Jurado, M. Á., Garolera, M., Segura, B., Sala-Llonch, R., Marqués-Iturria, I., et al. (2013). Alterations of the salience network in obesity: a resting-state fMRI study. *Human Brain Mapping*, *34*(11), 2786–2797. http://doi.org/10.1002/hbm.22104

Garrity, A. G., Pearlson, G. D., McKiernan, K., & Lloyd, D. (2007). Aberrant “default mode” functional connectivity in schizophrenia. *American Journal of Psychiatry,* 164(3):450-7.

Gautier, J. F., Chen, K., Salbe, A. D., Bandy, D., Pratley, R. E., Heiman, M., et al. (2000). Differential brain responses to satiation in obese and lean men. *Diabetes*, *49*(5), 838–846.

Gautier, J. F., Del Parigi, A., Chen, K., Salbe, A. D., Bandy, D., Pratley, R. E., et al. (2001). Effect of satiation on brain activity in obese and lean women. *Obes Res*, *9*(11), 676–684. http://doi.org/10.1038/oby.2001.92

Ghoorah, K., Campbell, P., & Kent, A. (2014). Obesity and cardiovascular outcomes: a review. *… Heart Journal,* 5(1):77-85. doi: 10.1177/2048872614523349.

Giannì, M. L., Roggero, P., & Morlacchi, L. (2014). Formula-fed infants have significantly higher fat-free mass content in their bodies than breastfed babies. *Acta Pediatria,*

103(7):e277-81. doi: 10.1111/apa.12643.
Gillman, M. W., Rich-Edwards, J. W., Huh, S., Majzoub, J. A., Oken, E., Taveras, E. M., & Rifas-Shiman, S. L. (2006). Maternal corticotropin-releasing hormone levels during pregnancy and offspring adiposity. *Obesity (Silver Spring, Md.)*, *14*(9), 1647–1653. http://doi.org/10.1038/oby.2006.189
Gilmore, J. H., Lin, W., Prastawa, M. W., Looney, C. B., Vetsa, Y. S. K., Knickmeyer, R. C., et al. (2007). Regional Gray Matter Growth, Sexual Dimorphism, and Cerebral Asymmetry in the Neonatal Brain. *Journal of Neuroscience*, *27*(6), 1255–1260. http://doi.org/10.1523/JNEUROSCI.3339-06.2007
Gilmore, J. H., Shi, F., Woolson, S. L., & Knickmeyer, R. C. (2012). Longitudinal development of cortical and subcortical gray matter from birth to 2 years. *Cerebral Cortex,* 22(11):2478-85.
Glover, G. (1991). Three-point dixon technique for true water/fat decomposition with B0 inhomogeneity correction. *Magnetic Resonance in Medicine, 18*(2), pp.371-383.
Gordon-Larsen, P., Nelson, M. C., Page, P., & Popkin, B. M. (2006). Inequality in the built environment underlies key health disparities in physical activity and obesity. *Pediatrics, 117*(2), pp.417-424.
Graham, A. M., Pfeifer, J. H., Fisher, P. A., Lin, W., Gao, W., & Fair, D. A. (2015). The potential of infant fMRI research and the study of early life stress as a promising exemplar. *Developmental Cognitive Neuroscience* , *12*, 12–39. http://doi.org/10.1016/j.dcn.2014.09.005
Greicius, M. D., Krasnow, B., Reiss, A. L., & Menon, V. (2003). Functional connectivity in the resting brain: a network analysis of the default mode hypothesis. *Proceedings of the National Academy of Sciences*, *100*(1), 253-258.
Grissom, N. M., Lyde, R., Christ, L., Sasson, I. E., Carlin, J., Vitins, A. P., et al. (2014). Obesity at conception programs the opioid system in the offspring brain. *Neuropsychopharmacology*, *39*(4), 801–810. http://doi.org/10.1038/npp.2013.193
Groen, W. B., Buitelaar, J. K., & Van Der Gaag, R. J. (2011). Pervasive microstructural abnormalities in autism: a DTI study. *Journal of Psychiatry Neuroscience,* 36(1):32-40.
Guerrieri, R., Nederkoorn, C., & Jansen, A. (2008). The interaction between impulsivity and a varied food environment: its influence on food intake and overweight. *International Journal of Obesity,* 32(4):708-14..
Guerrieri, R., Nederkoorn, C., Stankiewicz, K., & Alberts, H. (2007). The influence of trait and induced state impulsivity on food intake in normal-weight healthy women. *Appetite, 49*(1), pp.66-73.
Hallquist, M. N., Hwang, K., & Luna, B. (2013). The nuisance of nuisance regression: spectral misspecification in a common approach to resting-state fMRI preprocessing reintroduces noise and obscures functional. *Neuroimage,* 82:208-25.
Ham, T., Leff, A., de Boissezon, X., Joffe, A., & Sharp, D. J. (2013). Cognitive control and the salience network: an investigation of error processing and effective connectivity. *Journal of Neuroscience*, *33*(16), 7091–7098. http://doi.org/10.1523/JNEUROSCI.4692-12.2013
Hamilton, G., Smith, D. L. J., Bydder, M., Nayak, K. S., & Hu, H. H. (2011). MR properties of brown and white adipose tissues. *Journal of Magnetic Resonance Imaging : JMRI*, *34*(2), 468–473. http://doi.org/10.1002/jmri.22623
Hanley, J. A., & McNeil, B. J. (1982). The meaning and use of the area under a receiver

operating characteristic (ROC) curve. *Radiology,* 143(1):29-36.
Hanson, E. S., & Dallman, M. F. (1995). Neuropeptide Y (NPY) may integrate responses of hypothalamic feeding systems and the hypothalamo-pituitary-adrenal axis. *Journal of Neuroendocrinology*, *7*(4), 273–279.
Hazlett, H. C., Gu, H., & McKinstry, R. C. (2012). Brain volume findings in 6-month-old infants at high familial risk for autism. *American Journal of Psychiatry,* 169(6):601-8.
Hof, M. H. P., Vrijkotte, T. G. M., de Hoog, M. L. A., van Eijsden, M., & Zwinderman, A. H. (2013). Association between infancy BMI peak and body composition and blood pressure at age 5-6 years. *PLoS One*, *8*(12), e80517. http://doi.org/10.1371/journal.pone.0080517
Holstila, M., Virtanen, K. A., Grönroos, T. J., & Laine, J. (2013). Measurement of brown adipose tissue mass using a novel dual-echo magnetic resonance imaging approach: a validation study. *Metabolism, 62*(8), pp.1189-1198.
Homae, F., Watanabe, H., Otobe, T., Nakano, T., Go, T., Konishi, Y., & Taga, G. (2010). Development of global cortical networks in early infancy. *Journal of Neuroscience*, *30*(14), 4877–4882. http://doi.org/10.1523/JNEUROSCI.5618-09.2010
Hu, H. H., Börnert, P., & Hernando, D. (2012a). ISMRM workshop on fat–water separation: insights, applications and progress in MRI. *Magnetic Resonance in Medicine, 68*(2), pp.378-388.
Hu, H. H., Hines, C., Smith, D. L., & Reeder, S. B. (2012b). Variations in T 2* and fat content of murine brown and white adipose tissues by chemical-shift MRI. *Magnetic Resonance Imaging, 30*(3), 323-329.
Hu, H. H., Perkins, T. G., Chia, J. M., & Gilsanz, V. (2013a). Characterization of Human Brown Adipose Tissue by Chemical-Shift Water-Fat MRI. *American Journal of Roentgenology*, *200*(1), 177–183. http://doi.org/10.2214/AJR.12.8996
Hu, H. H., Smith, D. L. J., Nayak, K. S., Goran, M. I., & Nagy, T. R. (2010). Identification of brown adipose tissue in mice with fat-water IDEAL-MRI. *Journal of Magnetic Resonance Imaging : JMRI*, *31*(5), 1195–1202. http://doi.org/10.1002/jmri.22162
Hu, H. H., Tovar, J. P., Pavlova, Z., Smith, M. L., & Gilsanz, V. (2012). Unequivocal identification of brown adipose tissue in a human infant. *Journal of Magnetic Resonance Imaging : JMRI*, *35*(4), 938–942. http://doi.org/10.1002/jmri.23531
Hu, H. H., Yin, L., Aggabao, P. C., Perkins, T. G., Chia, J. M., & Gilsanz, V. (2013b). Comparison of brown and white adipose tissues in infants and children with chemical-shift-encoded water-fat MRI. *Journal of Magnetic Resonance Imaging : JMRI*, n/a–n/a. http://doi.org/10.1002/jmri.24053
Huang, H., Xue, R., Zhang, J., Ren, T., Richards, L. J., Yarowsky, P., ... & Mori, S. (2009). Anatomical characterization of human fetal brain development with diffusion tensor magnetic resonance imaging. *The Journal of Neuroscience*, *29*(13), 4263-4273.
Hube, F., Lietz, U., Igel, M., Jensen, P. B., Tornqvist, H., Joost, H. G., & Hauner, H. (1996). Difference in leptin mRNA levels between omental and subcutaneous abdominal adipose tissue from obese humans. *Hormone and Metabolic Research = Hormon- Und Stoffwechselforschung = Hormones Et Métabolisme*, *28*(12), 690–693. http://doi.org/10.1055/s-2007-979879
Hung, C. S., Lee, J. K., Yang, C. Y., Hsieh, H. R., Ma, W. Y., & Lin, M. S. (2014). Measurement of visceral fat: should we include retroperitoneal fat? *PLoS One,* e112355.
Huxley, R. R., Shiell, A. W., & Law, C. M. (2000). The role of size at birth and postnatal catch-

up growth in determining systolic blood pressure: a systematic review of the literature. *Journal of Hypertension,* 18(7):815-31.

Hüppi, P. S., Maier, S. E., Peled, S., Zientara, G. P., Barnes, P. D., Jolesz, F. A., & Volpe, J. J. (1998). Microstructural development of human newborn cerebral white matter assessed in vivo by diffusion tensor magnetic resonance imaging. *Pediatric Research*, *44*(4), 584–590. http://doi.org/10.1203/00006450-199810000-00019

Hwang, Y.-C., Hayashi, T., Fujimoto, W. Y., Kahn, S. E., Leonetti, D. L., McNeely, M. J., & Boyko, E. J. (2015). Visceral abdominal fat accumulation predicts the conversion of metabolically healthy obese subjects to an unhealthy phenotype. *International Journal of Obesity (2005)*. http://doi.org/10.1038/ijo.2015.75

Jahng, G. H., Song, E., Zhu, X. P., Matson, G. B., Weiner, M. W., & Schuff, N. (2005). Human Brain: Reliability and Reproducibility of Pulsed Arterial Spin-labeling Perfusion MR Imaging. *Radiology*, *234*(3), 909–916. http://doi.org/10.1148/radiol.2343031499

Janowitz, D., Wittfeld, K., Terock, J., Freyberger, H. J., Hegenscheid, K., Völzke, H., et al. (2015). Association between waist circumference and gray matter volume in 2344 individuals from two adult community-based samples. *Neuroimage*, *122*(C), 149–157. http://doi.org/10.1016/j.neuroimage.2015.07.086

Jauch-Chara, K., Binkofski, F., Loebig, M., Reetz, K., Jahn, G., Melchert, U. H., ... & Oltmanns, K. M. (2015). Blunted brain energy consumption relates to insula atrophy and impaired glucose tolerance in obesity. *Diabetes*, *64*(6), 2082-2091.

Johnson, W., Choh, A. C., Lee, M., & Towne, B. (2013). Characterization of the infant BMI peak: sex differences, birth year cohort effects, association with concurrent adiposity, and heritability. *American Journal of Human Biology,* 25(3):378-88.

Johnstone, A. M., Murison, S. D., Duncan, J. S., Rance, K. A., & Speakman, J. R. (2005). Factors influencing variation in basal metabolic rate include fat-free mass, fat mass, age, and circulating thyroxine but not sex, circulating leptin, or triiodothyronine. *The American Journal of Clinical Nutrition*, *82*(5), 941–948.

Jones, D. K., Knösche, T. R., & Turner, R. (2013). White matter integrity, fiber count, and other fallacies: The do"s and don"ts of diffusion MRI. *Neuroimage*, *73*(C), 239–254. http://doi.org/10.1016/j.neuroimage.2012.06.081

Kanoski, S. E., & Grill, H. J. (2015). Hippocampus contributions to food intake control: mnemonic, neuroanatomical, and endocrine mechanisms. *Biological Psychiatry,* S0006-3223(15)00771-4.

Karlsson, H. K., Tuulari, J. J., Hirvonen, J., Lepomäki, V., Parkkola, R., Hiltunen, J., et al. (2013). Obesity is associated with white matter atrophy: a combined diffusion tensor imaging and voxel-based morphometric study. *Obesity*, *21*(12), 2530–2537. http://doi.org/10.1002/oby.20386

Kaufmann, C. (2006). Brain activation and hypothalamic functional connectivity during human non-rapid eye movement sleep: an EEG/fMRI study. *Brain*, *129*(3), 655–667. http://doi.org/10.1093/brain/awh686

Kaul, S., Rothney, M. P., Peters, D. M., & Wacker, W. K. (2012). Dual-Energy X-Ray Absorptiometry for Quantification of Visceral Fat. *Obesity*, 20(6):1313-8.

Kelly, A. M. C., Di Martino, A., Uddin, L. Q., Shehzad, Z., Gee, D. G., Reiss, P. T., et al. (2009). Development of anterior cingulate functional connectivity from late childhood to early adulthood. *Cerebral Cortex*, *19*(3), 640–657. http://doi.org/10.1093/cercor/bhn117

Kelly, A. S., Barlow, S. E., Rao, G., Inge, T. H., Hayman, L. L., Steinberger, J., et al. (2013).

Severe Obesity in Children and Adolescents: Identification, Associated Health Risks, and Treatment Approaches: A Scientific Statement From the American Heart Association. *Circulation*, *128*(15), 1689–1712. http://doi.org/10.1161/CIR.0b013e3182a5cfb3

Kersbergen, K. J., Leemans, A., Groenendaal, F., van der Aa, N. E., Viergever, M. A., de Vries, L. S., & Benders, M. J. N. L. (2010). Microstructural brain development between 30 and 40weeks corrected age in a longitudinal cohort of extremely preterm infants. *Neuroimage*, *103*, 1–11. http://doi.org/10.1016/j.neuroimage.2014.09.039

Khanna, A., & Branca, R. T. (2012). Detecting brown adipose tissue activity with BOLD MRI in mice. *Magnetic Resonance in Medicine*. http://doi.org/10.1002/mrm.24118

Kim, D. J., Davis, E. P., Sandman, C. A., & Sporns, O. (2014). Longer gestation is associated with more efficient brain networks in preadolescent children. *Neuroimage,* 100:619-27.

Kim, H., Lepage, C., Maheshwary, R., Jeon, S., & Evans, A. C. (2016). NEOCIVET: Towards accurate morphometry of neonatal gyrification and clinical applications in preterm newborns. *Neuroimage,* 138:28-42.

Kinney, H.C., Kloman, A.S. and Gilles, F.H., (1988). Sequence of central nervous system myelination in human infancy. II. Patterns of myelination in autopsied infants. *Journal of Neuropathology & Experimental Neurology*, *47*(3), pp.217-234.

Knickmeyer, R. C., Gouttard, S., & Kang, C. (2008). A structural MRI study of human brain development from birth to 2 years. *The Journal of Neuroscience,* 28(47):12176-82.

Knuepfer, M. M., Eismann, A., & Schutze, I. (1995). Responses of single neurons in amygdala to interoceptive and exteroceptive stimuli in conscious cats. *American Journal of Physiology,* 268(3 Pt 2).

Koontz, M. B., Gunzler, D. D., Presley, L., & Catalano, P. M. (2014). Longitudinal changes in infant body composition: association with childhood obesity. *Pediatric Obesity*, *9*(6), e141–4. http://doi.org/10.1111/ijpo.253

Kostović, I., & Jovanov-Milošević, N. (2006). The development of cerebral connections during the first 20–45 weeks' gestation. *Seminars in Fetal and Neonatal Medicine*, *11*(6), 415–422. http://doi.org/10.1016/j.siny.2006.07.001

Kruithof, C. J., Gishti, O., Hofman, A., Gaillard, R., & Jaddoe, V. W. V. (2016). Infant weight growth velocity patterns and general and abdominal adiposity in school-age children. The Generation R Study. *European Journal of Clinical Nutrition*. http://doi.org/10.1038/ejcn.2016.60

Kulkarni, B., Mamidi, R. S., Balakrishna, N., & Radhakrishna, K. V. (2014). Body composition assessment in infancy and early childhood: comparison of anthropometry with dual-energy X-ray absorptiometry in low-income group children from India. *European Journal of Clinical Nutrition*, *68*(6), 658–663. http://doi.org/10.1038/ejcn.2014.37

Kullberg, J., Brandberg, J., Angelhed, J. E., & Frimmel, H. (2014). Whole-body adipose tissue analysis: comparison of MRI, CT and dual energy X-ray absorptiometry, *British Journal of Radiology,* 82(974):123-30.

Kullmann, S., Callaghan, M. F., Heni, M., & Weiskopf, N. (2016). Specific white matter tissue microstructure changes associated with obesity. *Neuroimage,* 125:36-44.

Kullmann, S., Heni, M., Linder, K., Zipfel, S., Häring, H.-U., Veit, R., et al. (2014). Resting-state functional connectivity of the human hypothalamus. *Human Brain Mapping*, *35*(12), 6088–6096. http://doi.org/10.1002/hbm.22607

Kullmann, S., Heni, M., Veit, R., Ketterer, C., Schick, F., Häring, H.-U., et al. (2011). The obese brain: Association of body mass index and insulin sensitivity with resting state network

functional connectivity. *Human Brain Mapping*, *33*(5), 1052–1061. http://doi.org/10.1002/hbm.21268
Kullmann, S., Pape, A.-A., Heni, M., Ketterer, C., Schick, F., Häring, H.-U., et al. (2013). Functional network connectivity underlying food processing: disturbed salience and visual processing in overweight and obese adults. *Cerebral Cortex*, *23*(5), 1247–1256. http://doi.org/10.1093/cercor/bhs124
Kullmann, S., Schweizer, F., Veit, R., & Fritsche, A. (2015). Compromised white matter integrity in obesity. *Obesity,* 16(4):273-81.
Kuo, L. E., Kitlinska, J. B., Tilan, J. U., Li, L., Baker, S. B., Johnson, M. D., et al. (2007). Neuropeptide Y acts directly in the periphery on fat tissue and mediates stress-induced obesity and metabolic syndrome. *Nature Medicine*, *13*(7), 803–811. http://doi.org/10.1038/nm1611
Kurth, F., Levitt, J. G., Phillips, O. R., Luders, E., Woods, R. P., Mazziotta, J. C., et al. (2012). Relationships between gray matter, body mass index, and waist circumference in healthy adults. *Human Brain Mapping*, *34*(7), 1737–1746. http://doi.org/10.1002/hbm.22021
Kurth, F., Levitt, J. G., Phillips, O. R., Luders, E., Woods, R. P., Mazziotta, J. C., et al. (2013). Relationships between gray matter, body mass index, and waist circumference in healthy adults. *Human Brain Mapping*, *34*(7), 1737–1746. http://doi.org/10.1002/hbm.22021
Kurth, F., Zilles, K., Fox, P. T., Laird, A. R., & Eickhoff, S. B. (2010). A link between the systems: functional differentiation and integration within the human insula revealed by meta-analysis. *Brain Structure and Function*, *214*(5-6), 519–534. http://doi.org/10.1007/s00429-010-0255-z
Lakens, D. (2013). Calculating and reporting effect sizes to facilitate cumulative science: a practical primer for t-tests and ANOVAs. *Frontiers in Psychology*, *4*, 863. http://doi.org/10.3389/fpsyg.2013.00863
Laskey, M. A. (1996). Dual-energy X-ray absorptiometry and body composition. *Nutrition,* 12(1):45-51.
Latini, F. (2015). New insights in the limbic modulation of visual inputs: the role of the inferior longitudinal fasciculus and the Li-Am bundle. *Neurosurgical Review,* 38(1):179-89.
Lau, A. Z., Chen, A. P., & Gu, Y. (2014). Noninvasive identification and assessment of functional brown adipose tissue in rodents using hyperpolarized 13C imaging. *International Journal of Obesity,* 38(1):126-31.
Lee, K., Cherel, M., & Budin, F. (2015). Early postnatal myelin content estimate of white matter via T1/T2w ratio. *SPIE Medical,* pp. 94171R-94171R .
Lee, Y., Chong, M., Liu, J., & Libedinsky, C. (2013). Dietary disinhibition modulates neural valuation of food in the fed and fasted states. *The American journal of Clinical Nutrition*, 97(5):919-25.
Lefèvre, J., Germanaud, D., Dubois, J., & Rousseau, F. (2015). Are Developmental Trajectories of Cortical Folding Comparable Between Cross-sectional Datasets of Fetuses and Preterm Newborns? *Cerebral Cortex,* p.bhv123.
Leptin replacement alters brain response to food cues in genetically leptin-deficient adults. (2007). Leptin replacement alters brain response to food cues in genetically leptin-deficient adults, 1–4.

Li, H., Chan, R. C. K., McAlonan, G. M., & Gong, Q.-Y. (2010). Facial emotion processing in schizophrenia: a meta-analysis of functional neuroimaging data. *Schizophrenia Bulletin*, *36*(5), 1029–1039. http://doi.org/10.1093/schbul/sbn190

Li, R., O'Connor, L., Buckley, D., & Specker, B. (1995). Relation of activity levels to body fat in infants 6 to 12 months of age. *The Journal of Pediatrics*, *126*(3), 353–357.

Lim, S. S., Vos, T., Flaxman, A. D., Danaei, G., Shibuya, K., Adair-Rohani, H., ... & Aryee, M. (2013). A comparative risk assessment of burden of disease and injury attributable to 67 risk factors and risk factor clusters in 21 regions, 1990–2010: a systematic analysis for the Global Burden of Disease Study 2010. *The lancet*, *380*(9859), 2224-2260.

Lidell, M. E., Betz, M. J., Leinhard, O. D., Heglind, M., Elander, L., Slawik, M., et al. (2013). Evidence for two types of brown adipose tissue in humans. *Nature Medicine*, 1–5. http://doi.org/10.1038/nm.3017

Lips, M. A., & Wijngaarden, M. A. (2014). Resting-state functional connectivity of brain regions involved in cognitive control, motivation, and reward is enhanced in obese females. *The American Journal of Clinical Nutrition,* 100(2):524-31.

Lobstein, T., & Dibb, S. (2005). Evidence of a possible link between obesogenic food advertising and child overweight. *Obesity Reviews,* 6(3):203-8.

Locke, A. E., Kahali, B., Berndt, S. I., Justice, A. E., & Pers, T. H. (2015). Genetic studies of body mass index yield new insights for obesity biology. *Nature,* 518(7538):197-206.

Lunati, E., Marzola, P., Nicolato, E., Fedrigo, M., Villa, M., & Sbarbati, A. (1999). In vivo quantitative lipidic map of brown adipose tissue by chemical shift imaging at 4.7 Tesla. *J Lipid Res*, *40*(8), 1395–1400.

Ma, J. (2004). Breath-hold water and fat imaging using a dual-echo two-point dixon technique with an efficient and robust phase-correction algorithm. *Magnetic Resonance in Medicine*, *52*(2), 415–419. http://doi.org/10.1002/mrm.20146

Ma, J. (2008). Dixon techniques for water and fat imaging. *Journal of Magnetic Resonance Imaging : JMRI*, *28*(3), 543–558. http://doi.org/10.1002/jmri.21492

Maayan, L., Hoogendoorn, C., Sweat, V., & Convit, A. (2011). Disinhibited eating in obese adolescents is associated with orbitofrontal volume reductions and executive dysfunction. *Obesity*, *19*(7), 1382–1387. http://doi.org/10.1038/oby.2011.15

Magnus, M. C., Olsen, S. F., Granström, C., Joner, G., Skrivarhaug, T., Svensson, J., et al. (2015). Infant Growth and Risk of Childhood-Onset Type 1 Diabetes in Children From 2 Scandinavian Birth Cohorts. *JAMA Pediatrics*, *169*(12), e153759. http://doi.org/10.1001/jamapediatrics.2015.3759

Malenka, R. C., Nestler, E., Hyman, S., Sydor, A., & Brown, R. Y. (2009). Molecular Neuropharmacology: A Foundation for Clinical Neuroscience. http://dx.doi.org/10.1176/appi.ajp.159.7.1251

Malik, S., McGlone, F., Bedrossian, D., & Dagher, A. (2008). Ghrelin Modulates Brain Activity in Areas that Control Appetitive Behavior. *Cell Metabolism*, *7*(5), 400–409. http://doi.org/10.1016/j.cmet.2008.03.007

Martin, L. E., Holsen, L. M., Chambers, R. J., Bruce, A. S., Brooks, W. M., Zarcone, J. R., et al. (2010). Neural mechanisms associated with food motivation in obese and healthy weight adults. *Obesity*, *18*(2), 254–260. http://doi.org/10.1038/oby.2009.220

Matsuzawa, Y., Funahashi, T., & Nakamura, T. (2011). The concept of metabolic syndrome: contribution of visceral fat accumulation and its molecular mechanism. *Journal of Atherosclerosis and Thrombosis*, *18*(8), 629–639.

McArdle, W. D., Katch, F. I., & Katch, V. L. (2010). Exercise physiology: nutrition, energy, and human performance. Lippincott Williams & Wilkins.
McCloskey, K., Burgner, D., Carlin, J. B., Skilton, M. R., Cheung, M., Dwyer, T., et al. (2016). Infant adiposity at birth and early postnatal weight gain predict increased aortic intima-media thickness at 6 weeks of age: a population-derived cohort study. *Clinical Science*, *130*(6), 443–450. http://doi.org/10.1042/CS20150685
McFadden, K. L., Cornier, M.-A., Melanson, E. L., Bechtell, J. L., & Tregellas, J. R. (2013). Effects of exercise on resting-state default mode and salience network activity in overweight/obese adults. *Neuroreport*, *24*(15), 866–871. http://doi.org/10.1097/WNR.0000000000000013
McPherson, K. (2014). Reducing the global prevalence of overweight and obesity. *The Lancet*, *384*(9945), 728–730. http://doi.org/10.1016/S0140-6736(14)60767-4
Menon, V., & Uddin, L. Q. (2010). Saliency, switching, attention and control: a network model of insula function. *Brain Structure and Function*, *214*(5-6), 655–667. http://doi.org/10.1007/s00429-010-0262-0
Mifflin, M. D., St Jeor, S. T., Hill, L. A., Scott, B. J., Daugherty, S. A., & Koh, Y. O. (1990). A new predictive equation for resting energy expenditure in healthy individuals. *The American Journal of Clinical Nutrition*, *51*(2), 241–247.
Miller, A. A., & Spencer, S. J. (2014). Obesity and neuroinflammation: a pathway to cognitive impairment. *Brain,* 42:10-21.
Modi, N., Thomas, E. L., Uthaya, S. N., Umranikar, S., Bell, J. D., & Yajnik, C. (2009). Whole body magnetic resonance imaging of healthy newborn infants demonstrates increased central adiposity in Asian Indians. *Pediatric Research*, *65*(5), 584–587. http://doi.org/10.1203/01.pdr.0000350364.10602.33
Monteiro, P. O. A., & Victora, C. G. (2005). Rapid growth in infancy and childhood and obesity in later life--a systematic review. *Obesity Reviews : an Official Journal of the International Association for the Study of Obesity*, *6*(2), 143–154. http://doi.org/10.1111/j.1467-789X.2005.00183.x
Monteiro, P. O. A., Victora, C. G., Barros, F. C., & Monteiro, L. M. A. (2003). Birth size, early childhood growth, and adolescent obesity in a Brazilian birth cohort. *International Journal of Obesity and Related Metabolic Disorders : Journal of the International Association for the Study of Obesity*, *27*(10), 1274–1282. http://doi.org/10.1038/sj.ijo.0802409
Morel, A., Gallay, M. N., Baechler, A., Wyss, M., & Gallay, D. S. (2013). The human insula: architectonic organization and postmortem MRI registration. *Neuroscience,* 236:117-35.
Morton, G. J., Meek, T. H., & Schwartz, M. W. (2014). Neurobiology of food intake in health and disease. *Nature Reviews Neuroscience,* 15(6):367-78.
Murray, E. A. (2007). The amygdala, reward and emotion. *Trends in Cognitive Sciences,* 11(11):489-97.
Nederkoorn, C., Braet, C., Van Eijs, Y., & Tanghe, A. (2006). Why obese children cannot resist food: the role of impulsivity. *Eating Behaviors,* 7(4):315-22.
Nie, J., Li, G., Wang, L., Shi, F., & Lin, W. (2014). Longitudinal development of cortical thickness, folding, and fiber density networks in the first 2 years of life. *Human Brain Mapping, 35*(8), pp.3726-3737.
O'Brien, G. D., Queenan, J. T., & Campbell, S. (1981). Assessment of gestational age in the second trimester by real-time ultrasound measurement of the femur length. Am J

Obstet Gynecol.
Oishi, K., Faria, A. V., & Mori, S. (2012). Advanced neonatal neuroMRI. *Magnetic Resonance Imaging Clinics of North America,* 20(1):81-91.
Oishi, K., Mori, S., Donohue, P. K., Ernst, T., Anderson, L., Buchthal, S., et al. (2011). Multi-contrast human neonatal brain atlas: Application to normal neonate development analysis. *Neuroimage*, *56*(1), 8–20. http://doi.org/10.1016/j.neuroimage.2011.01.051
Oliver, G., Wardle, J., & Gibson, E. L. (2000). Stress and food choice: a laboratory study. *Psychosomatic Medicine,* 62(6):853-65.
Ong, K. K., & Loos, R. (2006). Rapid infancy weight gain and subsequent obesity: systematic reviews and hopeful suggestions. *Acta Paediatrica,* 95(8):904-8.
Ong, K. K., Emmett, P., & Northstone, K. (2009). Infancy weight gain predicts childhood body fat and age at menarche in girls. *The Journal of Clinical Nutrition,* 94(5):1527-32.
Ongür, D., Lundy, M., Greenhouse, I., Shinn, A. K., Menon, V., Cohen, B. M., & Renshaw, P. F. (2010). Default mode network abnormalities in bipolar disorder and schizophrenia. *Psychiatry Research*, *183*(1), 59–68. http://doi.org/10.1016/j.pscychresns.2010.04.008
Ou, X., Andres, A., Pivik, R. T., Cleves, M. A., & Badger, T. M. (2015). Brain gray and white matter differences in healthy normal weight and obese children. *Journal of Magnetic Resonance Imaging : JMRI*. http://doi.org/10.1002/jmri.24912
Pan, H., Guo, J., & Su, Z. (2014). Advances in understanding the interrelations between leptin resistance and obesity. *Physiology & Behavior*, *130*, 157–169. http://doi.org/10.1016/j.physbeh.2014.04.003
Pannacciulli, N., Del Parigi, A., Chen, K., Le, D. S. N. T., Reiman, E. M., & Tataranni, P. A. (2006). Brain abnormalities in human obesity: A voxel-based morphometric study. *Neuroimage*, *31*(4), 1419–1425. http://doi.org/10.1016/j.neuroimage.2006.01.047
Pannacciulli, N., Le, D. S. N. T., Chen, K., Reiman, E. M., & Krakoff, J. (2007). Relationships between plasma leptin concentrations and human brain structure: A voxel-based morphometric study. *Neuroscience Letters*, *412*(3), 248–253. http://doi.org/10.1016/j.neulet.2006.11.019
Partridge, S. C., Mukherjee, P., Henry, R. G., Miller, S. P., Berman, J. I., Jin, H., et al. (2004). Diffusion tensor imaging: serial quantitation of white matter tract maturity in premature newborns. *Neuroimage*, *22*(3), 1302–1314. http://doi.org/10.1016/j.neuroimage.2004.02.038
Peng, X. G., Ju, S., Fang, F., & Wang, Y. (2013). Comparison of brown and white adipose tissue fat fractions in ob, seipin, and Fsp27 gene knockout mice by chemical shift-selective imaging and 1H-MR. *American Journal of Clinical Nutrition,* 304(2):E160-7.
Peng, Y., Gillis-Smith, S., Jin, H., Tränkner, D., Ryba, N. J. P., & Zuker, C. S. (2015). Sweet and bitter taste in the brain of awakebehaving animals. *Nature*, 1–12. http://doi.org/10.1038/nature15763
Peters, J., & Büchel, C. (2010). Neural representations of subjective reward value. *Behavioural Brain Research,* 213(2):135-41.
Peters, J., Dauvermann, M., Mette, C., Platen, P., Franke, J., Hinrichs, T., & Daum, I. (2009). **Voxel-based morphometry reveals an association between aerobic capacity and grey matter density in the right anterior insula**. *Neuroscience*, *163*(4), 1102–1108. http://doi.org/10.1016/j.neuroscience.2009.07.030
Pistollato, F., Chen, H. L., Schwartz, P. H., & Basso, G. (2007). Oxygen tension controls the expansion of human CNS precursors and the generation of astrocytes and

oligodendrocytes. *Molecular and Cellular Neurosci,* 35(3):424-35.
Pomarol-Clotet, E., Salvador, R., Sarró, S., Gomar, J., Vila, F., Martínez, A., et al. (2008). Failure to deactivate in the prefrontal cortex in schizophrenia: dysfunction of the default mode network? *Psychological Medicine*, *38*(8), 1185–1193. http://doi.org/10.1017/S0033291708003565
Poskitt, E. M., & Cole, T. J. (1977). Do fat babies stay fat? *Bmj,* doi: http://dx.doi.org/10.1136/bmj.1.6052.7.
Power, J. D., Barnes, K. A., Snyder, A. Z., Schlaggar, B. L., & Petersen, S. E. (2012). Spurious but systematic correlations in functional connectivity MRI networks arise from subject motion. *Neuroimage*, *59*(3), 2142–2154. http://doi.org/10.1016/j.neuroimage.2011.10.018
Prastawa, M., Gilmore, J. H., Lin, W., & Gerig, G. (2005). Automatic segmentation of MR images of the developing newborn brain. *Medical Image Analysis*, *9*(5), 457–466. http://doi.org/10.1016/j.media.2005.05.007
Provenzale, J. M., Isaacson, J., & Chen, S. (2012). Progression of Corpus Callosum Diffusion-Tensor Imaging Values During a Period of Signal Changes Consistent With Myelination. *American Journal of Roentgenology*, *198*(6), 1403–1408. http://doi.org/10.2214/AJR.11.7849
Puhl, R. M., & Heuer, C. A. (2010). Obesity stigma: important considerations for public health. *American Journal of Public Health,* 100(6): 1019–1028.
Puhl, R. M., & Latner, J. D. (2007). Stigma, obesity, and the health of the nation's children. *Psychological Bulletin,* 133(4):557-80.
Qiu, A., Fortier, M. V., Bai, J., Zhang, X., Chong, Y.-S., Kwek, K., et al. (2013). Morphology and microstructure of subcortical structures at birth: A large-scale Asian neonatal neuroimaging study. *Neuroimage*, *65*(C), 315–323. http://doi.org/10.1016/j.neuroimage.2012.09.032
Rabi, Y., Yee, W., Chen, S. Y., & Singhal, N. (2006). Oxygen saturation trends immediately after birth. *The Journal of Pediatrics,* 148(5):590-4.
Radaelli, T., Uvena-Celebrezze, J., Minium, J., Huston-Presley, L., Catalano, P., & Hauguel-de Mouzon, S. (2006). Maternal interleukin-6: marker of fetal growth and adiposity. *Journal of the Society for Gynecologic Investigation*, *13*(1), 53–57. http://doi.org/10.1016/j.jsgi.2005.10.003
Raji, C. A., Ho, A. J., Parikshak, N. N., Becker, J. T., Lopez, O. L., Kuller, L. H., et al. (2009). Brain structure and obesity. *Human Brain Mapping*, http://doi.org/10.1002/hbm.20870
Rasmussen, J. M., Entringer, S., Nguyen, A., van Erp, T. G. M., Guijarro, A., Oveisi, F., et al. (2013). Brown adipose tissue quantification in human neonates using water-fat separated MRI. *PLoS One*, *8*(10), e77907. http://doi.org/10.1371/journal.pone.0077907
Reilly, J. J., Methven, E., & McDowell, Z. C. (2003). Health consequences of obesity. *Archives of Disease in Obesity, 101*(Supplement 2), 518-525.
Rothemund, Y., Preuschhof, C., Bohner, G., Bauknecht, H.-C., Klingebiel, R., Flor, H., & Klapp, B. F. (2007). Differential activation of the dorsal striatum by high-calorie visual food stimuli in obese individuals. *Neuroimage*, *37*(2), 410–421. http://doi.org/10.1016/j.neuroimage.2007.05.008
Rutkowski, J. M., Davis, K. E., & Scherer, P. E. (2009). Mechanisms of obesity and related pathologies: The macro- and microcirculation of adipose tissue. *FEBS Journal*, *276*(20),

5738–5746. http://doi.org/10.1111/j.1742-4658.2009.07303.x
Saito, M., Okamatsu-Ogura, Y., Matsushita, M., Watanabe, K., Yoneshiro, T., Nio-Kobayashi, J., et al. (2009). High Incidence of Metabolically Active Brown Adipose Tissue in Healthy Adult Humans: Effects of Cold Exposure and Adiposity. *Diabetes*, *58*(7), 1526–1531. http://doi.org/10.2337/db09-0530
Saper, C. B., Chou, T. C., & Elmquist, J. K. (2002). The need to feed: homeostatic and hedonic control of eating. *Neuron,* 36(2):199-211.
Schroeter, M. L., Raczka, K., Neumann, J., & Cramon, von, D. Y. (2008). Neural networks in frontotemporal dementia--a meta-analysis. *Neurobiology of Aging*, *29*(3), 418–426. http://doi.org/10.1016/j.neurobiolaging.2006.10.023
Seeley, W. W., Menon, V., Schatzberg, A. F., Keller, J., Glover, G. H., Kenna, H., et al. (2007). Dissociable intrinsic connectivity networks for salience processing and executive control. *Journal of Neuroscience*, *27*(9), 2349–2356. http://doi.org/10.1523/JNEUROSCI.5587-06.2007
Seidell, J. C., Björntorp, P., Sjöström, L., & Kvist, H. (1990). Visceral fat accumulation in men is positively associated with insulin, glucose, and C-peptide levels, but negatively with testosterone levels. *Metabolism,* 39(9):897-901.
Serdula, M. K., Ivery, D., Coates, R. J., Freedman, D. S., Williamson, D. F., & Byers, T. (1993). Do obese children become obese adults? A review of the literature. *Preventive Medicine*, *22*(2), 167–177. http://doi.org/10.1006/pmed.1993.1014
Sesack, S. R., & Grace, A. A. (2010). Cortico-basal ganglia reward network: microcircuitry. *Neuropsychopharmacology,* 35(1):27-47.
Sescousse, G., Caldú, X., Segura, B., & Dreher, J. C. (2013). Processing of primary and secondary rewards: a quantitative meta-analysis and review of human functional neuroimaging studies. *Neuroscience & Biobehavioral Reviews,* 37(4):681-96.
Sharkey, R. J., Karama, S., & Dagher, A. (2015). Overweight is not associated with cortical thickness alterations in children. *Frontiers in Neuroscience*, *9*, 24. http://doi.org/10.3389/fnins.2015.00024
Silverwood, R. J., De Stavola, B. L., Cole, T. J., & Leon, D. A. (2009). BMI peak in infancy as a predictor for later BMI in the Uppsala Family Study. *International Journal of Obesity (2005)*, *33*(8), 929–937. http://doi.org/10.1038/ijo.2009.108
Simerly, R. (2006, November). Feeding signals and drugs meet in the midbrain. *Nature Medicine*, pp. 1244–1246. http://doi.org/10.1038/nm1106-1244
Simon, S. A., de Araujo, I. E., Gutierrez, R., & Nicolelis, M. A. L. (2006). The neural mechanisms of gustation: a distributed processing code. *Nature Reviews Neuroscience*, *7*(11), 890–901. http://doi.org/10.1038/nrn2006
Smith, S. M., Jenkinson, M., Woolrich, M. W., & Beckmann, C. F. (2004). Advances in functional and structural MR image analysis and implementation as FSL. *Neuroimage,* 23 Suppl 1:S208-19.
Smucny, J., Cornier, M.-A., Eichman, L. C., Thomas, E. A., Bechtell, J. L., & Tregellas, J. R. (2012). Brain structure predicts risk for obesity. *Appetite*, *59*(3), 859–865. http://doi.org/10.1016/j.appet.2012.08.027
Sonnenschein-van der Voort, A. M. M., Arends, L. R., de Jongste, J. C., Annesi-Maesano, I., Arshad, S. H., Barros, H., et al. (2014). Preterm birth, infant weight gain, and childhood asthma risk: a meta-analysis of 147,000 European children. *The Journal of Allergy and Clinical Immunology*, *133*(5), 1317–1329. http://doi.org/10.1016/j.jaci.2013.12.1082

Stanek, K. M., Grieve, S. M., Brickman, A. M., & Korgaonkar, M. S. (2011). Obesity Is Associated With Reduced White Matter Integrity in Otherwise Healthy Adults. *Obesity,* 19(3):500-4.

Steculorum, S. M., Collden, G., & Coupe, B. (2015). Neonatal ghrelin programs development of hypothalamic feeding circuits. *The Journal of Clinical Investigation, 125*(2), pp.846-858.

Steidle, G., Eibofner, F., & Schick, F. (2011). Quantitative diffusion imaging of adipose tissue in the human lower leg at 1.5 T. *Magnetic Resonance in Medicine*, *65*(4), 1118–1124. http://doi.org/10.1002/mrm.22699

Stephani, C., Fernandez-Baca Vaca, G., Maciunas, R., Koubeissi, M., & Lüders, H. O. (2010). Functional neuroanatomy of the insular lobe. *Brain Structure and Function*, *216*(2), 137–149. http://doi.org/10.1007/s00429-010-0296-3

Stettler, N., Kumanyika, S. K., Katz, S. H., Zemel, B. S., & Stallings, V. A. (2003). Rapid weight gain during infancy and obesity in young adulthood in a cohort of African Americans. *The American Journal of Clinical Nutrition*, *77*(6), 1374–1378.

Stoeckel, L. E., Kim, J., Weller, R. E., Cox, J. E., & Cook, E. W. (2009). Effective connectivity of a reward network in obese women. *Brain Research Bulletin,* 79(6):388-95.

Stoeckel, L. E., Weller, R. E., Cook, E. W., Twieg, D. B., Knowlton, R. C., & Cox, J. E. (2008). Widespread reward-system activation in obese women in response to pictures of high-calorie foods. *Neuroimage*, *41*(2), 636–647. http://doi.org/10.1016/j.neuroimage.2008.02.031

Symonds, M. E., Pope, M., Sharkey, D., & Budge, H. (2012). Adipose tissue and fetal programming. *Diabetologia*, *55*(6), 1597–1606. http://doi.org/10.1007/s00125-012-2505-5

Tau, G. Z., & Peterson, B. S. (2009). Normal Development of Brain Circuits. *Neuropsychopharmacology*, *35*(1), 147–168. http://doi.org/10.1038/npp.2009.115

Thomas Yeo, B. T., Krienen, F. M., Sepulcre, J., Sabuncu, M. R., Lashkari, D., Hollinshead, M., et al. (2011). The organization of the human cerebral cortex estimated by intrinsic functional connectivity. *Journal of Neurophysiology*, *106*(3), 1125–1165. http://doi.org/10.1152/jn.00338.2011

Tint, M. T., Fortier, M. V., Godfrey, K. M., & Shuter, B. (2016). Abdominal adipose tissue compartments vary with ethnicity in Asian neonates: Growing Up in Singapore Toward Healthy Outcomes birth cohort study. *The American Journal Clinical Nutrition,* 103(5):1311-7.

Toda, T., Homma, D., Tokuoka, H., Hayakawa, I., Sugimoto, Y., Ichinose, H., & Kawasaki, H. (2013). Birth Regulates the Initiation of Sensory Map Formation through Serotonin Signaling. *Developmental Cell*, *27*(1), 32–46. http://doi.org/10.1016/j.devcel.2013.09.002

Tomasi, D., Wang, G. J., Wang, R., Backus, W., & Geliebter, A. (2009). Association of body mass and brain activation during gastric distention: implications for obesity. *PLoS,* 4(8):e6847.

Tregellas, J. R., Wylie, K. P., Rojas, D. C., Tanabe, J., Martin, J., Kronberg, E., et al. (2011). Altered default network activity in obesity. *Obesity*, *19*(12), 2316–2321. http://doi.org/10.1038/oby.2011.119

Uddin, L. Q. (2015). Salience processing and insular cortical function and dysfunction. *Nature Reviews Neuroscience*, *16*(1), 55–61. http://doi.org/10.1038/nrn3857

van Bloemendaal, L., Ijzerman, R. G., & Jennifer, S. (2016). Alterations in white matter volume and integrity in obesity and type 2 diabetes. *Metabolic Brain Disorder,* 31: 621–629.
Van Essen, D. C., Smith, S. M., Barch, D. M., & Behrens, T. (2013). The WU-Minn human connectome project: an overview. *Neuroimage,* 80:62-79.
Van Kooij, B., De Vries, L. S., & Ball, G. (2012). Neonatal tract-based spatial statistics findings and outcome in preterm infants. *American Journal Neuroradiology,* 33(1):188-94.
Van Leemput, K., Maes, F., Vandermeulen, D., & Suetens, P. (1999). Automated model-based tissue classification of MR images of the brain. *IEEE Transactions on Medical Imaging*, *18*(10), 897–908. http://doi.org/10.1109/42.811270
van Marken Lichtenbelt, W. D., Vanhommerig, J. W., Smulders, N. M., Drossaerts, J. M., Kemerink, G. J., Bouvy, N. D., et al. (2009). Cold-activated brown adipose tissue in healthy men. *N Engl J Med*, *360*(15), 1500–1508. http://doi.org/10.1056/NEJMoa0808718
van Rooijen, B. D., van der Lans, A., & Brans, B. (2013). Imaging cold-activated brown adipose tissue using dynamic T2*-weighted magnetic resonance imaging and 2-deoxy-2-[18F] fluoro-D-glucose positron emission. *Investigative Radiology,* 48(10):708-14.
Vandenbergh, J., DuPont, P., Fischler, B., Bormans, G., Persoons, P., Janssens, J., & Tack, J. (2005). Regional brain activation during proximal stomach distention in humans: A positron emission tomography study. *Gastroenterology*, *128*(3), 564–573. http://doi.org/10.1053/j.gastro.2004.11.054
Verde, A. R. (2014). UNC-Utah NA-MIC framework for DTI fiber tract analysis, 1–12. http://doi.org/10.3389/fninf.2013.00051/abstract
Virtanen, K. A., Lidell, M. E., Orava, J., Heglind, M., Westergren, R., Niemi, T., et al. (2009). Functional brown adipose tissue in healthy adults. *N Engl J Med*, *360*(15), 1518–1525. http://doi.org/10.1056/NEJMoa0808949
Volkow, N. D., & Wise, R. A. (2005). How can drug addiction help us understand obesity? *Nature Neuroscience*, *8*(5), 555–560. http://doi.org/10.1038/nn1452
Volkow, N. D., Wang, G. J., Tomasi, D., & Baler, R. D. (2013). Obesity and addiction: neurobiological overlaps. *Obesity Reviews,* 14(1):2-18.
Wang, G. J., Tomasi, D., Backus, W., Wang, R., & Telang, F. (2008). Gastric distention activates satiety circuitry in the human brain. *Neuroimage,* 39(4):1824-31.
Wang, L., Shi, F., Yap, P.-T., Lin, W., Gilmore, J. H., & Shen, D. (2013). Longitudinally guided level sets for consistent tissue segmentation of neonates. *Human Brain Mapping*, *34*(4), 956–972. http://doi.org/10.1002/hbm.21486
Wang, Y., Li, D., Haacke, E. M., & Brown, J. J. (1998). A three‚Äêpoint dixon method for water and fat separation using 2D and 3D gradient‚Äêecho techniques. *Journal of Magnetic Resonance Imaging : JMRI*, *8*(3), 703–710.
Whitaker, R. C., Wright, J. A., Pepe, M. S., Seidel, K. D., & Dietz, W. H. (1997). Predicting obesity in young adulthood from childhood and parental obesity. *New England Journal of Medicine*, *337*(13), 869–873. http://doi.org/10.1056/NEJM199709253371301
Wijngaarden, M. A., Veer, I. M., Rombouts, S. A. R. B., van Buchem, M. A., Willems van Dijk, K., Pijl, H., & van der Grond, J. (2015). Obesity is marked by distinct functional connectivity in brain networks involved in food reward and salience. *Behavioural Brain Research*, *287*, 127–134. http://doi.org/10.1016/j.bbr.2015.03.016
Winkler, A. M., Ridgway, G. R., Webster, M. A., & Smith, S. M. (2014). Permutation inference

for the general linear model. *Neuroimage,* 92:381-97.
Wise, R. A. (2004). Dopamine, learning and motivation. *Nature Reviews Neuroscience,* doi:10.1038/nrn1406.
Wise, R. A., & Rompré, P. P. (1989). Brain dopamine and reward. *Annual Review of Psychology,* 40:191-225.
Yan, J., & Scott, T. R. (1996). The effect of satiety on responses of gustatory neurons in the amygdala of alert cynomolgus macaques. *Brain Research, 740*(1), pp.193-200.
Yoshida, S., Oishi, K., Faria, A. V., & Mori, S. (2013). Diffusion tensor imaging of normal brain development. *Pediatric Radiology*, *43*(1), 15–27. http://doi.org/10.1007/s00247-012-2496-x
Yushkevich, P. A., Piven, J., Hazlett, H. C., Smith, R. G., Ho, S., Gee, J. C., & Gerig, G. (2006). User-guided 3D active contour segmentation of anatomical structures: significantly improved efficiency and reliability. *Neuroimage*, *31*(3), 1116–1128. http://doi.org/10.1016/j.neuroimage.2006.01.015
Zanin, E., Ranjeva, J.-P., Confort-Gouny, S., Guye, M., Denis, D., Cozzone, P. J., & Girard, N. (2012). White matter maturation of normal human fetal brain. An in vivo diffusion tensor tractography study. *Brain and Behavior*, *1*(2), 95–108. http://doi.org/10.1002/brb3.17
Zeller, M. H., & Modi, A. C. (2006). Predictors of health-related quality of life in obese youth. *Obesity (Silver Spring, Md.)*, *14*(1), 122–130. http://doi.org/10.1038/oby.2006.15
Zhan, L., Jahanshad, N., Ennis, D. B., Jin, Y., Bernstein, M. A., Borowski, B. J., et al. (2012). Angular versus spatial resolution trade-offs for diffusion imaging under time constraints. *Human Brain Mapping*, *34*(10), 2688–2706. http://doi.org/10.1002/hbm.22094
Zhang, B., Tian, D., Yu, C., Zhang, J., Tian, X., Deneen, von, K. M., et al. (2015). Altered baseline brain activities before food intake in obese men: a resting state fMRI study. *Neuroscience Letters*, *584*, 156–161. http://doi.org/10.1016/j.neulet.2014.10.020
Zhang, Y., Brady, M., & Smith, S. (2001). Segmentation of brain MR images through a hidden Markov random field model and the expectation-maximization algorithm. *IEEE Transactions on Medical Imaging,* 20(1):45-57.